

ABSTRACT

BARILOVITS, STEPHEN. Experimental Study of a Unique Multi-Row Meltblowing Fiber Formation Process and the Web Structures Produced Thereby. (Under the direction of Drs. Saad A. Khan and Eunyoung Shim.)

Nano- and micro-polymeric fibers find widespread use in our lives in the form of engineered fabrics that require high surface areas and/or small pore sizes. These fabrics are used in high efficiency filtration, medical apparel, thermal and acoustic insulation. Meltblowing technology is a preferred method of producing such fibers, having been well studied and solidly established in the industry. A multi-row variant of the traditional process has also been commercialized, offering a higher maximum throughput and potentially producing stronger fibers with a wider range of polymer resins. Despite the commercial availability and possible advantages of multi-row meltblowing, it has not yet been publically studied in detail. In an effort to provide a better and more consolidated understanding of this process and its capabilities, this research was conducted to experimentally examine the fiber formation process and explain how it creates fibers and web structures.

Unlike traditional meltblowing, multi-row meltblowing uses cylindrical spinnerets, each of which is surrounded by an annular air stream. A symmetric, two-spinning-row die configuration was selected to investigate the fiber formation process using this spinneret design. A single polypropylene resin was used for all experiments. Fiber spinning process variables included air temperature, air speed, polymer throughput, and Die-Collector Distance (DCD). Observations included scanning electron microscopy of fiber diameters and web structures, high-resolution infrared thermography of polymer jets, three-dimensional air speed and temperature profiles, and ultra-high-speed videography and high-resolution stop-motion photography of spinning fibers.

Fiber diameters depended predominantly on polymer throughput and air temperature, with higher air speeds reducing diameters only at high polymer throughputs. Median diameters from the various processing conditions ranged from 0.76 to 13.8 μm . Infrared thermography demonstrated that significant heat transfer occurs between the polymer and the air immediately prior to spinning. Air temperature and velocity profiles were measured in the absence of spinning fibers to estimate the environment around the fibers during spinning. An empirical model was developed to predict median fiber diameter using the knowledge of thermal and physical conditions within the first centimeter of fiber spinning. Agreement of this model with the measured fiber diameters demonstrates that total fiber diameter attenuation is largely determined by conditions of the polymer jet very close to the spinnerets.

Careful examination of the polymer jets using ultra-high-speed videography and high-resolution photography revealed, for some conditions, a pulsation of the polymer jet, causing it to swell and retract periodically with frequencies of about 1 – 4 Hz. The pulsation exhibits different behavior from “draw resonance” and is observed to allow both large and small fibers to be formed from a single spinneret. Adjusting processing conditions to produce smaller fibers results in more severe pulsation, causing jet breakage and shot formation as the median fiber diameter drops below 1.0 μm . The jet pulsation increases the relative width of the diameter distributions and alters their shapes. Fiber diameters were distributed normally for larger median diameters to skewed-lognormal for small median diameters. The pulsation of the polymer jet certainly reduces median fiber diameters but may also limit diameter attenuation by causing shot formation.

Multi-row effects were studied using dies with two, four, and six spinning rows. Despite a parabolic air temperature profile across the width of the die, fiber diameters and distribution widths were only slightly increased when formed with more spinning rows. More spinning rows did,

however, clearly increase the incidence of spun fusion web defects and thereby increased effective fiber diameters even when individual diameters remained essentially unchanged.

This work provides an understanding of the commercial multi-row meltblowing process as it stands. While it is beyond the scope of this work to make design modifications, it is hoped that the results can guide those skilled in the art to make improvements in versatility and control of fibers and web structures. Future work should focus on aerodynamic and fluid mechanics to explain the origins and possible control mechanisms of the polymer jet instability observed here. While spun fusion can certainly be reduced, more research is needed to suggest the advantages and drawbacks of the various reduction methods available.

© Copyright 2018 Stephen Barilovits
All Rights Reserved

Experimental Study of a Unique Multi-Row Meltblowing Fiber Formation Process
and the Web Structures Produced Thereby

by
Stephen Barilovits

A dissertation submitted to the Graduate Faculty of
North Carolina State University
in partial fulfillment of the
requirements for the degree of
Doctor of Philosophy

Chemical Engineering

Raleigh, North Carolina

2018

APPROVED BY:

Dr. Eunkyong Shim
Committee Co-Chair

Dr. Saad A. Khan
Committee Co-Chair

Dr. Orlin Velev

Dr. Behnam Pourdeyhimi

DEDICATION

To my mother, Dr. Jane K. Laurent.

BIOGRAPHY

Stephen Barilovits IV is from Charlotte, NC with family roots traced to central Florida. On his mother's side, Steve is a third generation of PhD recipients. He attended high school at Canon School in Concord, NC where he discovered an interest in the sciences, especially chemistry from Tony Almond, an exceptional teacher. In high school, Steve also worked to develop a small neighborhood tree protection job into a larger business. Over several years he grew this business to serve hundreds of customers, residential, commercial, and city governments. For his bachelor's degree, Steve studied chemistry (biochemistry track), minoring in physics and biology at UNC-Chapel Hill. After graduating with Highest Honors in 2012, he took a gap year to travel with his future wife, Rebecca. They spent more than four months abroad before returning to attend graduate school in fall 2013. Transitioning to study chemical engineering for its focus on the applications of chemistry and physics, Steve pursued his doctorate at North Carolina State University. His work there focused on heterogeneous catalysis and on a meltblown fiber formation process with the Nonwovens Institute.

ACKNOWLEDGEMENTS

One of the most rewarding parts of my experience as a graduate student has been the ability to collaborate with others, learn from them, and solve problems together. First and foremost, I thank Dr. Eunkyong Shim for her guidance in navigating this journey, from solving the day-to-day problems that arise in experimentation, to guidance of the project overall. She is uniquely devoted to her students which explains her track record of success stories. I have been lucky to have her on my team. I thank Dr. Saad Khan threefold: first for his encouragement and efforts to usher me into the field of chemical engineering, second for his support and guidance on the research project, and third for his advice on my personal development. I thank Dr. Behnam Pourdeyhimi for his experienced feedback on this project and advice for the effective communication of the work.

Almost all of my experimental work involved Nonwovens Institute staff and technicians who provided invaluable assistance in the successful execution of experimental objectives. I extend my thanks to Bruce Anderson for all the imaging help in this highly imaging-intensive project, to Eric Lawrence and William Barnes for their help in numerous successful fiber-forming trials and experiments, to Amy Minton for help in material characterization, and to Abhay Joojode for his rheological help and spinneret-blocking advice.

I would also like to thank all of my industrial advisors, who offered excellent feedback, advice, and help during the course of this project. I especially thank Doug Brown and Jeff Stark of Biax-Fiberfilm Corporation for sharing their intimate knowledge of their equipment and process. I thank Raul Farer of Freudenberg for his active engagement in the project and valuable advice in interpretation of experimental results. Last but not least, I thank Annette Schenk of MANN+HUMMEL for her tremendous help in analyzing the numerous fiber diameters.

I thank the students in the Khan Research Group as well as the Nonwovens Institute. I especially thank Miika Niikinmaa for giving me many good and novel ideas on the project and effective presentation of results. I also thank Salvatore Luiso for working together with me on rheological calculations.

Finally, I would like to thank my department and funding sources. I thank the Nonwovens Institute and member companies for funding this work. I thank the Department of Chemical and Biomolecular Engineering for accepting me to the program despite my non-traditional background, and for providing me some excellent and challenging courses that taught me the field. Special thanks to Sandra Bailey, the welcoming face of the department, who consistently provided accurate information and support to me over these years.

TABLE OF CONTENTS

LIST OF TABLES	ix
LIST OF FIGURES	x
Chapter 1 – Introduction and Background.....	1
1.1 Nonwovens Background and Industry Future.....	1
1.2 Meltblowing for Fine Fiber Production.....	2
1.3 Multi-Row Meltblowing Using Annular Spinnerets	7
1.4 References	12
Chapter 2 - Experimental Investigation of the Fiber Formation Process and Web Structures using an Annular Meltblowing Spinneret.....	14
2.1 Abstract	14
2.2 Introduction	15
2.3 Experimental	19
2.3.1 Material	19
2.3.2 Material Characterization	19
2.3.3 Dual-Row Meltblowing.....	20
2.3.4 Infrared Thermography of Spinning Fibers.....	24
2.3.5 Air Temperature and Velocity Profiling	25
2.4 Results and Discussion.....	26
2.4.1 Air Temperature and Velocity Profiles in the Fiber-Forming Region	26
2.4.2 Temperature of Spinning Fibers.....	31
2.4.3 Polymer Thermal and Rheological Characterization	37
2.4.4 Two-Row Meltblowing Fiber Diameter Distributions	39
2.4.5 DCD Effects on Fiber Size and Bonding Distance	42
2.5 Conclusions	45
2.6 References	48
2.7 Supplementary Information.....	50

2.7.1 Tracking of Lateral Fiber Motions	50
2.7.2 Online Measurement of Fiber Bending Instabilities Using Back-Folding Distance	54
2.7.3 Bulk Fiber Speed	56
Chapter 3 - Meltblown Polymer Jet Pulsation: Observations and Effects on Fiber Diameter Distribution in an Annular Meltblowing Spinneret Design	58
3.1 Abstract	58
3.2 Introduction	59
3.3 Experimental	63
3.3.1 Material	63
3.3.2 Dual-Row Meltblowing.....	63
3.3.3 Ultra-High-Speed Videography	67
3.3.4 High-Resolution Photography	68
3.3.5 Fiber Diameter Measurement	68
3.4 Results and Discussion	68
3.4.1 Fiber Diameter Distributions.....	68
3.4.2 Pulsation of the Polymer Jet	73
3.5 Conclusions:	84
3.6 References	86
Chapter 4 - High Throughput Multi-Row Meltblowing: Effects of Increasing Fiber-Forming Rows on Fiber Diameter Distributions and Web Defects.....	91
4.1 Abstract	91
4.2 Introduction	91
4.3 Experimental	95
4.3.1 Material	95
4.3.2 Multirow Meltblowing	96
4.3.3 Air Temperature and Velocity Profile.....	100

4.3.4	Fiber Diameter Measurement	102
4.4	Results and Discussion	102
4.4.1	Air Temperature and Velocity Profile	102
4.4.2	Fiber Diameters and Distributions	107
4.4.3	Web Defect: Spun Fusion.....	113
4.5	Conclusions	119
4.6	References	120
4.7	Supplementary Information.....	122
4.7.1	Fiber Diameter Measurement Using a Semi-Automated Method.....	122
4.7.2	Processing Conditions and Fiber Diameter Distributions	124
Chapter 5	- Summary and Conclusions	130

LIST OF TABLES

Table 2.1	Process variables and their specific conditions.....	24
Table 2.2	Air cavity conditions as they affect the air temperature and velocity 1.0 cm in front of the fiber-forming spinnerets.	31
Table 2.3	Back-folding distance (in centimeters) of fibers undergoing bending instability during fiber formation. Distances for when the centerline air temperature drops to 120 °C, the crystallization temperature of PP, are shown for reference. * Indicates that fibers were so small that they were barely visible; determining back-folding events was very difficult for these conditions.....	55
Table 2.4	Bulk fiber speed at 8 cm from the spinnerets compared to air speed at the same location, for all conditions	57
Table 3.1	Process variables and their specific conditions.....	67
Table 3.2	Fiber diameter distributions as defined by Shapiro-Wilk test results. Subscripts of normal and lognormal indicate test result statistics from the fiber diameters and the logarithm of the diameters, respectively. All distributions observed satisfy one and only of the shown criteria.	70
Table 3.3	Median fiber diameter, distribution type and distribution dispersity for each 26 samples collected. Distributions indicated by * are shown as histograms in Figure 3.3.	72
Table 3.4	Median fiber diameters, processing conditions, and jet pulsation amplitude.....	78
Table 4.1	Process variables and their specific conditions.....	100
Table 4.2	Processing condition by condition identifying number. Fabrics formed from all condition for 2, 4, and 6 fiber spinning rows.	124
Table 4.3	Fiber diameter distribution dispersities for each condition and number of fiber spinning rows.	125

LIST OF FIGURES

Figure 1.1	Traditional Meltblowing Equipment [14]. (a) The meltblowing process; (b) Fiber-forming die.	5
Figure 1.2	Multi-Row Meltblowing Die [29]. (a) Cross sectional view; (b) Die face view.	8
Figure 2.1	(a) Side schematic representation of the multi-row meltblowing design and fiber formation process. (b) Photo of an eight-polymer-row die face, with two air-only outlets at the die edge. (Photo courtesy of Biax Fiberfilm Corp)	17
Figure 2.2	(a) Schematic side view of the 2-row meltblowing process; (b) Schematic front view of the die face showing red polymer extrusion from the fiber forming spinnerets, blue hash steel spinneret wall and studs, and white hot air releasing annuli; (c) Relevant dimensions of the spinnerets (not shown: spinnerets extend 3.0 mm past the air annuli face, and spinneret studs extend 1.5 mm past the same face).	21
Figure 2.3	Side schematic view of the locations where air temperature and velocities were measured.	25
Figure 2.4	Air temperature and velocity measurements for various positions in front of the die face for the single processing condition where air cavity temperature and pressure were 240 °C, and 97 kPa, respectively. Red star (★) location measurements are shown for other processing conditions in Table 2.2. (a) Air temperature profile. (b) Air velocity profile. (c) Air temperature and velocity within the air stream measured 1.0 cm in front of the spinnerets.	27
Figure 2.5	(a) Side view IR photographs of spinning fibers; air velocity was 56 m/s and polymer throughput 0.17 grams/hole/minute for both images shown. (b) Air temperature and speed effect on relative fiber temperature as a function of distance from the spinnerets (polymer throughput was 0.10 gram/hole/minute). (c) Air temperature and polymer throughput effect on relative fiber temperature as a function of distance from the spinnerets.	33
Figure 2.6	Temperature equilibration fraction as a function of polypropylene throughput for a spinneret length of 2.5 cm. $\theta = TPP - TiTw - Ti$, where T_{pp} is the fiber spinning temperature, T_i is the polymer melt temperature, and T_w is the air cavity temperature.	36
Figure 2.7	Rheological characterization of LyondellBasell MF 650W Polypropylene. (a) Viscosity versus shear rates collected from parallel plate and capillary rheometers. (b) Viscosity versus temperature in the	

	low shear limit with exponential extrapolation $A \exp(-BT)$, where $A = 7.60 \times 10^6 \text{ Pa}\cdot\text{s}$ and $B = 2.59 \times 10^{-2} \text{ }^\circ\text{K}^{-1}$	38
Figure 2.8	Fiber diameter distributions for each air speed, air temperature, and polymer throughput level listed in Table 2.1. DCD was 40 cm for all conditions. Samples marked with * toward the right of the figure indicate the presence of any amount of shot. Shot and fly for the rightmost condition prevented the sample from being collected and analyzed.	40
Figure 2.9	DCD effect on fiber diameter	43
Figure 2.10	Determining bonding distance by SEM inspection. Processing conditions: throughput = 0.17 gram/hole/minute, air temperature = 240 °C, air speed = 56 m/s. (a) Heavily bonded. (b) Highest DCD exhibiting bonding: portions of fibers crossing at high angles are visibly bonded. (c) DCD greater than bonding distance: fibers crossing at high angles that clearly touch are not visibly bonded.....	44
Figure 2.11	Fiber bonding distances compared to distance for the centerline air temperature to reach 120 °C.....	46
Figure 2.12	Fiber lateral motion for air temperature of 166 °C, air speed of 46 m/s, and polymer throughput of 0.17 gram/hole/minute. (a) A fiber tracked over 20 ms at 3 and 6 cm from the spinneret outlet. (b) A fiber tracked over 20 ms at 9 and 11.2 cm from the spinneret outlet.	52
Figure 2.13	Amplitude of fiber lateral motion oscillations for various distances from the spinneret outlet.....	53
Figure 2.14	Schematic representation of back-folding distance.	55
Figure 3.1	(a) Side schematic representation of the multi-row meltblowing design and fiber formation process. (b) Photo of an eight polymer row die face, with two air-only outlets at the die edge. (Photo courtesy of Biax Fiberfilm Corp)	61
Figure 3.2	(a) Schematic side view of the 2-row meltblowing process; (b) Schematic front view of the die face showing red polymer extrusion from the fiber forming spinnerets, blue hash steel spinneret wall and studs, and white hot air releasing annuli; (c) Relevant dimensions of the spinnerets (not shown: spinnerets extend 3.0 mm past the air annuli face and spinneret studs extend 1.5 mm past the same face).	63
Figure 3.3	Representative fiber diameter distributions as histograms with 1 μm bin size.....	70

Figure 3.4	Fiber diameter distributions by number and by mass fraction, histograms with 1 μm bin size. Data sets were taken from Figures 3.3(a), (d), and (e), respectively for (a), (b), and (c). Dispersion: $D = \sigma/D_{\text{med}}$	73
Figure 3.5	In the region of fiber bending instabilities, a large fiber is clearly visible along with many smaller fibers that are difficult to discern given the image resolution.....	74
Figure 3.6	Top-down view of spinnerets from an ultra-high speed cine showing a sharp increase of polymer released from one spinneret into a larger fiber. Five spinneret columns are visible in this field of view, and the release of polymer from a second spinneret is visible in the rightmost image. The median fiber diameter collected from this condition was 0.76 μm	75
Figure 3.7	High resolution photos of the polymer jet issuing from a single spinneret at different moments during the jet pulsation.....	76
Figure 3.8	Shot particle; median diameter of fibers was 0.76 μm	79
Figure 3.9	Polymer jet diameter profile with time, for three polymer flow rates. Air temperature was 240 $^{\circ}\text{C}$, air speed was 56 m/s.	80
Figure 3.10	Polymer jet pulsation as caused by the annular spinneret aerodynamic configuration.....	81
Figure 3.11	Jet pulsation period for high amplitude conditions.....	82
Figure 3.12	Fiber diameters from large (2-row) capillaries and from small (4-row) capillaries. For all diameters shown, air temperature was 166 $^{\circ}\text{C}$, polymer throughput was 0.05 gram/hole/minute, and DCD was 40 cm (a) Air speed 56 m/s. (b) Air speed 68 m/s.....	89
Figure 4.1	Annular meltblowing spinneret.	94
Figure 4.2	(a) Schematic side view of the multirow meltblowing process for six, four, and two fiber forming rows; (b) Schematic front view of the 6-row die face showing red polymer extrusion from the fiber forming spinnerets, blue hash steel spinneret wall and studs, and white hot air releasing annuli; (c) Relevant dimensions of the spinnerets (not shown: spinnerets extend 3.0 mm past the air annuli face and spinneret studs extend 1.5 mm past the same face).....	97
Figure 4.3	Side schematic view of the locations where temperature and velocity measurements were measured.	101

Figure 4.4	Air temperature and velocity measured across the air stream 1 cm in front of spinnerets. Spinnerets were “dry”, i.e. no fibers were formed during the measurement. Measurement type by numeral: I. Air Temperatures; II. Air Speeds. Air cavity conditions by letter: (a) 48.3 kPa, 182 °C; (b) 48.3 kPa, 240 °C; (c) 68.9 kPa, 182 °C; (d) 68.9 kPa, 240 °C.....	104
Figure 4.5	Fiber diameter for different number of spinning rows relative to the average for all rows, for various processing conditions.	108
Figure 4.6	Cumulative fiber diameter distributions from all conditions where DCD = 40 cm, for two, four, and six fiber spinning rows. Each distribution results from approximately 3000 fiber diameters measured.	110
Figure 4.7	Fiber diameter distribution dispersity for all conditions (where DCD = 40 cm), spun from 2, 4, and 6 spinneret rows.....	112
Figure 4.8	Fiber fusion counting procedure: a line is draw approximately perpendicular to the machine direction of the fiber orientation. Individual and fused fibers are counted that cross this line. This procedure applied to this image gives 43 fibers total (fused or individual), 22 fibers involved in 10 fusions. 22/43 or 51% of fibers are fused.	114
Figure 4.9	Effect of processing conditions on the incidence of fiber fusion. (a) Air temperature effects (for DCD = 40 cm, averaged across row number, air velocity, and polymer throughput); (b) Air velocity effects (for DCD = 40 cm, averaged across row number, air temperature, and polymer throughput); (c) Polymer throughput effects (for DCD = 40 cm, averaged across row number, air temperature and air velocity); (d) DCD effects (averaged across all conditions and row number).	115
Figure 4.10	Fiber fusion rates for all processing conditions (where DCD = 40 cm) for fibers spun from 2, 4 and 6 fiber forming spinneret rows.	117
Figure 4.11	Fiber diameter distributions as determined manually (using ImageJ software) shown in red, and using a semi-automated program (AutoFiber from Mann+Hummel Group) shown in blue. Kolmogorov-Smirnov two sample test p-values shown. Processing conditions: (a) air temperature of 166 °C, air speed of 55 m/s, polymer throughput of 0.10 ghm, DCD of 15 cm; (b) air temperature of 166 °C, air speed of 55 m/s, polymer throughput of 0.10 ghm, DCD of 20 cm; (c) air temperature of 166 °C, air speed of 55 m/s, polymer throughput of 0.10 ghm, DCD of 30 cm; (d) air temperature of 166 °C, air speed of 55 m/s, polymer throughput of 0.10 ghm, DCD of 40 cm.....	123
Figure 4.12	Fiber diameter distributions as cumulative distributions for all samples collected. Distributions in blue are for the sample collected from the 2-	

row case, red from the 4-row case, and green from the 6-row case.
Table 4.2 displays processing conditions for each condition number.
Kolmogorov-Smirnov two sample test p-values shown: P_{2/6} shows the
p-value results when 2 and 6-row distributions are compared,
analogously for the other two pairs.125

1 Chapter 1 – Introduction and Background

1.1 Nonwovens Background and Industry Future

While nonwoven textiles trace their origin to ancient or even prehistoric wool feltmaking [1], as a cohesive industry the field is less than a century old. A need to convert fibrous material not suitable for yarn making into useful products, along with other considerations, led to the development of revolutionary technologies capable of producing textile-like fibrous products without weaving or knitting operations [2]. While the origins of the modern industry cannot be pinpointed, critical ideation leading to the modern industry certainly include needle looming equipment from the 1870s, adhesive bonding techniques from the 1920s, and integrated spun-laid processes from the 1950s-1970s. Nonwoven production technologies encompass numerous subsidiary technologies, most of which have become industries in their own right. While this thesis concerns only a spun-laid process, more specifically a particular meltblowing process, the reader not familiar with the nonwovens industry is encouraged to consult textbook references on the field [2], [3]. Only to put the research into context, a cursory overview of nonwovens and their applications is given here.

INDA, the Association of the Nonwoven Fabrics Industry, defines a nonwoven as “a primarily fibrous assembly – other than traditional paper, woven, or knit – which has been engineered to some level of structural integrity by physical and/or chemical means” [4]. Nonwovens today find use in a tremendous number of products and applications, both disposable and durable. Examples of products core to the industry include wipes, disposable clothing, interlinings, carpet backings, filters, geotextiles, automotive parts, and medical supplies, to name just a few. The industry employs the term “engineered fabrics” to emphasize that the fabrics are highly tailored to specific applications and to dispel the perception of the fabrics as cheap and

therefore necessarily lower performance alternatives to traditional textiles. Indeed, nonwovens often have cost and/or production speed advantages over traditional textiles, as well as advantages in the diversity of possible structures and materials with which to make them.

The future of the global nonwovens industry arguably lies in increasing production capacity to serve developing markets and the incorporation of novel materials to create new products or existing products with more desirable properties. The nonwovens market is more mature in western Europe and North America than it is in the rest of the world. A growing middle class in some of the world's most populous countries drives increasing consumption of nonwoven-containing goods in those areas. Higher production capacity and cost reduction will therefore continue to be priorities of the industry for the foreseeable future. However, the expected increase in nonwoven consumption, especially disposables, also fuels environmental concerns related to sustainability and biodegradation. The future of the nonwoven industry in its established markets may even depend on its ability to meet regulatory demands by replacing fossil-fuel-based polyolefins with sustainably sourced and/or biodegradable components [5]. Thus, efforts are currently being made to develop novel materials and to modify processes to economically produce nonwoven products from these new materials.

1.2 Meltblowing for Fine Fiber Production

An important subset of nonwoven products requires high surface area and/or small pore sizes for optimal performance. Some examples include filtration, bio-separation, medical barrier fabrics, and thermal and acoustic insulation. High specific surface area (surface area per unit mass or volume) is needed for efficient conversion of raw material into surface area available for particle capture or surface functionalization. Specific surface area is inversely proportional to fiber

diameter, so small fiber diameters yield high surface area fabrics. Pore size is a more complex function of fabric properties but is directly proportional to fiber diameter [6], so small fiber diameters also reduce fabric pore sizes. The finest natural fibers used commonly in textiles such as silk, fine wools and cottons typically have diameters larger than 10 μm . Synthetic polymeric fiber production methods such as monocomponent spunbonding and melt spinning also rarely produce fibers less than 10 μm in diameter.

Fine fiber production technologies include bicomponent spunbonding, meltblowing, solution blowing, and electrospinning. When performed with polymers that have little affinity for one another, segmented pie bicomponent spunbonding followed by mechanical fiber fracturing can produce fibrous shards of less than 1 μm , but more commonly greater than 2 μm [7]. Common polymer combinations include polyethylene (PE)/polyethylene terephthalate (PET), PE/polypropylene (PP), Nylon/PET, and copolymer variants of these [2]. The Islands-in-the-Sea (I/S) spunbonding technique can also produce submicron fibers but requires the use of solvents to remove the sea component [8]. Meltblowing can produce single-component continuous fibers with diameters of 2-5 μm [9], or less than 500 nm at significantly reduced throughput rates [10]. Solution blowing [11] and electrospinning [12] can produce fibers of less than 100 nm. Although they exist in the industry, these processes are slow and are not environmentally responsible because they involve solvents. Meltblowing and bicomponent spunbonding are certainly the industrially preferred methods of fine fiber production. Although meltblowing produces structurally weak fibers compared to spunbonding, it has the advantage of producing bonded fabrics in a single step. Meltblown fibers are often sandwiched between monocomponent spunbonded layers, in so-called SMS fabrics, for applications that require both strength and small fibers.

The meltblowing process evolved from the solution blowing process, which has been employed industrially to produce polymeric fibers since the 19th century [11]. Most researchers cite the work of Van Wente, who was working for the Naval Research Laboratory in search of methods of producing submicron organic fibers, as the first to demonstrate the viability of the meltblowing process [13]. Exxon later patented and scaled the process up to a commercial technology [14], [15]. These works describe a method of producing fine fibers in a single integrated process from a thermoplastic polymer melt, see Figure 1.1.

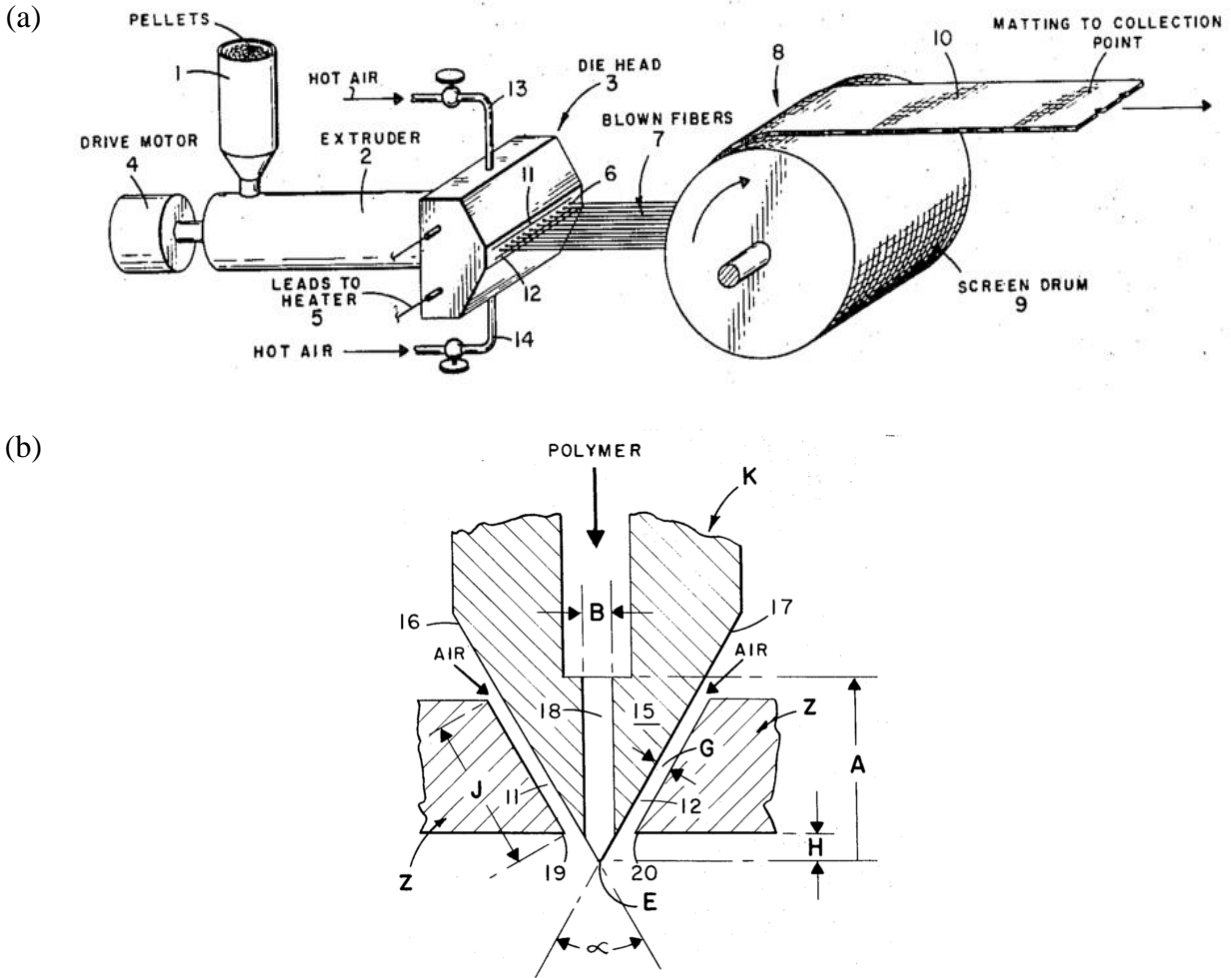


Figure 1.1 Traditional Meltblowing Equipment [14]. (a) The meltblowing process; (b) Fiber-forming die.

Polymer chips are heated, melted, and pushed with high pressure by an extruder into small capillaries of a fiber-forming die. The die has a triangular cross section with capillary orifices located at the edge of the triangle, as shown in Figure 1.1(b). Two converging curtains of high-velocity hot air are directed toward the capillary outlets and serve to rapidly accelerate and draw the polymer into a jet, subsequently transforming it into a fine fiber that is collected on a belt. The collection belt often contains suction underneath to pull the fibers into a mat and prevent “fly”, uncollected fibers that are released into the room air.

The term polymer jet is used to describe the molten polymer in the region close to the capillary outlet where rapid axial acceleration dominates the dynamics of fiber formation. As the polymer jet speed approaches the air speed and the jet becomes quite narrow, it is typically referred to as a fiber from this point on. This fine fiber has a low bending rigidity, allowing it to undergo complex bending motions that further reduce cross sectional diameters [16]. Fibers also may crystallize before, during, or after they are collected. The distance over which fibers traverse, termed the Die-Collector Distance (DCD), dictates in large part the extent to which fibers will crystallize in the air prior to collection. For sufficiently short DCDs, fibers do not fully crystallize before collection and have a tacky surface, allowing the fibers to bond to one another immediately upon collection. Such *autogenous* bonding is a unique capability of the meltblowing process, allowing for the production of stiff, heavily bonded fabrics or flexible, lightly bonded ones based on DCD variations alone [2].

Regardless of the DCD used, most of the fiber draw down occurs while the polymer is still molten [17]; therefore, little or no crystalline orientation can develop [18]. Melt spinning and spunbonding techniques, by contrast, purposefully draw fibers within or below the polymer crystallization temperature range, conditions that align crystals in ordered structures and thereby create strong fibers [19], [20]. In this way, the mechanisms that allow for production of very fine fibers in meltblowing also inhibit their ability to provide mechanical integrity. Additionally, the small capillary sizes required to produce fine fibers limits the variety of polymers compatible with the process. Compatible polymers typically have Melt Flow Rate (MFR) values (a value inversely proportional to the viscosity, for more information see the standard measurement technique ASTM D1238) of 400 to 1,600 [2]. Polypropylene is currently most widely used, due to its low cost, low

density, and hydrophobicity, which prevents the need to pre-dry the polymer pellets before meltblowing.

The process and equipment described above are commonly used and well-studied, but variants to the traditional meltblowing process have also been patented and commercialized. For example, the air outlets have been modified to create supersonic air jets [21], the effects of which have been studied [22]. Additionally, several machinery variations have been made to enable meltblowing of multi-component fibers [23]–[25]. Significant deviations from the traditional design can allow for the production of hollow fibers in a meltblowing process [26], [27]. While these variations can create structures that the traditional die design cannot, they retain the fundamental limitations of meltblowing: weak fibers and a limited choice of highly compatible polymers.

1.3 Multi-Row Meltblowing Using Annular Spinnerets

One commercial variant to the meltblowing process has claimed to alleviate some of these pervasive drawbacks while increasing total fiber throughput. The process, patented by Biax-Fiberfilm Corp, distributes molten polymer to an array of cylindrical capillaries, each of which is surrounded by an annular attenuating air stream [28], [29]. The annular drawing air is necessary to isolate fibers from one another to help prevent molten jets from colliding during fiber formation in a multi-row case. A schematic diagram of the die is shown in Figure 1.2.

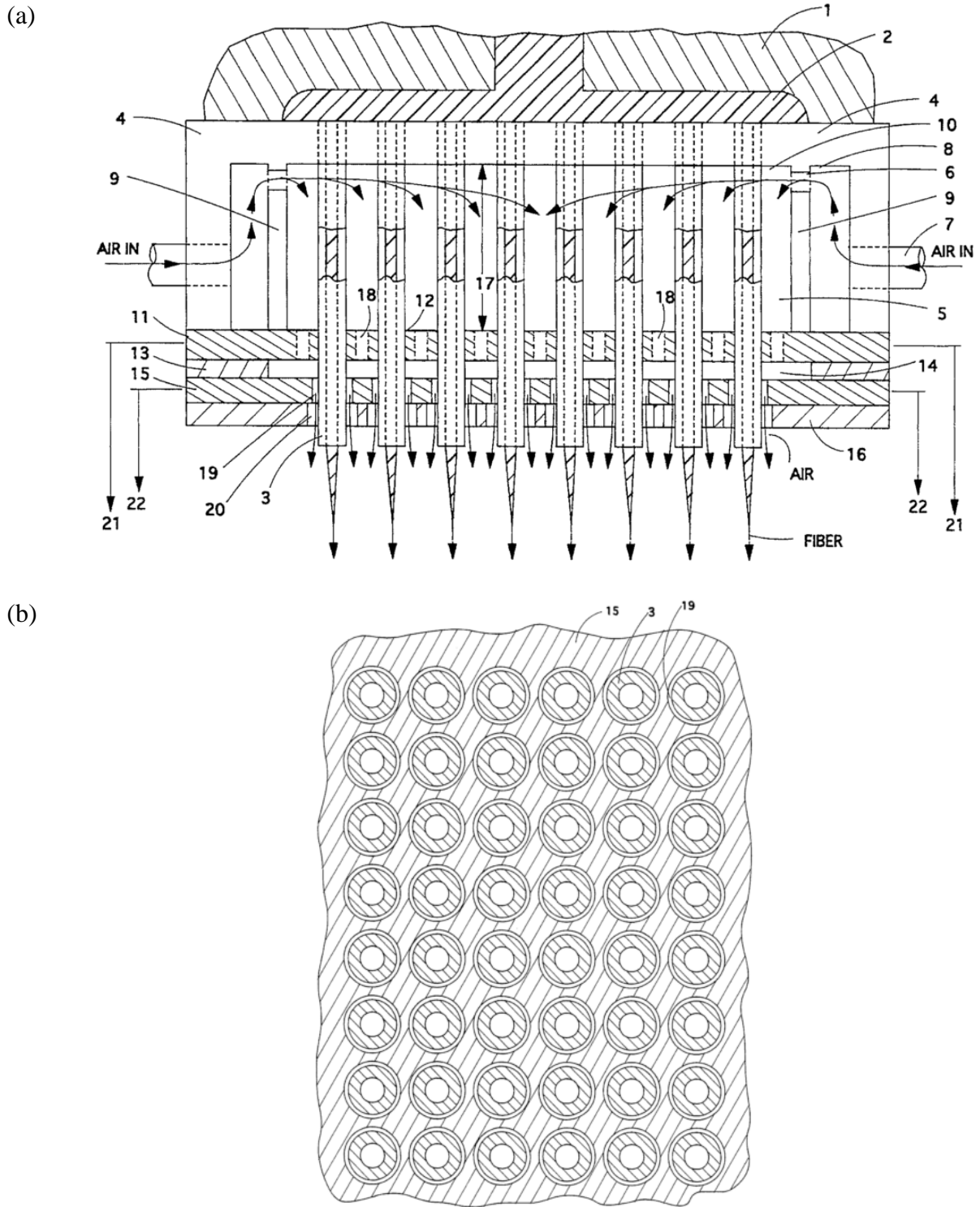


Figure 1.2 Multi-Row Meltblowing Die [29]. (a) Cross sectional view; (b) Die face view.

Referring to the numbered labels of Figure 1.2, the design requires capillaries (#3) to traverse an air cavity (#5), putting the polymer and air into thermal contact prior to fiber spinning. Not shown in Figure 1.2(a), the polymer distribution (#2) is typically achieved using a series of modular distribution plates to distribute polymer from the extrusion pipe evenly to each capillary. The capillaries, also known as spinnerets, extend several millimeters past the air annuli outlets (#19) to allow the air stream to become directed parallel to the spinnerets and assist in isolating the polymer jets from one another. Capillaries flush with the air annuli outlets, or recessed behind them, as is sometimes the case for slot dies [10], can cause polymer jets to collide with one another during spinning [29]. Also not shown in Figure 1.2, spinnerets may be blocked from emitting polymer. Many commercial dies contain “air curtain” rows, perimeter spinnerets whose capillaries are blocked from spinning fibers but still release air. The objective of air curtain rows is to insulate the interior polymer jets from cool entraining room air, reducing fiber diameter and diameter distributions.

Multi-row meltblowing can operate at higher total polymer throughput rates than can a single row. More spinnerets can be used in a multi-row design even though inter-spinneret spacing is greater in the multi-row case. More than twelve-row-containing dies are sold commercially [30]. Higher throughput meltblowing in the traditional design can be achieved by increasing capillary size and/or increasing per-capillary flow rate via higher extrusion pressures. Achieving higher throughput using either method will likely come at the cost of producing larger fibers. Additionally, excessive extrusion pressures run the risk of causing catastrophic die fracture or “unzipping” of the triangular-shaped dies [31]. A greater total number of spinnerets fed by an extruder reduces the operating pressures on the multi-row variant required to achieve a desired throughput rate.

Equipment manufacturers also claim that fibers produced using the annular meltblowing design are stronger and can be made from a wider variety of polymers than traditional meltblowing. The process has been termed “Spun-blown®” to emphasize that fibers made with the process have fiber sizes similar to meltblowing, but strength intermediate between weak traditional meltblown fibers and stronger spunbonded fibers [30]. Lower extrusion pressures can allow the use of polymers of higher viscosity (and lower MFRs). Even if little crystalline orientation develops, the ability to operate with higher viscosity and higher molecular weight polymers can alone produce stronger structures [20]. The ability to change polymer temperature immediately prior to fiber spinning can minimize thermal degradation of polymers, also creating stronger fibers.

Although the fiber formation process for traditional meltblowing, and many variants to that die configuration, have been studied extensively, the multi-row annular spinneret design has not yet been studied openly and systematically. It is known that the aerodynamics close to the spinnerets are of critical importance to the fiber formation process in the traditional design [32], so it cannot be assumed that the findings from slot-die meltblowing studies can be applied to this altered design. The design has the potential to produce strong, fine fibers at high throughput and with a variety of polymers and may therefore play an important role in the production of high-performance nonwovens for years to come. A better understanding of the process advantages and limitations is needed for appropriate application of the technology. The goal of this work is to provide the first thorough understanding of this fiber and web formation process.

This following work is divided into three content chapters, and introductions for each are included separately. Chapter 2 is a detailed investigation of the fiber and web formation process from a single die geometry. Chapter 3 examines the fiber diameter distributions and their causes from the same die geometry. Chapter 4 investigates the effects of increasing the number of fiber-

forming spinneret rows on fiber diameters, distributions, and web defects. Chapter 5 contains summary and conclusions. All fiber spinning was accomplished using exclusively a meltblowing grade (MFR 500) polypropylene resin, a polymer known to the industry to be compatible with the equipment over a wide range of conditions. The work was conducted between 2015 and 2018 at the Nonwovens Institute, a partnership between academia, industry, and government at North Carolina State University. This forum has provided the capability to conduct research on commercial processes, which ensures that the results reflect an industrial reality. While the research is fundamentally academic in nature, members from industry, including the manufacturers and patent holders of the multi-row meltblowing equipment described, have provided feedback and advice during the course of this work.

1.4 References

- [1] B. Gordon, *Feltmaking*. Watson-Guption Publications, New York, 1980.
- [2] S. Batra and B. Pourdeyhimi, *Introduction to Nonwovens Technology*. 2012.
- [3] S. J. Russell, *Handbook of nonwovens*. Woodhead Publishing Limited and CRC Press LLC, Boca Raton, FL, 2007.
- [4] “INDA Annual Report,” 2014.
- [5] A. Koukoulas, “Nonwovens and the Sustainability Imperative,” in *RISE 2017*, 2017.
- [6] K. Matsumoto, T. Yunoki, and K. Nakamura, “Effect of fiber diameter, porosity and basis weight on pore size and pore size distribution of stainless steel non-woven fiber filter,” *KAGAKU KOGAKU RONBUNSHU*, vol. 30, no. 1, pp. 79–86, 2004.
- [7] R. Groten, J. Baravian, and G. Riboulet, “United States Patent (19),” 5970583, 1999.
- [8] A. Durany, N. Anantharamaiah, and B. Pourdeyhimi, “High surface area nonwovens via fibrillating spunbonded nonwovens comprising Islands-in-the-Sea bicomponent filaments: Structure-process-property relationships,” *J. Mater. Sci.*, vol. 44, no. 21, pp. 5926–5934, 2009.
- [9] X. Wang and Q. Ke, “Experimental Investigation of Adhesive Meltblown Web Production Using Accessory Air,” *Polym. Eng. Sci.*, vol. 46, no. 1, pp. 1–7, 2006.
- [10] C. J. Ellison, A. Phatak, D. W. Giles, C. W. Macosko, and F. S. Bates, “Melt blown nanofibers : Fiber diameter distributions and onset of fiber breakup,” *Polymer (Guildf)*, vol. 48, pp. 3306–3316, 2007.
- [11] M. E. S., G. M. Glenn, A. P. Klamczynski, W. J. Ortis, and L. H. C. Mattoso, “Solution Blow Spinning: A New Method to Produce Micro- and Nanofibers from Polymer Solutions,” *J. Appl. Polym. Sci.*, vol. 113, no. 4, pp. 2322–2330, 2009.
- [12] D. H. Reneker and I. Chun, “Nanometre diameter fibres of polymer, produced by electrospinning,” *Nanotechnology*, vol. 7, pp. 216–223, 1996.
- [13] V. Wentz, “Superfine Thermoplastic Fibers,” *Ind. Eng. Chem. Res.*, pp. 342–346, 1955.
- [14] J. P. Keller and R. R. Buntin, “Melt-Blowing Die For Producing Nonwoven Mats,” 3825380, 1974.
- [15] R. Butin, J. P. Keller, and J. Harding, “Non-Woven Mats by Melt Blowing,” 3849241, 1974.
- [16] A. L. Yarin, S. Sinha-ray, and B. Pourdeyhimi, “Meltblowing : II-linear and nonlinear waves on viscoelastic polymer jets,” *J. Appl. Phys.*, vol. 108, 2010.
- [17] B. Haynes, “An experimental and analytical investigation on the production of microfibers using a single hole melt blowing process,” 1991.

- [18] B. R. R. Bresee and W. Ko, "Fiber Formation During Melt Blowing," *Int. Nonwovens J.*, 2003.
- [19] S. Fischer, O. Marti, T. Diesner, and B. Rieger, "Small-Angle X-ray Scattering on Melt-Spun Polypropylene Fibers : Modeling and Data Reduction," *Macromolecules*, vol. 43, pp. 5009–5015, 2010.
- [20] J. Schultz, *Polymer Chrstalization: The Development of Crystalline Order in Thermoplastic Polymers*. Oxford University Press, New York, 2001.
- [21] A. S. . Fabbriante, G. F. Ward, and T. J. Fabbriante, "Micro-Denier Nonwoven Materials Made Using Modular Die Units," 6,114,017, 2000.
- [22] D. H. Tan, P. K. Herman, A. Janakiraman, F. S. Bates, S. Kumar, and C. W. Macosko, "Influence of Laval nozzles on the air flow field in melt blowing apparatus," *Chem. Eng. Sci.*, vol. 80, pp. 342–348, 2012.
- [23] V. Bansal, M. Davis, and E. Rudisill, "APPARATUS FOR MAKING MULTICOMPONENT MELTBLOWN FIBERS AND WEBS," 7008207, 2006.
- [24] M. A. Allen, "METHOD FOR MELTBLOWING MULTI- COMPONENT LIQUID FILAMENTS," 6946093, 2005.
- [25] B. Haynes and M. C. Cook, "DIE FOR PRODUCING MELTBLOWN MULTICOMPONENT FIBERS AND MELTBLOWN NONWOVEN FABRICS," 7150616, 2006.
- [26] L. B. Torobin, "Method and Apparatus for Producing Microfilaments," 4363646, 1982.
- [27] C. Torobin, L., Finlow, "Method and Apparatus for Producing High Efficiency Fibrous Media Incorporating Discontinuous Sub-Micron Diameter Fibers, and Web Media Formed Thereby," 6183670, 2001.
- [28] E. C. A. Schwarz, "Apparatus and Process of Melt-Blowing A Fiberforming Thermoplastic Polymer and Product Produced Thereby," 4380570, 1983.
- [29] E. Schwarz, "Apparatus and Process for Uniformly Melt-Blowing A Fiberforming Thermoplastic Polymer in a Spinnerette Assembly of Multiple Rows of Spinning Orifices," 5476616, 1995.
- [30] Biax Fiberfilm, "Spun-blown Meltblown Systems," 2015. [Online]. Available: <http://www.biax-fiberfilm.com/spunblownmeltblown/>.
- [31] G. F. Ward, "Meltblown nanofibres for nonwoven filtration applications," *Filtr. Sep.*, vol. 38, no. 9, pp. 42–43, 2001.
- [32] A. L. Yarin, S. Sinha-ray, and B. Pourdeyhimi, "Meltblowing : Multiple polymer jets and fi ber-size distribution and lay-down patterns," *Polymer (Guildf)*, vol. 52, no. 13, pp. 2929–2938, 2011.

2 Chapter 2 - Experimental Investigation of the Fiber Formation Process and Web Structures using an Annular Meltblowing Spinneret

Stephen Barilovits, Eunkyong Shim, Saad A. Khan, Behnam Pourdeyhimi

Department of Chemical and Biomolecular Engineering and the Nonwovens Institute, North Carolina State University, Raleigh, NC (USA).

This chapter is under revision for publication.

2.1 Abstract

The Spunblown® process is a commercial variant of the traditional meltblowing process. Molten polymer, often polypropylene, is extruded from an array of outlets, each of which is individually surrounded by a concentric high velocity air stream. To provide the first thorough understanding of this unique process, we have experimentally investigated the effects of critical processing parameters on the fiber and web formation process. Air temperature, air speed, and polymer throughput have been related to fiber diameter distribution and distance to solidification. Median fiber diameters ranged from less than 1 μm to almost 14 μm . The accuracy of an empirical model relating processing conditions to fiber diameters shows that diameter attenuation for the entire process is largely determined by the first centimeter of fiber spinning. Air temperature effects on polymer jets were investigated using high-resolution infrared thermography and indicated that substantial heat transfer occurs between the air and molten polymer prior to spinning. A detailed three-dimensional air temperature and velocity profile, measured in the absence of spinning fibers, is presented for an array of supplied temperatures and air cavity pressures. Web analysis shows that smaller fibers in cooler air streams require shorter die-collector-distances to form bonded fabrics.

2.2 Introduction

A nonwoven fabric is a fibrous sheet or web structure that is held together not by intricate knitting or stitching operations but by much faster mechanical, thermal, or chemical means [1]. Nonwovens find use in a wide range of applications, from medical gowns, wipes, and diaper liners, to geotextiles, carpeting, and apparel interlinings. Industry worldwide sales were nearly \$36 billion in 2014. Many important nonwoven applications such as filtration, barrier fabric, and insulation require high surface and/or small pore sizes, both of which require small fiber diameters. Technologies have therefore been developed to produce ever smaller fibers. Electrospinning technology produces the industry's most narrow fiber diameters, often less than 100 nm, but requires solvents and is orders of magnitude slower than other techniques [2].

Meltblowing is a commercial nonwoven manufacturing technology for producing random oriented microfibrinous webs and fabrics. The technique is the industrially preferred method of rapidly producing very fine fibers. In the typical design, a thermoplastic polymer melt is pushed through the small capillaries of a die and then accelerated by two converging jet streams of heated air. Fibers simultaneously accelerate, cool, and stretch, becoming much narrower before reaching a collection belt. In most cases, a turbulent whipping action farther from the die face contributes to reduced fiber diameters [3]. Most fibers produced will have diameters between 2 and 10 μm , sufficiently fine for most filtration and barrier fabric applications [4]. Because meltblowing elongates polymer melts before crystallization, very little crystalline orientation develops. Pure meltblown nonwovens have low strength [5]. Even when small pore size and high surface area are required, many applications require more strength than meltblown fabrics alone can provide. One of the most popular uses of meltblown fibers are in so-called SMS fabrics where a meltblown fabric is sandwiched between two stronger spunbonded fabrics.

Meltblowing technology has advanced from proof-of-concept experiments in the 1950s to a highly productive and versatile commercial system. Exxon first commercialized the process in the 1970s using what has become the industry standard linear meltblowing die [6]. In this setup, molten polymer is pushed through a single row of capillary outlets and attenuated into fibers by converging air curtains. This design has been studied experimentally and theoretically, and has been modified to create supersonic air streams and multicomponent fibers [7]–[11]. Departures from the standard linear die have also been patented and commercialized, but not as thoroughly studied [12]–[14].

One such alternate meltblowing design that has been gaining commercial interest in recent years allows for multiple fiber spinning rows. This multi-row meltblowing die distributes molten polymer to an array of capillary outlets, each of which is surrounded by a concentric air stream. Such a design can allow for a higher single-pass throughput, see Figure 2.1.

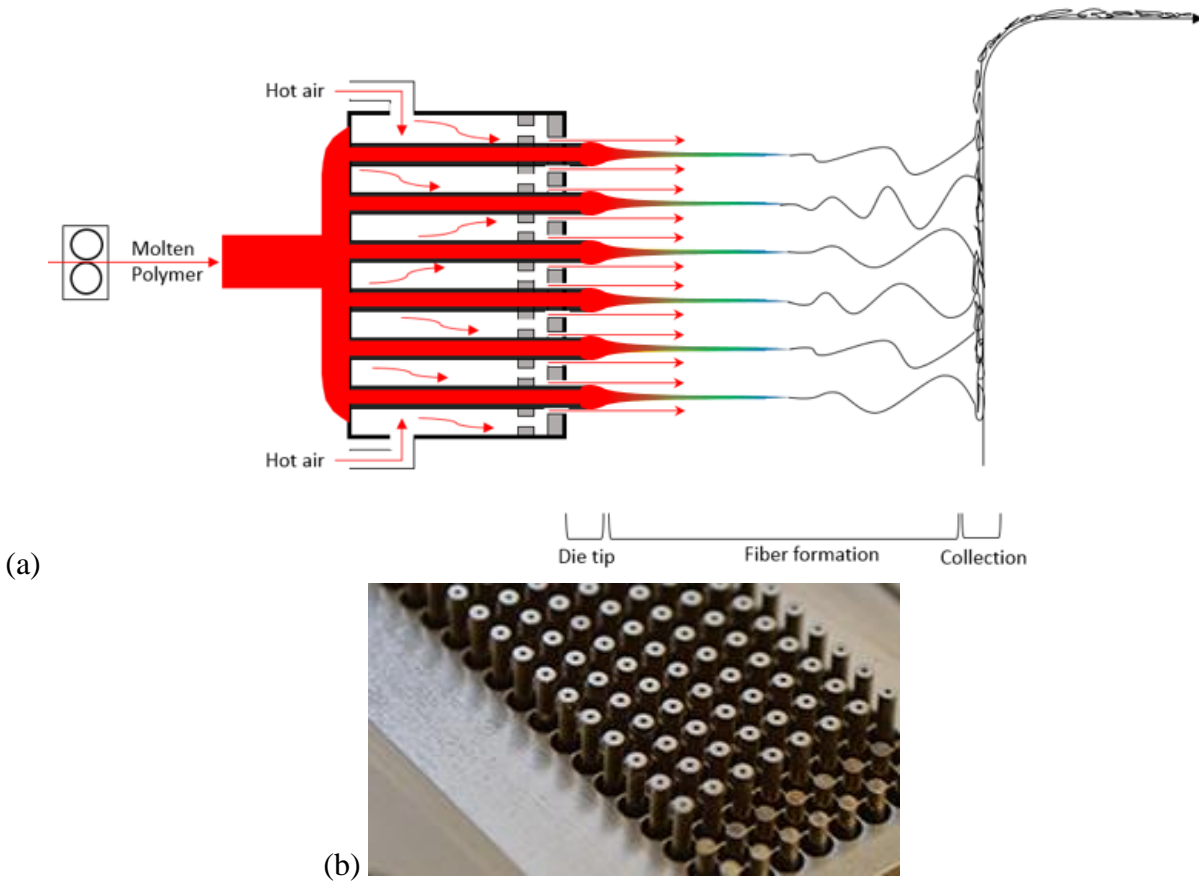


Figure 2.1 Multi-row meltblowing process. (a) Side schematic representation of the multi-row meltblowing design and fiber formation process. (b) Photo of an eight-polymer-row die face, with two air-only outlets at the die edge. (Photo courtesy of Biax Fiberfilm Corp)

Multi-row meltblowing differs from the traditional single-row meltblowing system most noticeably in the relative positioning of the fiber-forming spinnerets and the attenuating air stream. It is known that the aerodynamics near the spinnerets is of critical importance to meltblown fiber diameters and other fabric properties [6], [9], [15], [16]. Therefore, the conclusions from the detailed experimental and theoretical studies on the single-row geometry can hardly be applied to the multi-row variant. To the best of our knowledge, no systematic experimental or theoretical report exists for the annular spinneret design capable of multi-row meltblowing, and any published information is limited to its patents.

In this research, we have conducted an experimental study of the fiber formation process of the annular meltblowing spinneret configuration. For a single polymer and die geometry, we have investigated the effects of air temperature, air velocity, polymer throughput, and Die-Collector Distance (DCD) on fiber diameters, distance to solidification, and web defects such as shot. These results are put into context by measurements important to the mechanisms of fiber draw down, which have two critical aspects: air-to-polymer momentum transfer and polymer extensibility. Air-to-polymer momentum transfer, as well as fiber cooling rate, requires knowledge of the air speed and temperature in the fiber-forming region. These have been measured using a pitot tube and thermocouple in a manner similar to Begnir et al [17] and show the impact of air and die geometry choices on fiber environment. Because polymer extensibility is a strong function of the steady shear viscosity [18], the temperature-dependent viscosity and the polymer temperature during fiber formation are important parameters for the production of meltblown fibers and webs. The temperature-dependent zero shear viscosity was determined for this polymer for the thermally stable melt temperature range. High-resolution IR thermography has been previously established as a non-contact method for on-line fiber temperature measurement of meltblowing fibers [19]. We use this technique to validate calculations of the polymer temperature close to the spinnerets, the region in which most polymer acceleration occurs. An empirical relationship between processing conditions and median fiber diameters is presented. IR thermography and the air profiles are used to explain the effects of these processing conditions on the DCDs required to produce bonded fabrics.

2.3 Experimental

2.3.1 Material

All experiments used LyondellBasell MF 650W Isotactic Polypropylene, a commercial meltblowing grade homopolymer resin. The manufacturer states that polymerization was metallocene catalyzed, so the molecular weight distribution is expected to be low. The stated melt flow rate at 230 °C and a 2.16 kg mass was 500 g/10 min using ASTM D1238, and the density at 23 °C was 0.90 g/cm³ using ASTM D792.

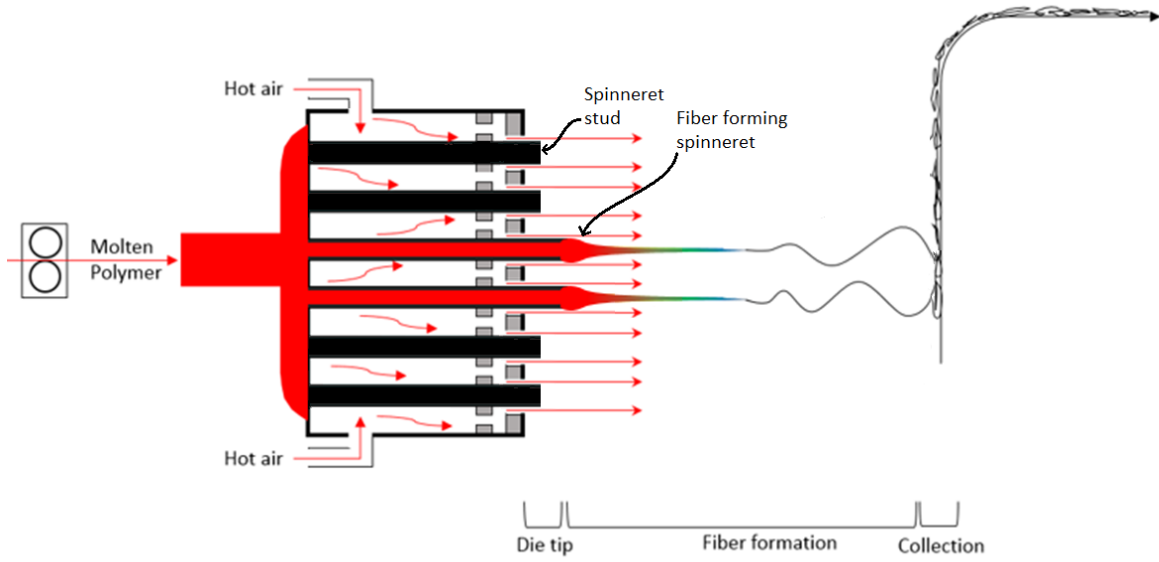
2.3.2 Material Characterization

Polymer thermal properties were measured in duplicate using a TA Instruments first-generation Discover Series Differential Scanning Calorimeter (DSC) and Thermogravimetric Analyzer (TGA). TGA and DSC heating experiments were conducted at 5 °K per minute, and DSC cooling was performed at 10 °K per minute. Steady shear and dynamic oscillatory flow behavior of the molten polymer was characterized using a 25 mm diameter parallel plate TA Instruments Discovery Hybrid Rheometer HR-3. Dynamic oscillatory rheology was measured from 0.1 rad/s to 600 rad/s and related to steady shear viscosity using the Cox-Mertz relationship [20]. Steady shear viscosity was measured at shear rates from about 800 s⁻¹ to about 7500 s⁻¹ using an Instron CAEST SR20 Capillary Rheometer. Capillary measurements were adjusted for end effects and wall slip using the Bagley and Rabinowitz corrections, respectively [21], [22]. Steady shear viscosity versus shear rate from 0.1 s⁻¹ to about 7500 s⁻¹ is presented for several temperatures in the range of 170 – 240 °C.

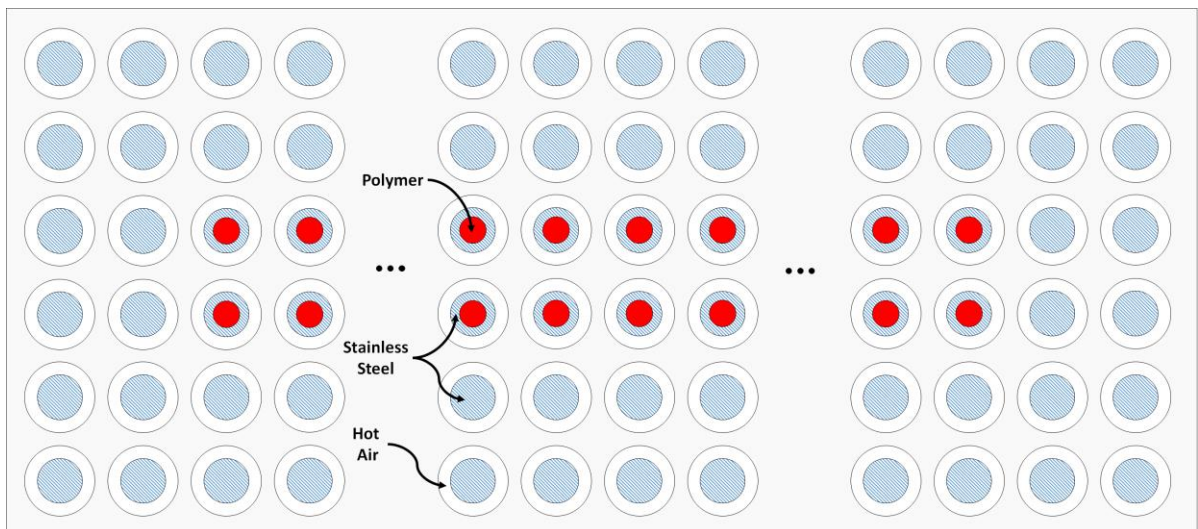
2.3.3 *Dual-Row Meltblowing*

A pilot-scale two-row meltblowing die was selected to study the unique annular spinneret design. The equipment and die used, termed the Spunblown® process, was manufactured by Biax-Fiberfilm Corporation [14], [23]. The die was 38 cm in width, contained two fiber spinning rows with a total of 368 spinnerets. The adjacent fiber-forming spinneret rows were surrounded on all sides by two air-only (non-fiber-forming) rows, which serve to insulate the spinning fibers from cool air entrainment. The total number of air annuli, both those surrounding the fiber-forming spinnerets and spinneret studs, was 1128. The inner diameter of the fiber-forming spinnerets was 508 μm . Schematic representations of the specific die and system are displayed in Figure 2.2.

Figure 2.2 (a) Schematic side view of the 2-row meltblowing process; (b) Schematic front view of the die face showing red polymer extrusion from the fiber forming spinnerets, blue hash steel spinneret wall and studs, and white hot air releasing annuli; (c) Relevant dimensions of the spinnerets (not shown: spinnerets extend 3.0 mm past the air annuli face, and spinneret studs extend 1.5 mm past the same face).

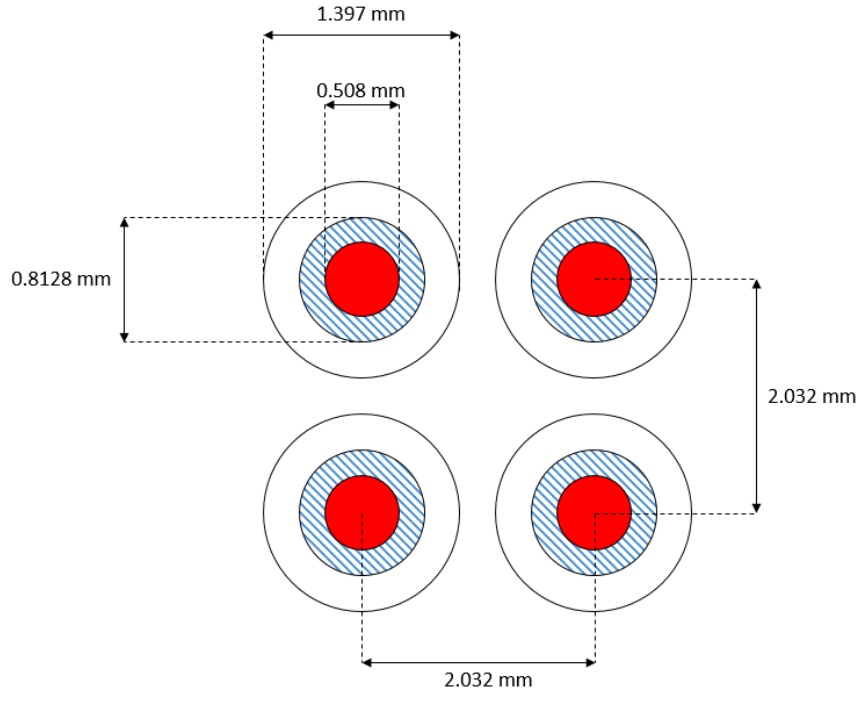


(a)



(b)

Figure continues to next page.



(c)

In the multi-row meltblowing die design, molten polymer is pushed through a series of distribution plates and into 2.5 cm long cylindrical spinnerets. The spinnerets traverse an air cavity (see Figure 2.2a) and emit the polymer several millimeters in front of the die face. Hot air flows into the air cavity and escapes through the annuli surrounding the spinnerets and spinneret studs. In these experiments, four process variables were investigated: air cavity temperature, air cavity pressure, polymer flow rate, and DCD. Their conditions spanned the range of typical safe use of the equipment and polymer and are shown in Table 2.1. DCD was not varied in the full factorial manner and was set to 40 cm for most conditions. Other important process parameters were held nearly constant: melt temperature was about 240 °C, die temperature was 220 °C, collector speed was 3.05 m/min, and collector suction was set to 40% of machine maximum.

Table 2.1 Process variables and their specific conditions

Process Variable	Conditions
Air Cavity Temperature (°C)	166, 182, 240
Air Cavity Pressure (kPa)	48.3, 68.9, 97.2
Polymer Throughput (gram/hole/minute)	0.050, 0.100, 0.170
Die-Collector Distance (cm)	15.0, 20.0, 25.0, 30.0, 35.0, 40.0

2.3.4 *Infrared Thermography of Spinning Fibers*

IR thermography was employed to quantify the relative temperature of the fibers during the spinning process. A FLIR T650sc Camera with 13.1mm lens was used in all experiments. To determine the IR emissivity of polypropylene fibers, a 1 mm diameter polypropylene monofilament fiber was heated uniformly, and the temperature was measured both by a K-type thermocouple and by IR imaging. The emissivity value that produced the best match between measured and IR calculated temperature was found to be approximately 0.83.

2.3.5 Air Temperature and Velocity Profiling

The air temperature and velocity profiles in front of the spinnerets were measured using a K-type thermocouple and FlowKinetics FKT 2DP1A-C device with a 7.94 mm diameter pitot tube attachment, respectively. Absolute velocity measurements require simultaneous air temperature measurement, which was accomplished by mounting the thermocouple about two centimeters away from the pitot tube in the positive x-direction (see Figure 2.3), so as not to disturb the air flow near the pitot tube. Both devices were mounted on a robotically controlled stage (Benchtop PRO 2424 from CNC Router Parts) to take measurements at locations of a repeatable accuracy of ± 0.02 mm for a 3D array of positions. The locations of the measured sites are shown in Figure 2.3, and measurements were performed for each of the nine air cavity temperature and pressure conditions shown in Table 2.1.

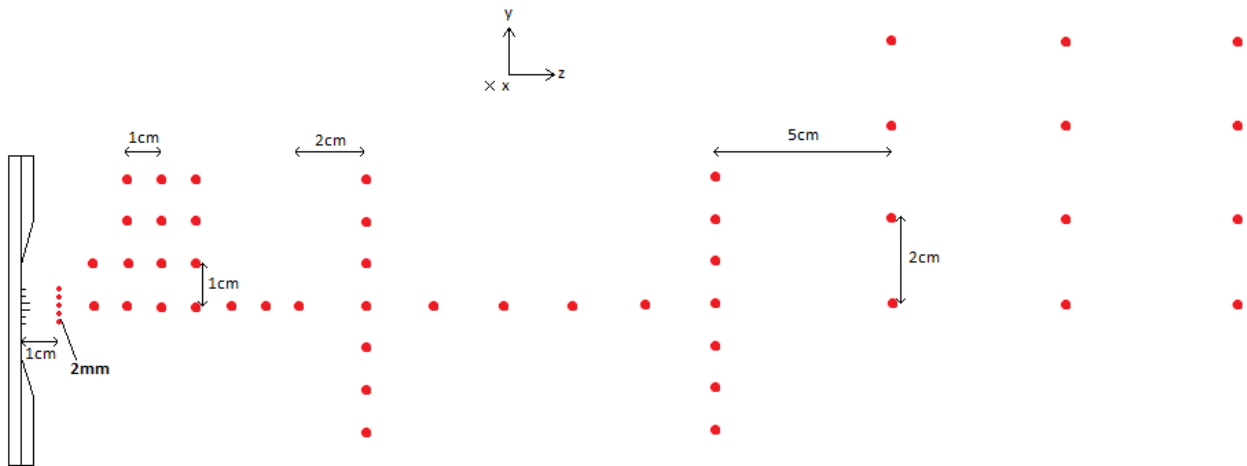


Figure 2.3 Side schematic view of the locations where air temperature and velocities were measured.

A FlowKinetics FKT Series pressure and temperature monitoring system was used to continually record data averaged over each half second. The probes were held at each position for

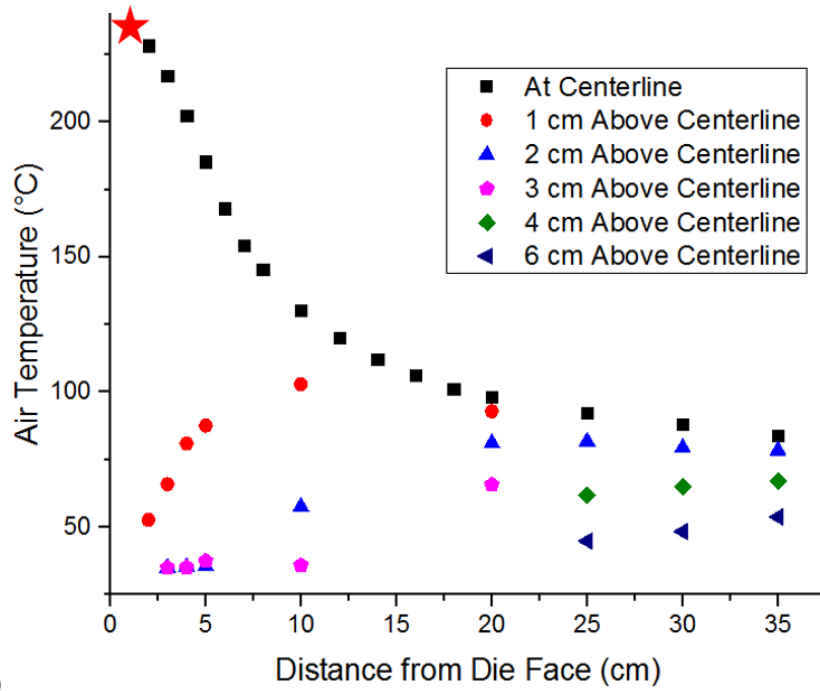
20 seconds, and the values reported here were averaged over the last 8 seconds of that hold time. This procedure allowed the probes to equilibrate to the new environment of each position.

2.4 Results and Discussion

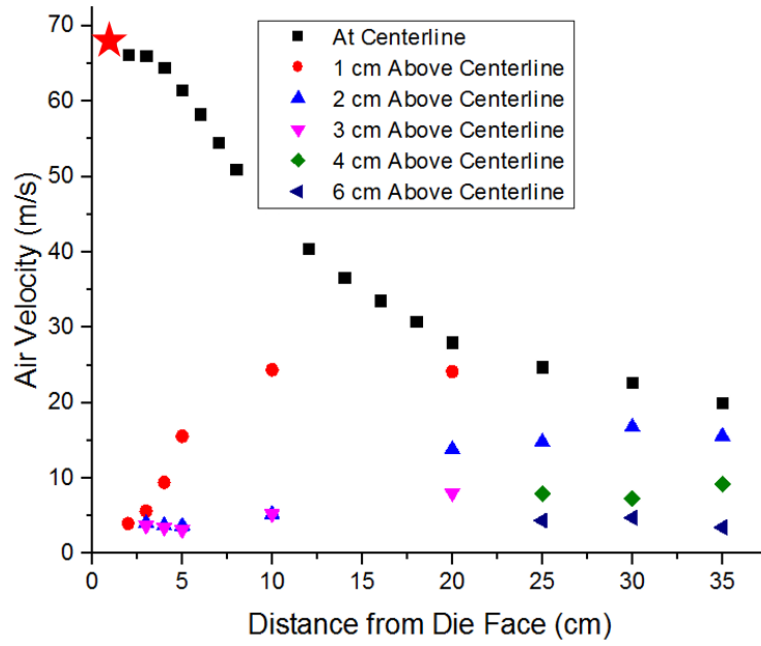
2.4.1 Air Temperature and Velocity Profiles in the Fiber-Forming Region

Air temperature and velocity were measured simultaneously at every point shown in Figure 2.3 and for every air cavity temperature and pressure combination shown in Table 2.1. Results from the highest temperature and pressure combination are shown in Figure 2.4.

Figure 2.4 Air temperature and velocity measurements for various positions in front of the die face for the single processing condition where air cavity temperature and pressure were 240 °C, and 97 kPa, respectively. Red star (★) location measurements are shown for other processing conditions in Table 2.2. (a) Air temperature profile. (b) Air velocity profile. (c) Air temperature and velocity within the air stream measured 1.0 cm in front of the spinnerets.

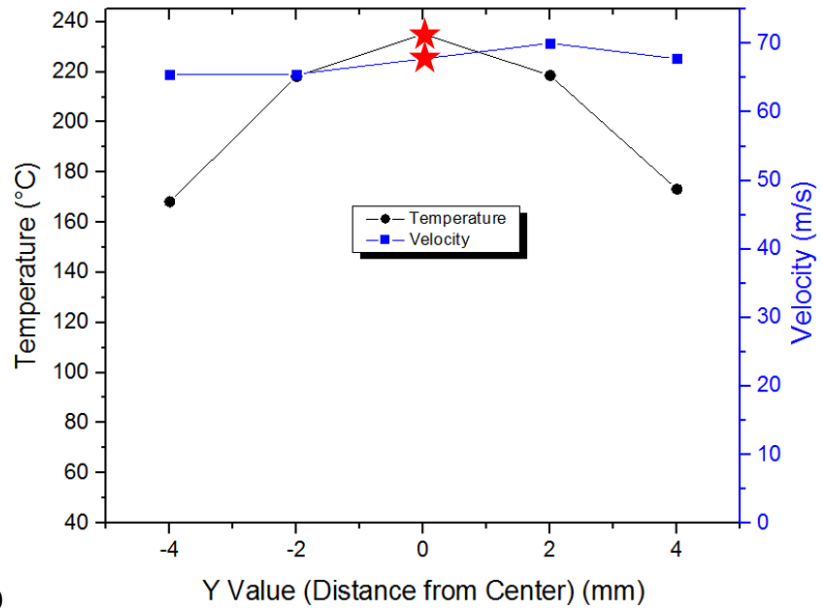


(a)



(b)

Figure continues to next page.



(c)

Figure 2.4(a) and Figure 2.4(b) show centerline and above centerline air conditions. The air profile was assumed to be symmetric about the centerline, which was verified at 10 and 20 cm from the die face. Figure 2.4 shows that the air heat dissipates more rapidly than does the air momentum; this is especially noticeable close to the spinneret as seen in Figure 2.4(c). In that figure, air heat dissipation is clear because the temperature profile is parabolic in shape, while the air speed profile is essentially flat. Heat and momentum dissipation trends are also seen for off-centerline air temperature values in Figure 2.4(a), which approach centerline values more rapidly than the off-centerline air speed values approach centerline values in Figure 2.4(b). Fiber-forming spinnerets are located at ± 1 mm along the Y-coordinate, close enough to the center that the air surrounding the fibers 1 cm past the spinnerets is still approximately 220 °C. Figure 2.4(c) shows the dramatic effect of the non-fiber-forming spinneret stud rows that emit only air (located at ± 3 and ± 5 mm) and serve to effectively insulate the fibers at the center from cooler room air. If the spinneret studs were converted to fiber-forming rows, those fibers would be exposed to cooler air much earlier in the fiber-forming process. The cooler air would cool the polymer jet, reducing its extensibility and presumably resulting in thick fibers formed at the perimeter of the die and fine fibers formed at the center. In essence, the particular die configuration studied here has been designed to minimize fiber diameter distribution caused by the cool air entrainment effect.

Figure 2.4 shows the full air profile for one processing condition, and while the general shape of the profile does not change between conditions, the temperature and velocity of the air stream across conditions nearest to the fiber-forming spinnerets (positions stated in Figure 2.4) are shown in Table 2.2. These values are of greatest importance because conditions affecting the fiber formation very close to the spinneret largely determine the fiber diameters produced by the process.

Table 2.2 Air cavity conditions as they affect the air temperature and velocity 1.0 cm in front of the fiber-forming spinnerets.

Air Cavity Pressure Effects		Air Cavity Temperature Effects	
Air Cavity Pressure (kPa)	Air Velocity at 1.0 cm (m/s)	Air Cavity Temperature (°C)	Air Temperature at 1.0 cm (°C)
48.3	46	166	168
68.9	56	182	183
97.2	68	240	235

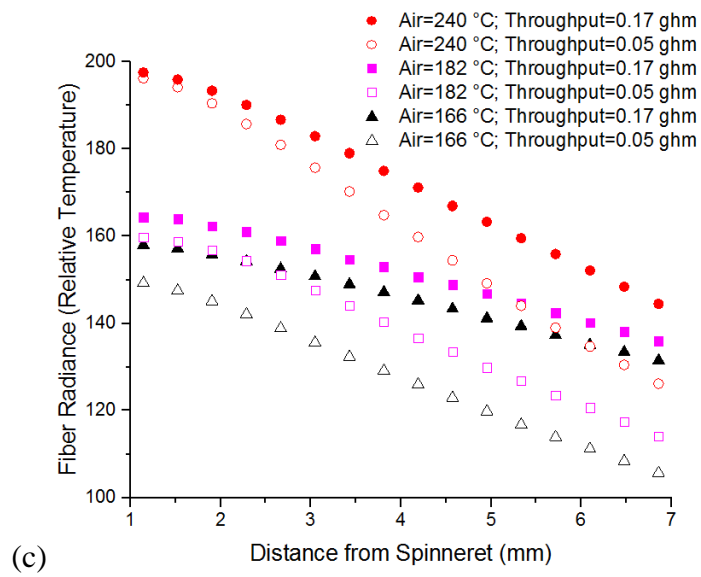
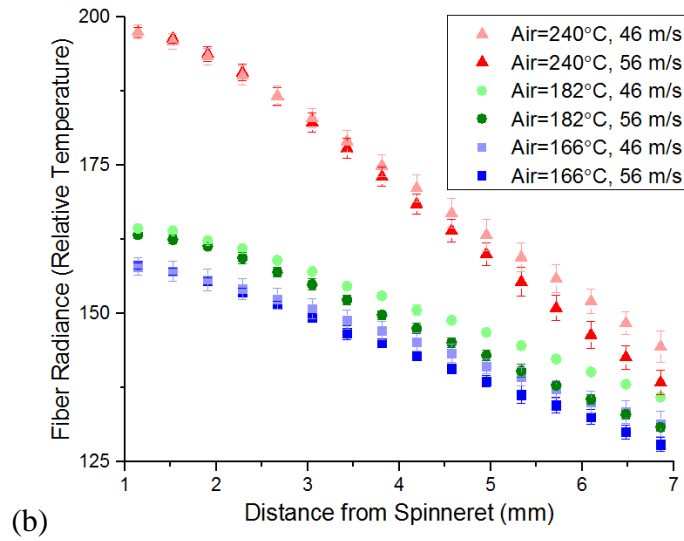
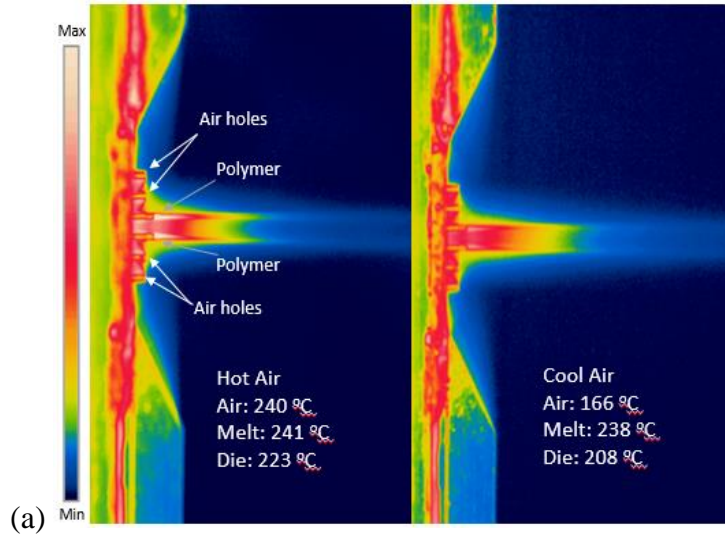
Changes in air cavity pressures and temperatures did not appreciably affect the air temperatures or velocities, respectively, just in front of the spinnerets. Air temperature just in front of the spinnerets deviates from air cavity values likely due to heat transfer with the die, which was attempted to be held constant at 220 °C. The air velocity values shown in Table 2.2 are used below to develop an empirical model for the effect of air speed on median fiber diameter.

2.4.2 *Temperature of Spinning Fibers*

Online fiber heat measurements of meltblowing fibers were taken using high-resolution infrared imaging. We do not use this method to determine absolute fiber temperatures and instead use it compare fiber radiances very close to the spinnerets for varying processing parameters. Accurate temperature measurement of meltblowing fibers over any considerable distance is a significant challenge that we circumvent by limiting our conclusions to those taken from relative total IR radiance. Suffice it to say that it is known that the infrared emissivity of fibers, which is necessary for the accurate determination of temperature from radiance, is a function of the fiber diameter [19], [24]. By just 1 cm from the spinnerets, the polymer jet can have a diameter less than 50 μm and vibrate in excess of 5000 Hz with an amplitude several times greater than the fiber diameter. Only very high-speed and high-resolution IR imaging taken simultaneously with fiber diameter measurements can provide a reliable absolute temperature measurement of meltblowing

fibers. By assuming that radiance is proportional to temperature, little understanding of the heat transfer properties of the system is lost. Moreover, fiber spinning temperature, the temperature of the polymer melt just as it emerges from the spinneret, can be accurately calculated and used to verify this assumption. Figure 2.5 shows IR images of the spinning fibers at two air temperatures and the radiance plots of the fibers for several air temperatures and speeds.

Figure 2.5 (a) Side view IR photographs of spinning fibers; air velocity was 56 m/s and polymer throughput 0.17 grams/hole/minute for both images shown. (b) Air temperature and speed effect on relative fiber temperature as a function of distance from the spinnerets (polymer throughput was 0.10 gram/hole/minute). (c) Air temperature and polymer throughput effect on relative fiber temperature as a function of distance from the spinnerets.



As can be seen from Figure 2.5, the fiber spinning temperature is a strong function of air temperature, even though the melt temperature entering the spinnerets was hardly changed between the conditions. Higher air speeds universally resulted in faster initial cooling rates of the fibers than did lower air speeds. Higher polymer throughputs made for slower initial cooling rates. Taking these observations together, we conclude that finer fibers cool more quickly than do larger fibers. Also, when air temperature was 182 °C or 166 °C, higher polymer throughput increased the maximum fiber temperatures observed. Melt temperature entering the spinnerets was held constant at 240 °C, so this dependence results from changes in residence time of the polymer inside the spinneret.

Absolute fiber spinning temperature is determined analytically rather than by measurement. This calculation is simplified by neglecting the radial temperature gradient and assuming a plug flow profile inside the capillaries. The result from performing the energy balances, the temperature of the polymer in Kelvin (T_{PP}) as a function of axial distance, x , is

$$T_{pp}(x) = T_w + (T_i - T_w)e^{-\beta x} \quad (1)$$

where $\beta = \frac{2h}{\rho C_p v_x R}$; and $h = Nu \frac{k}{2R}$. T_w is the air temperature inside the air cavity, T_i is the process “melt temperature”, the temperature of the polymer as it enters the capillary, Nu is the Nusselt number for plug flow in the thermal entrance region of a pipe with constant wall temperature [25], k is the thermal conductivity of polypropylene [26], C_p is the constant pressure heat capacity of polypropylene [26], v_x is the axial velocity of the polymer, R is the radius of the capillary, and ρ is the melt density of polypropylene. The capillaries are approximately 2.5 cm long, so $T_{PP}(x=2.5\text{cm})$ can be used to find the initial temperature of the spinning fibers.

This relationship can be used to make a useful plot showing the heat transfer as a function of the polymer throughput, in a plot similar to that shown in the process original patent [14].

Letting $\theta = \frac{T_{PP}-T_i}{T_w-T_i}$, which represents the fraction of temperature equilibration achieved in the spinnerets prior to spinning, and solving this quantity for different throughputs produces Figure 2.6.

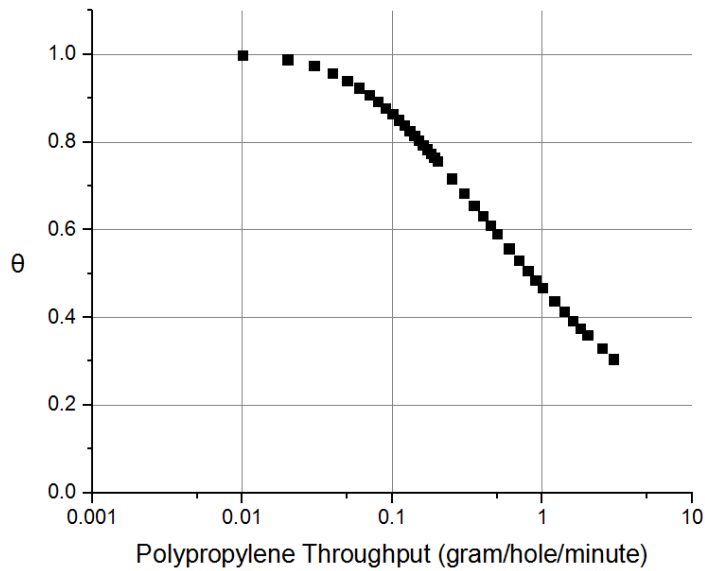


Figure 2.6 Temperature equilibration fraction as a function of polypropylene throughput for a spinneret length of 2.5 cm. $\theta = \frac{T_{PP}-T_i}{T_w-T_i}$, where T_{pp} is the fiber spinning temperature, T_i is the polymer melt temperature, and T_w is the air cavity temperature.

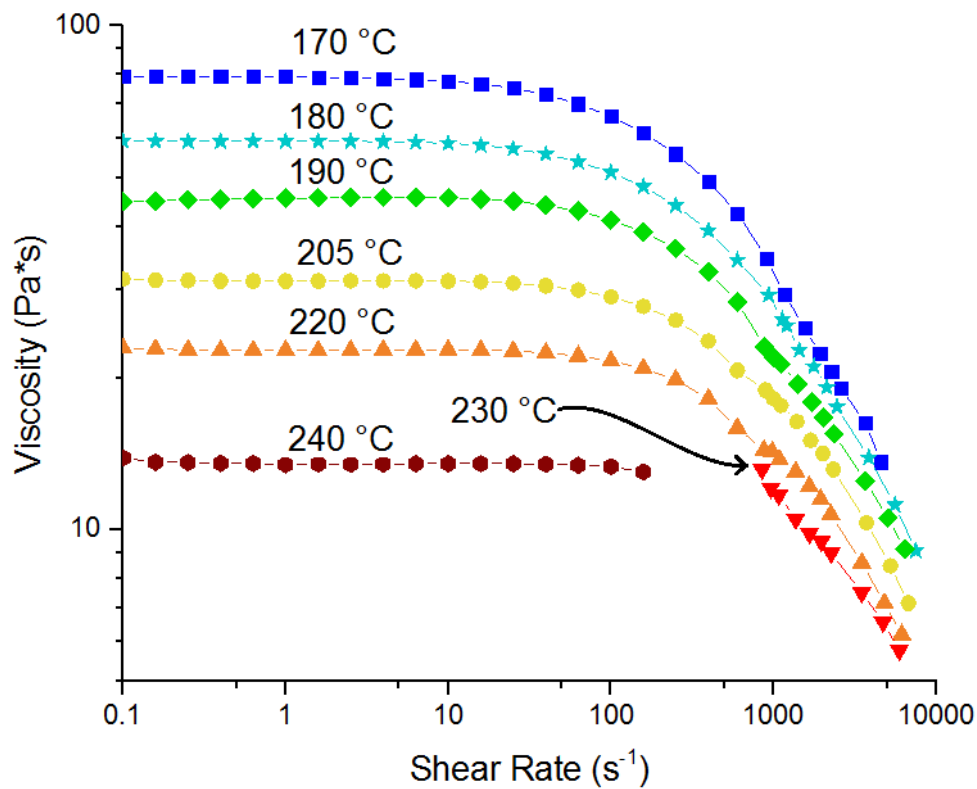
Figure 2.6 can be used to predict the fiber spinning temperature of polypropylene for the annular meltblowing spinneret configuration for any of the available capillary geometries (provided the length of the capillary is 2.5 cm, the capillary length for most commercially available dies). In accordance with Figure 2.6, the IR-determined relative fiber spinning temperature in **Figure 2.5(c)** shows that higher polymer throughput increases the fiber spinning temperature for conditions where the air temperature is lower than the polymer melt temperature. This difference in fiber spinning temperatures from throughput changes also increases for a greater air/melt

temperature difference, as is predicted. These calculations therefore validate the air temperature and polymer throughput effects on fiber spinning temperature seen experimentally in **Figure 2.5**.

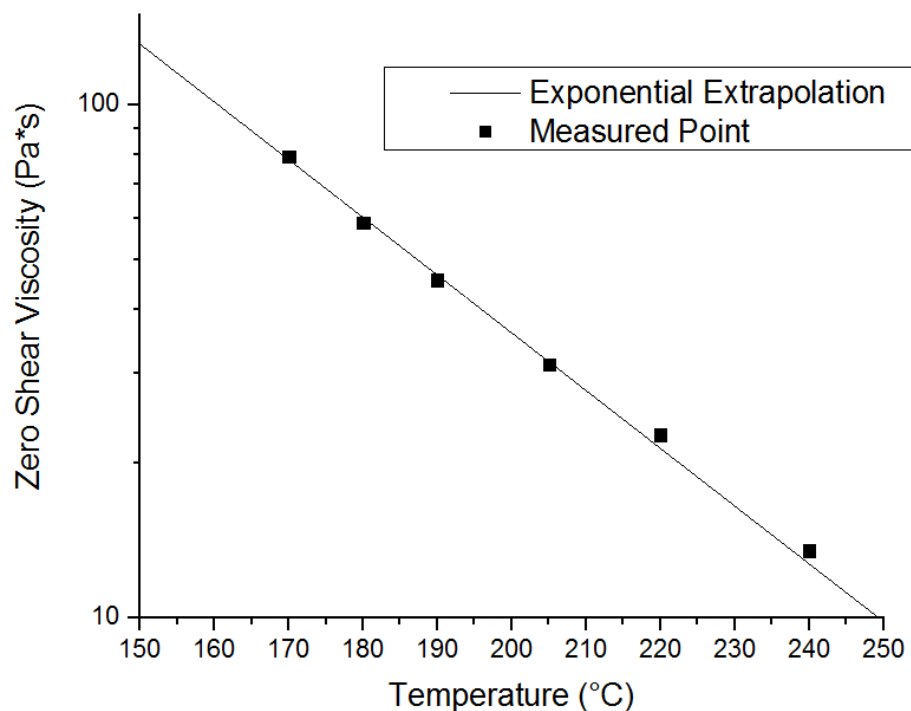
2.4.3 Polymer Thermal and Rheological Characterization

To provide a processing temperature range for this polypropylene resin (LyondellBasell MF 650W), DSC and TGA experiments were performed to give the lower and upper bounds, respectively. The thermal profiles show that this resin must be heated to at least 170 °C to ensure complete melting, but not above about 250 °C to prevent thermal degradation. DSC also shows that crystallization of the quiescent melt of this polymer does not begin until it is cooled to about 120 °C, indicating that fiber spinning is possible in the range of 120 to 250 °C.

The rheological properties of the polymer were also characterized to generalize the findings of the processability of this particular polymer and to relate steady shear viscosity to the attenuation rate of the fibers. Viscosity was measured as a function of shear rate for several temperatures in the range of 170 – 240 °C. The viscosity-temperature relationship in the low shear Newtonian plateau can be fit using the exponential form $A \exp(-BT)$, where A and B are constants chosen to best fit the data in that range.



(a)



(b)

Figure 2.7 Rheological characterization of LyondellBasell MF 650W Polypropylene. (a) Viscosity versus shear rates collected from parallel plate and capillary rheometers. (b) Viscosity versus temperature in the low shear limit with exponential extrapolation $A \exp(-BT)$, where $A = 7.60 \times 10^6 \text{ Pa}\cdot\text{s}$ and $B = 2.59 \times 10^{-2} \text{ }^\circ\text{K}^{-1}$.

Figure 2.7 shows that the viscosity of this polymer can be adjusted between 10 and 80 Pa·s within the temperature operating limits given from DSC and TGA. The temperature dependence of the zero-shear viscosity gives a useful indication of the relative extensibility of the polymer melt, and in the following section, with the knowledge of the fiber spinning temperature discussed above, it is used to model the dependence of the fiber diameter on the air temperature.

2.4.4 Two-Row Meltblowing Fiber Diameter Distributions

To provide an understanding of the general capabilities of this spinneret design for the production of fine fibers, webs were analyzed for each condition of a trial spanning the conditions shown in Table 2.1. A full factorial experiment was conducted for air temperature, air velocity, and polymer throughput variables, along with five conditions in which DCD was varied over an additional four levels. Fibrous samples were collected from each condition and fiber diameters measured manually from SEM images. Fiber diameter distributions where the DCD was 40 cm are presented as box plots as a function of processing condition in Figure 2.8. Each fiber diameter distribution shown is the result of about 200 individual fibers measured manually, chosen at random.

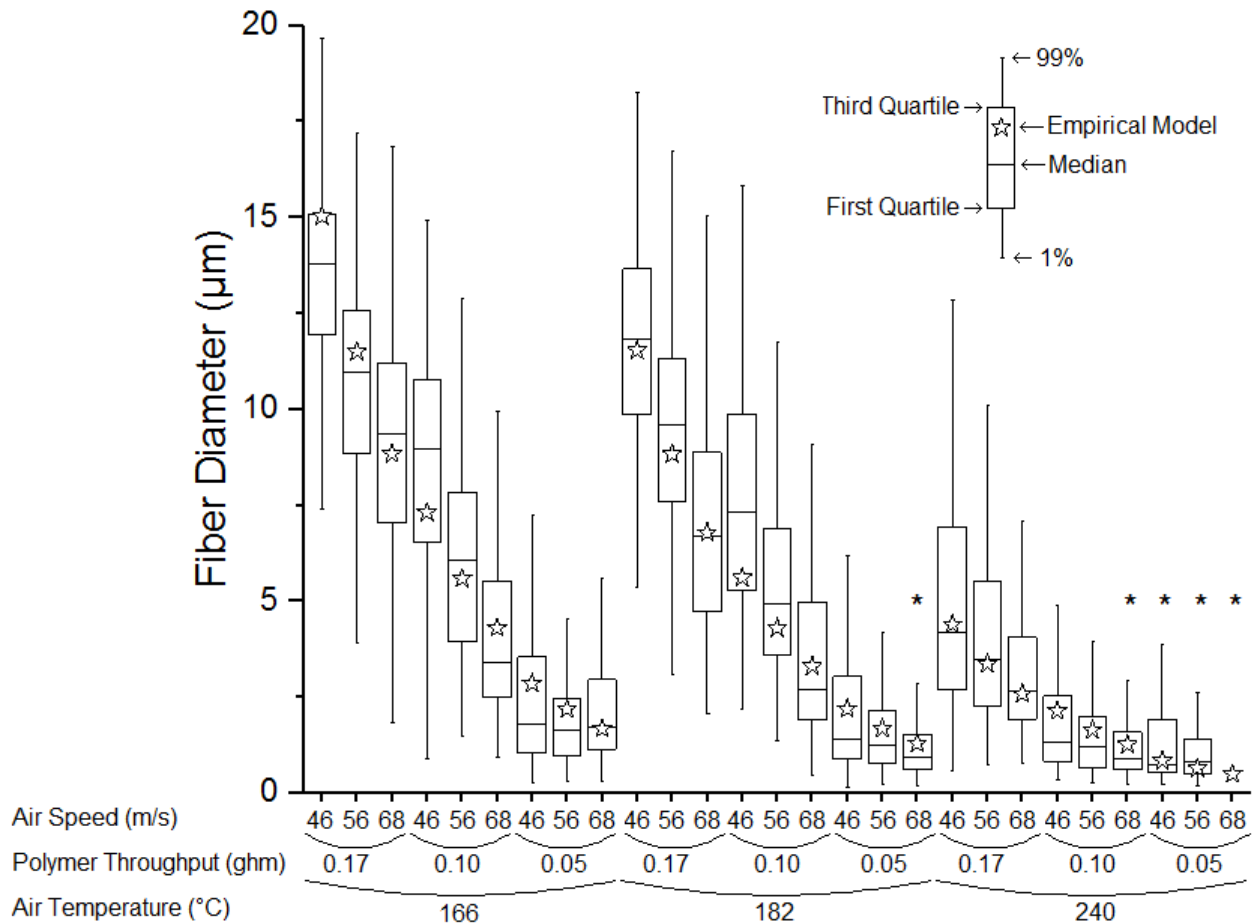


Figure 2.8 Fiber diameter distributions for each air speed, air temperature, and polymer throughput level listed in Table 2.1. DCD was 40 cm for all conditions. Samples marked with * toward the right of the figure indicate the presence of any amount of shot. Shot and fly for the rightmost condition prevented the sample from being collected and analyzed.

Median fiber diameters shown in Figure 2.8 ranged from 0.76 μm to 13.8 μm . Samples containing the smallest fiber diameters also contained shot defects. Shot refers to polymer droplets deposited in the web caused by fiber breakage near the spinneret. All conditions that produced median fiber diameters of less than 1.19 μm produced some quantity of shot, increasingly so for smaller fibers. Figure 2.8 shows that fiber diameter depends most significantly on polymer throughput and air temperature. Air speed is most effective in reducing the diameters of high and medium throughput samples. Following the dimensional analysis of Shambaugh [27], the fiber diameter was fit to an empirical model using two dimensionless quantities: the air to polymer mass

flow ratio and the air to (zero shear) polymer viscosity ratio. The mass flow ratio takes into account polymer throughput and air speed effects, while the viscosity ratio takes into account air temperature effects. Among numerous forms available, the form

$$d = C_1 + C_2 M^a \eta^b \quad (2)$$

showed the best fit to the data. M represents the air to polymer mass flow ratio, d the modeled fiber diameter in micrometers, and η the air to polymer dynamic viscosity ratio, with C_1 , C_2 , a , and b constants to be chosen. The air mass flow was calculated using the centerline air velocity one centimeter in front of the spinnerets (shown in Table 2.2) through the cross sectional area of the rectangle that encloses the air annuli that surround the fiber-forming spinnerets (373.25 x 3.42 mm). Thus the effect of the air-only rows is ignored in this empirical model. Air viscosity as a function of temperature was found via reference [28]. Polymer viscosities were found by first calculating the temperature of the polymer at the spinneret tip using equation (1), then finding the viscosity of the polymer at that temperature using the exponential extrapolation shown in Figure 2.7. The values $C_1 = 0.0100 \mu\text{m}$, $C_2 = 0.05247 \mu\text{m}$, $a = -1.48$, and $b = -0.768$ produced the modeled points shown in Figure 2.8; the R^2 value for this regression with respect to the median fiber diameters was 0.97.

In developing this empirical model, we seek less to predict fiber diameters than to establish a basis for understanding the fiber formation process. The fact that such an accurate prediction of median fiber diameter can be made from information pertaining to just the first centimeter of the polymer jet illustrates the importance of the initial axial acceleration in determining total diameter by all mechanisms. For example, while the two mechanisms of fiber draw down are entirely different, greater fiber diameter reduction from rapid bending motions downstream can occur for

conditions of greater axial acceleration of the polymer jet near the spinneret (see supplementary information for fiber bending instabilities).

This model also shows the relative importance of air temperature, speed, polymer throughput, and polymer viscosity in causing fiber diameter reduction for this spinneret design. The fact that the exponent a is nearly twice the magnitude of b shows that polymer throughput and air velocity has a greater effect on fiber diameter than does polymer viscosity. It is, however, the value of b that is of greater importance in practice. This is because achieving fine fibers through polymer viscosity modification by appropriate resin selection can be more economical than by increasing heated air volumes and/or reducing polymer throughput. Commercial meltblowing operations typically seek to produce fibers quickly, as measured in kilograms per meter of die per hour, and a reduction in total polymer throughput is moving in the wrong direction economically. Also, the primary cost associated with the meltblowing process is the energy required to heat the large volumes of air [16]. Therefore, it is costly to reduce fiber diameters by increasing air speed and temperature. This empirical model can be used as the basis for resin and condition selection as well as to analyze the tradeoffs involved for producing fibers of a desired diameter.

2.4.5 DCD Effects on Fiber Size and Bonding Distance

To examine the effect of DCD on fiber diameter and bonding distance, DCD was varied between 15 and 40 cm for five select conditions. Figure 2.9 shows mean fiber diameters for these DCD variations.

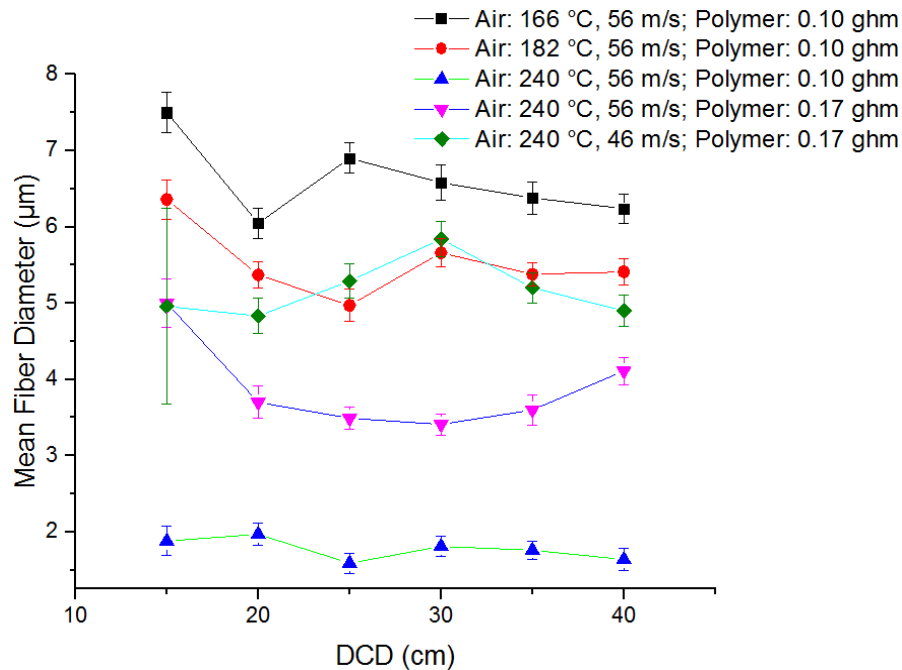


Figure 2.9 DCD effect on fiber diameter

The effect of DCD on fiber diameter was largely insignificant for 20 cm and beyond, and at 15 cm all samples showed substantial bonding between fibers. Fiber bonding refers to fibers contacting the collecting belt while still partially molten and sticking together. This indicates that reducing the DCD will not increase the fiber diameter without also causing significant fiber bonding. This also provides further understanding of the fiber formation process, in that fibers continue to attenuate, albeit modestly, even farther from the die up to the point that they crystalize.

One of the advantages of meltblowing processes in the manufacture of nonwoven fabrics is the ability to cause fiber bonding in the same step as fiber formation. This is achieved by adjusting the DCD appropriately to a desired bonding extent. In other words, fiber bonding occurs on a gradient from entirely bonded films at low DCDs to unbonded loose webs where no fibers are bonded. For the purposes of this investigation, the presence or absence of any fiber bonding was used to describe the effect of DCD on fiber bonding. The fiber bonding distance was determined

by noting the highest DCD, in 5 cm increments, in which fibers could be seen in the SEM images with some molten part bonding high angle crossing fibers together; see Figure 2.10.

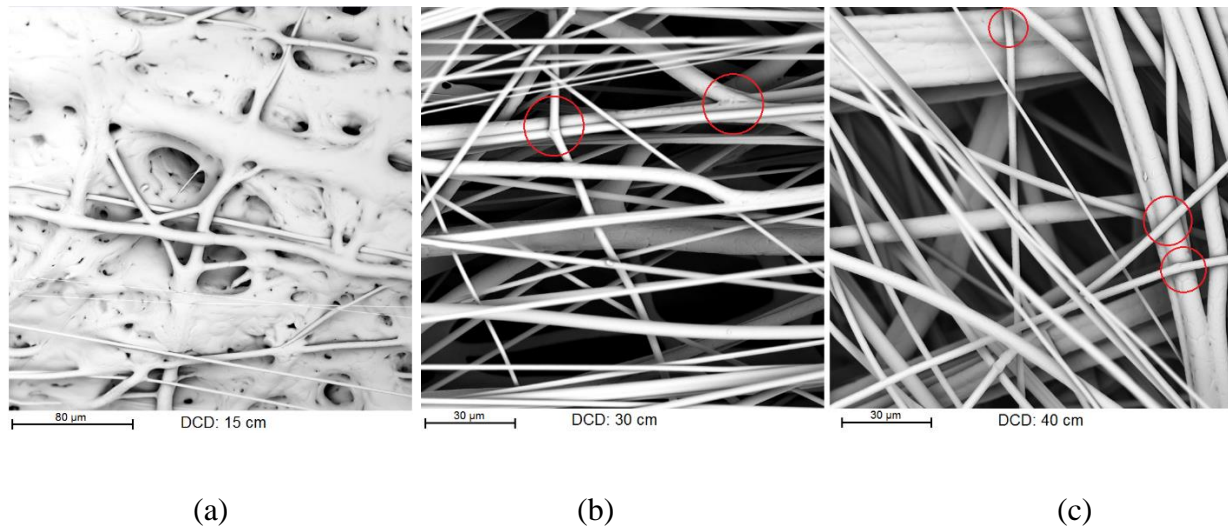


Figure 2.10 Determining bonding distance by SEM inspection. Processing conditions: throughput = 0.17 gram/hole/minute, air temperature = 240 °C, air speed = 56 m/s. (a) Heavily bonded. (b) Highest DCD exhibiting bonding: portions of fibers crossing at high angles are visibly bonded. (c) DCD greater than bonding distance: fibers crossing at high angles that clearly touch are not visibly bonded.

The fiber bonding distance for each of these conditions is shown in comparison to the air profile, as shown by the distance from the spinnerets at which the centerline air temperature reached 120 °C, the crystallization temperature of polypropylene. See Figure 2.11.

2.5 Conclusions

This experimental work serves as a basis for understanding the fiber and web formation process of the annular variant of the meltblowing process. Thermal exposure of the polymer melt to the attenuating air stream prior to fiber spinning is a unique aspect of the annular meltblowing design. The air-polymer heat transfer allows for rapid alteration of the melt temperature immediately before spinning. The impact of air temperature on fiber diameters is explained by the effect of temperature-dependent viscosity of the polymer melt. Experimental variations in air temperature, air speed, polymer throughput, and DCD spanned a wide range of conditions to test the limits and capabilities of the process. Webs were collected containing fibers with median diameters from submicron to more than 10 μm . Shot formation occurred when median fiber diameters were less than 1.2 μm . Investigation of the effects of processing conditions on fiber diameters show that fiber diameters can be accurately predicted by knowledge of the air profile and polymer properties associated with the first centimeter of fiber spinning.

While most experiments were conducted for high DCDs to examine the effects of processing conditions on loose-web fiber diameters, DCD variations show those effects on inter-fiber bonding, an important web characteristic. Lower polymer throughput, lower air temperature, and higher air speed reduce the collection distance required to produce bonded fabrics. DCD variations have significant impact on the extent to which fibers are bonded but a modest impact on individual diameters. Extension of the conclusions of this work to the various spinneret and die geometries possible may lead to improvements of the design and capabilities of the process but will require extensive experimentation. Computational modeling of the process, similar to what has been done for the traditional meltblowing die, is instead recommended.

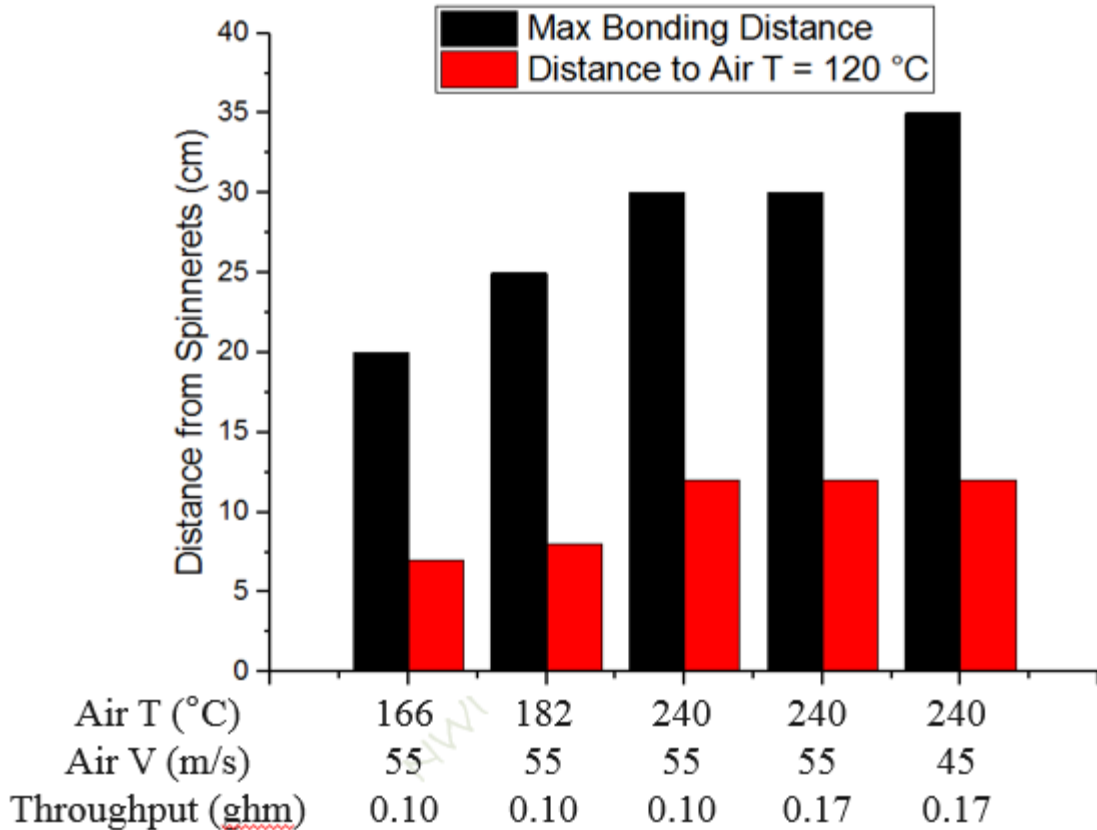


Figure 2.11 Fiber bonding distances compared to distance for the centerline air temperature to reach 120 °C.

Figure 2.11 demonstrates that higher air temperature increased bonding distance, but polymer throughput had no noticeable effect (i.e., any effect was less than the 5 cm increment). Higher air speed resulted in a shortened bonding distance, a less intuitive result that can be explained by the faster attenuation rate at higher air speed. Infrared thermography in **Figure 2.5(b)** showed that smaller fibers cool more quickly than larger fibers, which reduces the DCD required for those fibers to bond on the collection belt. Figure 2.11 also shows that while the air profile farther from the die (see centerline values shown in Figure 2.4(a)) correlates to the bonding distance, the fiber temperature exceeds the centerline air temperature. If the air and polymer temperature were equivalent, we would expect to see fiber bonding distance match the distance at which the centerline air temperature reaches the crystallization temperature of polypropylene.

Instead, fibers are still molten 15-25 cm past the point at which the centerline air temperature drops below 120 °C. These results highlight the importance of the air profile in the fiber-forming region: a 5 cm extension of the distance for the air temperature to reach 120 °C corresponds to a 10 cm extension to the bonding distance, even though the smaller fibers formed at higher air temperatures also cool more quickly. Because fiber diameters continue to reduce until the fibers have crystalized, an alteration in the bonding distance also affects the fiber diameters. These insights suggest that modifications to the air temperature profile farther from the die can have controllable effects on both the fibers and webs formed in this process.

2.6 References

- [1] INDA, “INDA | About Nonwovens <http://www.inda.org/about-nonwovens/>,” 2017. [Online]. Available: <http://www.inda.org/about-nonwovens/>.
- [2] D. H. Reneker and I. Chun, “Nanometre diameter fibres of polymer, produced by electrospinning,” *Nanotechnology*, vol. 7, pp. 216–223, 1996.
- [3] A. L. Yarin, S. Sinha-ray, and B. Pourdeyhimi, “Meltblowing : II-linear and nonlinear waves on viscoelastic polymer jets,” *J. Appl. Phys.*, vol. 108, 2010.
- [4] S. Batra and B. Pourdeyhimi, *Introduction to Nonwovens Technology*. 2012.
- [5] C. J. Ellison, A. Phatak, D. W. Giles, C. W. Macosko, and F. S. Bates, “Melt blown nanofibers : Fiber diameter distributions and onset of fiber breakup,” *Polymer (Guildf)*., vol. 48, pp. 3306–3316, 2007.
- [6] J. P. Keller and R. R. Buntin, “Melt-Blowing Die For Producing Nonwoven Mats,” 3825380, 1974.
- [7] A. L. Yarin, S. Sinha-ray, and B. Pourdeyhimi, “Meltblowing : Multiple polymer jets and fiber-size distribution and lay-down patterns,” *Polymer (Guildf)*., vol. 52, no. 13, pp. 2929–2938, 2011.
- [8] M. Uyttendaele and R. L. Shambaugh, “Melt Blowing : General Equation Development and Experimental Verification,” *AICHE J.*, vol. 36, no. 2, pp. 175–186, 1990.
- [9] D. H. Tan, C. Zhou, C. J. Ellison, S. Kumar, C. W. Macosko, and F. S. Bates, “Meltblown fibers: Influence of viscosity and elasticity on diameter distribution,” *J. Nonnewton. Fluid Mech.*, vol. 165, no. 15–16, pp. 892–900, 2010.
- [10] B. Haynes and M. C. Cook, “Die for Producing Meltblown Multicomponent Fibers and Meltblown Nonwoven Fabrics,” 7150616, 2006.
- [11] A. S. . Fabbricante, G. F. Ward, and T. J. Fabbrincante, “Micro-Denier Nonwoven Materials Made Using Modular Die Units,” 6,114,017, 2000.
- [12] V. T. Marla, R. L. Shambaugh, and D. V Papavassiliou, “Using Swirl Dies To Spin Solid and Hollow Fibers,” *Ind. Eng. Chem. Res.*, vol. 45, pp. 2331–2340, 2006.
- [13] C. Torobin, L., Finlow, “Method and Apparatus for Producing High Efficiency Fibrous Media Incorporating Discontinuous Sub-Micron Diameter Fibers, and Web Media Formed Thereby,” 6183670, 2001.
- [14] E. C. A. Schwarz, “Apparatus and Process of Melt-Blowing A Fiberforming Thermoplastic Polymer and Product Produced Thereby,” 4380570, 1983.
- [15] V. Wente, “Superfine Thermoplastic Fibers,” *Ind. Eng. Chem. Res.*, pp. 342–346, 1955.
- [16] B. Haynes, “An experimental and analytical investigation on the production of microfibers using a single hole melt blowing process,” 1991.

- [17] A. Begenir, S. Michielsen, and B. Pourdeyhimi, "Melt-Blowing Thermoplastic Polyurethane and Polyether-Block-Amide Elastomers : Effect of Processing Conditions and Crystallization on Web Properties," *Polym. Eng. Sci.*, vol. 49, pp. 1340–1349, 2009.
- [18] H. M. Laun, H. Schuch, H. M. Laun, and H. Schuch, "Transient Elongational Viscosities and Drawability of Polymer Melts * Republic of Germany," *J. Rheol. (N. Y. N. Y.)*, vol. 119, no. 1989, 1994.
- [19] V. T. Marla, R. L. Shambaugh, and D. V Papavassiliou, "Online Measurement of Fiber Diameter and Temperature in the Melt-Spinning and Melt-Blowing Processes," *Ind. Eng. Chem. Res.*, vol. 48, no. 18, pp. 8736–8744, 2009.
- [20] W. P. Cox and E. H. Merz, "Correlation of Dynamic and Steady Flow Viscosities," *J. Polym. Sci.*, vol. 28, no. 118, pp. 619–622, 1958.
- [21] E. B. Bagley, "End corrections in the capillary flow of polyethylene," *J. Appl. Phys.*, vol. 28, no. 5, pp. 624–627, 1957.
- [22] B. Rabinowitsch, "Zeitschrift für physikalische Chemie," *Zeitschrift für Phys. Chemie*, vol. 145, no. 1, pp. 1–26, 1929.
- [23] E. Schwarz, "Apparatus and Process for Uniformly Melt-Blowing A Fiberforming Thermoplastic Polymer in a Spinnerette Assembly of Multiple Rows of Spinning Orifices," 5476616, 1995.
- [24] V. T. Marla, R. L. Shambaugh, and D. V Papavassiliou, "Use of an Infrared Camera for Accurate Determination of the Temperature of Polymer Filaments," *Ind. Eng. Chem. Res.*, vol. 46, pp. 336–344, 2007.
- [25] W. J. Beek and R. Eggink, *De Ingenieur*. 1962.
- [26] J. E. Mark, Ed., *Physical Properties of Polymers Handbook*, 2nd ed. Springer New York, 2006.
- [27] R. L. Shambaugh, "A Macroscopic View of the Melt-Blowing Process for Producing Microfibers," *Ind. Eng. Chem. Res.*, vol. 27, pp. 2363–2372, 1988.
- [28] Y. S. Touloukian, S. C. Saxena, and P. Hestermans, *Viscosity: Thermophysical Properties of Matter*, 1st ed. IFI/Plenum, New York, 1975.

2.7 Supplementary Information

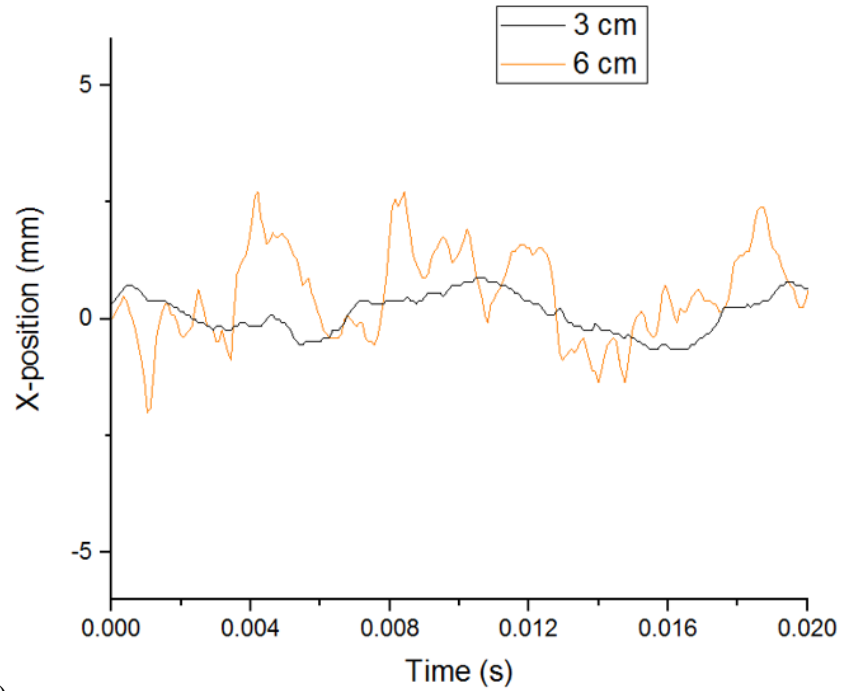
2.7.1 *Tracking of Lateral Fiber Motions*

To understand the extent to which fiber bending or flapping motions can contribute to fiber diameter reduction, researchers have utilized high-speed videography to directly monitor these motions with time [29], [30]. Each of these studies monitored fibers formed using a single-orifice homemade slot-die device, with polymer flow rates of 1 gram per minute or higher. For this study, a Phantom v1612 Ultrahigh-Speed Camera was used visualize and track the rapid motions of the spinning fibers studied here. The camera was equipped with a Canon 180 mm Macro lens whose face was positioned 18 cm from the fibers at the center of the die, giving a minimum spatial resolution of about 80 μm . Two plasma light sources (Hive Lighting, Killer Maxi Par Kit) capable of delivering 500,000 lux of continuous light was used to illuminate fibers directly, and as a backlight source. Video recordings were made for 1-2 second intervals for each of the 27 conditions varying air cavity temperature and pressure, and polymer throughput. Each condition was recorded at two video resolution and frame speed combinations: 128x800 (1 cm x 6.4 cm) at 58,252 frames/second, and 128x128 (1 cm x 1 cm) at 310,000 frames/second.

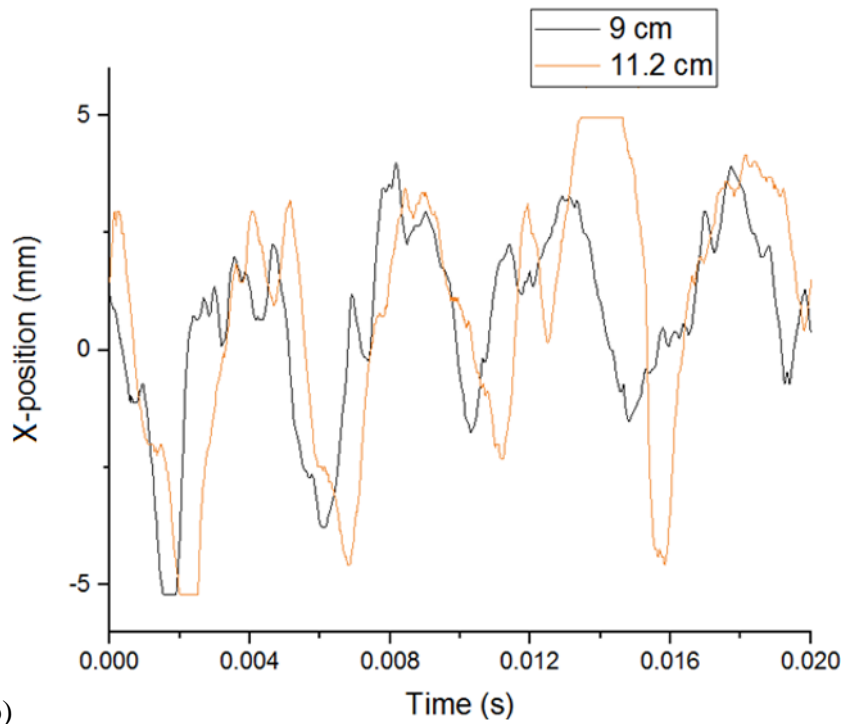
Despite using state-of-the-art high-speed imaging equipment, monitoring fiber lateral motion from a multi-spinneret device at low polymer flow rates is still a challenge. The principal difficulty is the inability to use automated object tracking software, which fails due to insufficient resolution for the object size and the presence of multiple fibers in an image. Much higher polymer throughputs from a single-orifice die allowed the use of such software in the previous works [29]. While extremely time-consuming, these motions can be tracked manually for higher throughput conditions, frame-by-frame, to plot the lateral motion of a single fiber with time. Care must be

taken to ensure the same fiber is being tracked at all times, especially after two or more fibers overlap in the image.

Lateral fiber motions were manually tracked for one condition that produced the largest fibers made in this study: air temperature of 166 °C, air speed of 46 m/s, and polymer throughput of 0.17 gram/hole/minute. A single fiber's x-position was monitored at several z-distances: 3, 6, 9 and 11.2 cm from the spinnerets, for 20 milliseconds. This range was not simultaneously visible due to the 6.4 cm field of view, so the same fiber was tracked at distances of 3 and 6 cm, but a different one tracked for 9 and 11.2 cm. The x-motion of the fiber versus time is plotted in Figure 2.12.



(a)



(b)

Figure 2.12 Fiber lateral motion for air temperature of 166 °C, air speed of 46 m/s, and polymer throughput of 0.17 gram/hole/minute. (a) A fiber tracked over 20 ms at 3 and 6 cm from the spinneret outlet. (b) A fiber tracked over 20 ms at 9 and 11.2 cm from the spinneret outlet.

While the movements are not sinusoidal, if the amplitude is described as the difference between opposite maximal excursions from the mean, then the amplitude of fiber lateral movements increases as the fiber moves away from the spinnerets. Figure 2.12(b) shows the fiber leaving the field of view at 0.002 and 0.014 s. The increase of amplitude from these images is shown in Figure 2.13.

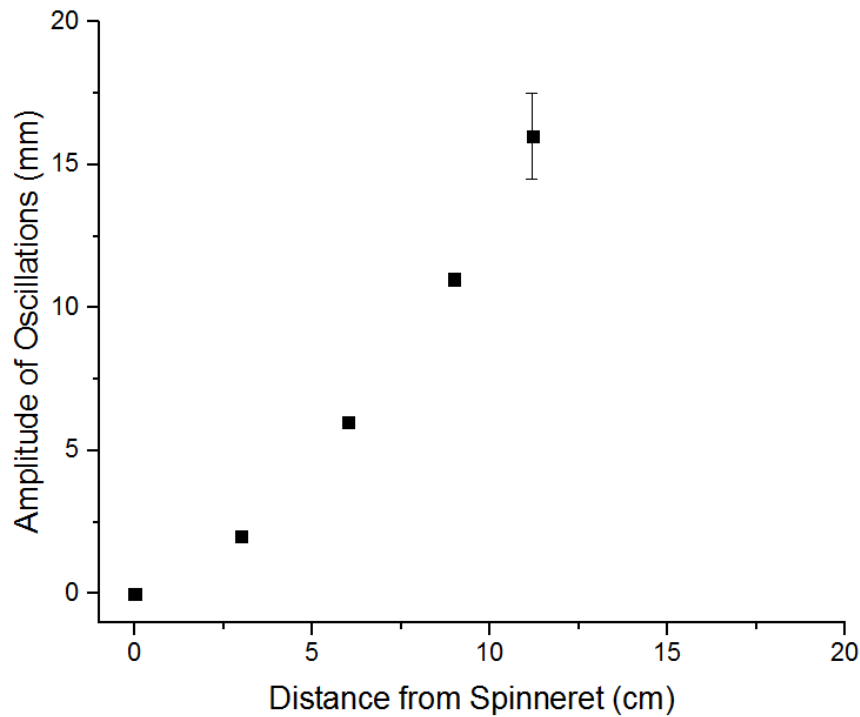


Figure 2.13 Amplitude of fiber lateral motion oscillations for various distances from the spinneret outlet.

At 9 cm and 11.2 cm from the spinneret, the fiber began to exit the field of view, leading to some uncertainty in the amplitude of oscillation, especially at 11.2 cm. The frequency of fiber motion is more complex than amplitude: there are several layers of smaller whipping motions within larger fiber movements. These small amplitude motions are of very high frequency, in excess of 10,000 Hz, and are much higher than such frequencies previously reported [29], [30]. To make accurate observations of high-speed phenomena, the measurement timescale must be more

than twice the speed of the motions to be measured [31]. This means that to monitor the fast motions of meltblown fiber vibrations with time requires ultra-high-speed videography. Camera speeds prior to this work were not sufficiently fast enough to observe these motions if they occurred at all, given the different polymer flow rates and aerodynamic configurations studied.

While Figure 2.12 must be created using direct manual fiber tracking, it is not necessary to track intermediate positions to create a plot like Figure 2.13. Provided the fibers are large enough to discern at all, amplitudes can be more quickly determined from individual fiber observation and the recording of extreme points only. This has not been done systematically for the other conditions, but qualitatively, amplitudes of fiber motions for conditions spinning smaller fibers than the condition shown in Figure 2.12 and Figure 2.13 appear to be larger at shorter distances from the spinneret.

2.7.2 Online Measurement of Fiber Bending Instabilities Using Back-Folding Distance

Clearly, the continuous tracking of individual fibers using high-speed videography is not feasible for a multi-spinneret design where fibers are commonly less than 5 μm in diameter. Although even the manual tracking of fiber motion is impossible when fibers become very fine, their movement over short times can be detected for almost all spinning conditions. This can allow for measurement of spinning aspects such as bulk fiber speed, discussed below, and distance to the first occurrences of back-folding. Back-folding distance, shown in Figure 2.14, refers to the shortest distance at which a fiber folds back on itself, causing the local fiber axis to be perpendicular to the die face [32]. Back-folding distance in conjunction with knowledge of the air profile can be used as an indicator of the extent to which bending motions can contribute to fiber size reduction.

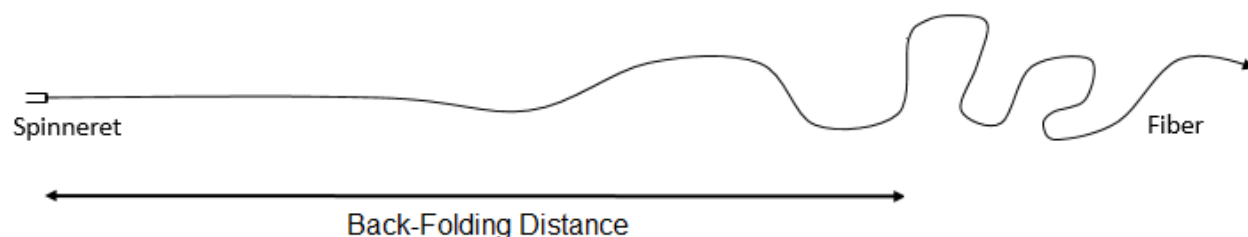


Figure 2.14 Schematic representation of back-folding distance.

Back-folding distances for each processing condition where DCD was 40 cm were measured and are shown in Table 2.3.

Table 2.3 Back-folding distance (in centimeters) of fibers undergoing bending instability during fiber formation. Distances for when the centerline air temperature drops to 120 °C, the crystallization temperature of PP, are shown for reference. * Indicates that fibers were so small that they were barely visible; determining back-folding events was very difficult for these conditions.

Air Temperature (°C)	Polymer Throughput (ghm)	Air Speed (m/s)		
		46	56	68
165 (Air T = 120 °C at 7 cm)	0.17	>11.2	11.2	10.7
	0.10	11	8.5	8.4
	0.05	8.2	7	6.8
182 (Air T = 120 °C at 8 cm)	0.17	10.7	9.9	9.2
	0.10	10.2	8.8	6.1
	0.05	5.3*	5.1*	4.3*
240 (Air T = 120 °C at 12 cm)	0.17	6	5.5	4.8
	0.10	4.4	4.2	4.1
	0.05	2.9*	2.9*	2.9*

Back-folding distance gives indication of both the acceleration rate of the polymer jet and the distance over which bending motions can contribute to fiber stretching. As shown in Table 2.4, fiber velocities matched the centerline air velocities measured at the respective location in front of the die face. Therefore, a back-folding region of a fiber has essentially reached the bulk average speed of the air stream at that location, and the distances shown in Table 2.3 correlate to the distance required to accelerate the polymer stream to the local air speed. Higher air temperatures,

higher air speeds, and lower polymer throughputs result in more rapid fiber acceleration. In contrast to fibers that undergo back-folding at higher distances, fibers that back-fold earlier have accelerated more quickly and to a higher velocity and will undergo complex bending motions in a warmer environment and for a longer time before reaching the collection belt. Fine and warmer fibers have a lower bending rigidity than cooler and thicker fibers [3], allowing them to more completely follow the turbulent eddies of the air stream, further reducing their diameter. In this way, an additional fiber diameter reduction mechanism can play an increasing role in fiber diameter reduction when the initial axial acceleration is higher. This gives further indication that the conditions affecting the fiber formation very close to the spinneret largely determine the final fiber diameters resulting from all attenuating mechanisms.

2.7.3 Bulk Fiber Speed

Bulk fiber speed refers to the steady movement of waves on the fibers in the direction of the air stream. Measurements were taken at video speeds of 310,000 frames/second with a resolution of 128x128 pixels (1 cm x 1cm). Fiber speeds were calculated by noting the number of frames that passed for a fiber feature to traverse the 128 pixels of the field of view, the center of which was at about 8 cm from the spinnerets. At least ten fiber features were observed and their speeds calculated for each condition, with 95% confidence intervals displayed from the standard error of the mean measurement. These speeds are shown in Table 2.4.

Table 2.4 Bulk fiber speed at 8 cm from the spinnerets compared to air speed at the same location, for all conditions

Number	Air Temp (°C)	Air Speed (m/s)	Throughput (ghm)	Bulk Fiber Speed at 8 cm from die (m/s)	Air Speed at 8 cm from die (m/s)
1	166	56	0.1	42.8 ± 2.4	40.9
2	166	68	0.1	47.1 ± 2.9	49.2
3	166	46	0.1	32.1 ± 1.4	34.1
4	166	56	0.05	36.0 ± 2.4	40.9
5	166	68	0.05	49.6 ± 2.0	49.2
6	166	46	0.05	30.3 ± 1.3	34.1
7	166	56	0.17	40.7 ± 1.0	40.9
8	166	68	0.17	49.3 ± 2.3	49.2
9	166	46	0.17	35.6 ± 1.0	34.1
10	182	56	0.1	40.7 ± 1.4	41.8
11	182	68	0.1	45.7 ± 1.0	48.7
12	182	46	0.1	32.2 ± 1.0	33.8
13	182	56	0.05	38.4 ± 1.6	41.8
14	182	68	0.05	46.6 ± 1.9	48.7
15	182	46	0.05	27.5 ± 0.6	33.8
16	182	56	0.17	40.3 ± 0.8	41.8
17	182	68	0.17	46.1 ± 1.4	48.7
18	182	46	0.17	32.4 ± 0.9	33.8
19	240	56	0.1	42.7 ± 1.2	42.3
20	240	68	0.1	53.8 ± 1.8	51.0
21	240	46	0.1	30.7 ± 1.1	35.9
22	240	56	0.05	41.3 ± 2.5	42.3
23	240	68	0.05	51.9 ± 1.9	51.0
24	240	46	0.05	36.3 ± 1.8	35.9
25	240	56	0.17	43.7 ± 0.9	42.3
26	240	68	0.17	50.6 ± 1.7	51.0
27	240	46	0.17	31.7 ± 1.5	35.9

Table 2.4 verifies the assumptions that bulk fiber speed nearly matches air speed and that fiber speed with the air stream does not exceed the air speed. Thus, mass-balance calculations that find fiber speeds exceeding the air speed anywhere in the process must result from stretching of the fibers by complex bending and folding patterns.

3 Chapter 3 - Meltblown Polymer Jet Pulsation: Observations and Effects on Fiber Diameter Distribution in an Annular Meltblowing Spinneret Design

Stephen Barilovits, Eunkyong Shim, Saad A. Khan, Behnam Pourdeyhimi

Department of Chemical and Biomolecular Engineering and the Nonwovens Institute, North Carolina State University, Raleigh, NC (USA).

This chapter is under revision for publication.

3.1 Abstract

We have investigated the fibers formed by the meltblowing spinneret configuration which has each cylindrical spinneret individually surrounded by annular air stream. Fiber diameter distributions are observed to be more varied and more disperse than traditional meltblowing. Distributions are normally distributed for large fiber samples, lognormally distributed for small fibers, and lognormally distributed with a positive skew for the smallest fibers. The presence of a few large fibers in otherwise fine fibrous samples skews the distributions and increases their relative dispersity. Using ultra-high speed videography and high resolution photography we observe the distribution to originate from a pulsation of the polymer jet near the spinneret tip. The pulsation behavior is described in detail and its origins attributed, not to an example of draw resonance, but to the aerodynamic configuration of an annular meltblowing spinneret. The pulsation is seen to reduce the median fiber diameter, but also to increase the dispersity and risk causing “shot” defects to arise.

3.2 Introduction

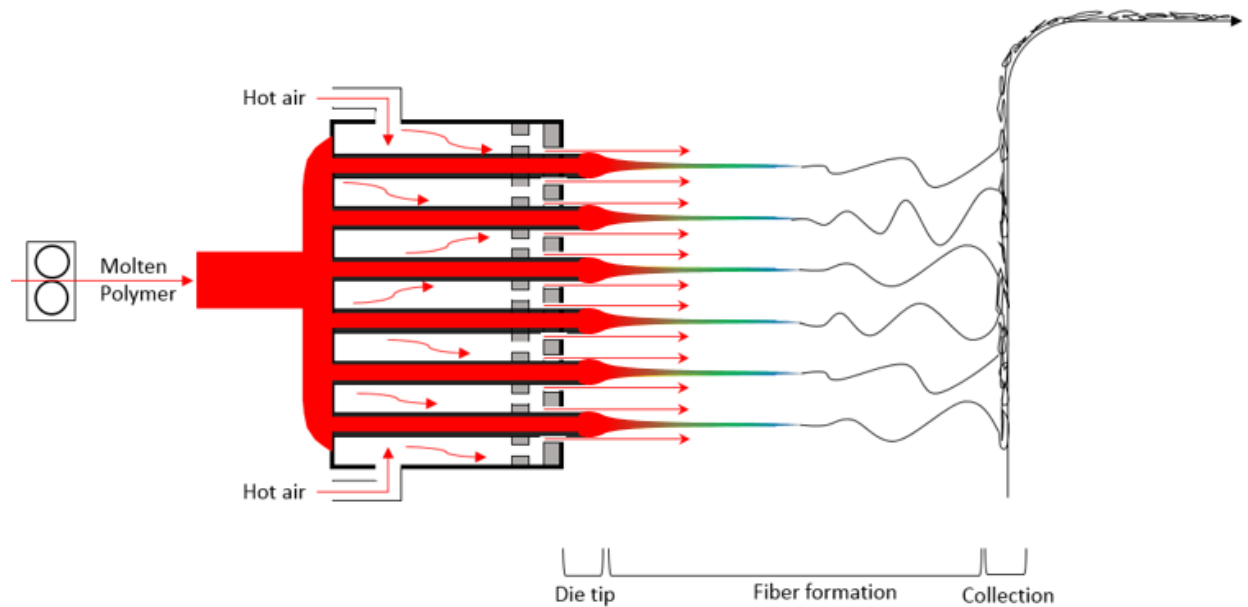
Nonwovens refer to sheet or lofty products composed primarily of fibers held together not by intricate weaving or knitting methods, but by faster mechanical, chemical, or thermal means.[1] Nonwovens can be found in a wide range of applications for uses in home, industrial, electronic, and medical areas. Example uses are quite commonplace such as cushioning, wipes, liners for thermal and acoustic insulation, filtration, and geotextiles, but the fabrics are often highly engineered with diverse components and technologies required. The nonwovens industry worldwide sales were \$36 billion in 2014. [2]

Nonwovens performance in many applications depend on the fabric pore size and surface area, both of which are directly affected by the fiber diameter. Smaller pores and higher surface area provide more efficient filtration and better barrier properties and a greater ability to functionalize the fabrics. Technologies such as electrospinning, melt blowing, and solution blowing have been developed to produce fibers with minimal diameters, often below 1 μm . [3]–[5] Meltblowing is the preferred method of producing fine polymeric fibers industrially because it is high throughput, does not use solvents, and can be used for a wide range of thermoplastic resins. Fibers produced by meltblowing commonly have diameters between 2 and 10 μm . [6] Meltblown fibers are produced by extruding a thermoplastic resin from the fine capillaries of a die into a heated, high velocity air stream which attenuates the fibers and carries them to a collection belt. The traditional “slot die” design, patented and commercialized by Exxon the in the 1970s, extrudes the polymer through a row of capillaries to the edge of a v-shaped die while two converging air curtains extend the polymer jet into fine fibers.[6] The design has been the subject of much experimental and theoretical work, giving a solid understanding of the ability of the process to

draw a polymer jet down to a fine fiber. [7]–[11] Other die geometries have been patented and commercialized, but not nearly as well studied. [12]–[15]

One such alternate meltblowing design that has been gaining commercial interest in recent years allows for multiple fiber spinning rows. This multi-row meltblowing die distributes molten polymer to an array of capillary outlets, each of which is surrounded by a concentric air stream. Such a design can allow for a higher single-pass throughput than a single row, see Figure 3.1.

(a)



(b)



Figure 3.1 (a) Side schematic representation of the multi-row meltblowing design and fiber formation process. (b) Photo of an eight polymer row die face, with two air-only outlets at the die edge. (Photo courtesy of Biax Fiberfilm Corp)

Multi-row meltblowing differs from the traditional single-row meltblowing system most importantly in the relative positioning of the fiber forming spinnerets and the attenuating air stream. The capabilities of this aerodynamic configuration in fiber and web formation have been studied experimentally, but no reports have been made regarding the causes of the fiber diameter distribution for this geometry. For some applications, such as air filtration, a wider fiber diameter

distribution can be advantageous, but for others, such as liquid filtration and tissue scaffolding, a narrow distribution is required.[16] There is a need in meltblowing processes, therefore, not just the ability to control the fiber diameter but also to control the fiber diameter distribution.

In this work, we examine specifically the fiber diameter distribution of the multi-row meltblowing aerodynamic configuration, and its response to processing conditions. Distribution profiles vary by processing condition, but widen relative to the median diameter as smaller fibers are formed. We quantify the dispersity of the fiber diameters using the standard deviation divided by the median fiber diameter. We note that air entrainment effects cannot explain the fiber diameter distributions for the symmetric two-row die geometry we have studied. To provide insight on the causes of the fiber diameter distribution, we have examined the fiber formation process using ultra-high-speed videography and high-resolution photography. For conditions with wider fiber diameter distribution, we observe both large and small fibers in the air stream far from the die ruling out lay-down and bending instability effects as a substantial contributor to the distribution. Rather, the principal cause of a wide fiber diameter distribution is a fluctuation of fiber-forming throughput that originates at the tip of every spinneret. The pulsation amplitude of the polymer jet at the spinneret is here shown to correspond excellently to the dispersity of fiber diameters. Air temperature and polymer throughput effects show that the pulsation is fundamentally different from “draw resonance” which has been observed in melt spinning. We hypothesize that this pulsation originates instead from the presence of a region in front of the spinneret that is protected from the high-speed air flow which allows the buildup of polymer there.

3.3 Experimental

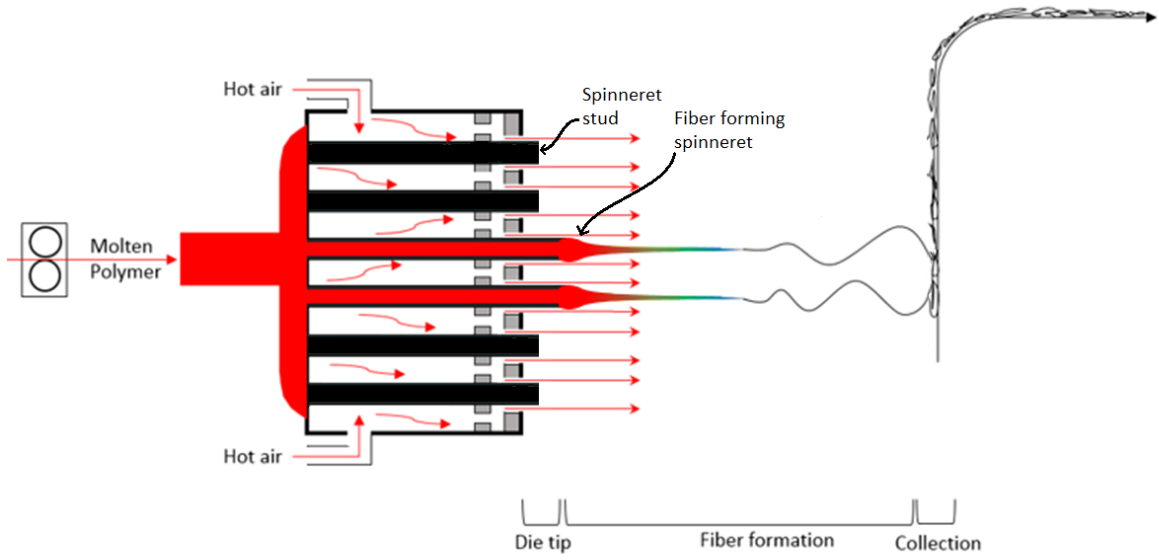
3.3.1 Material

All experiments used LyondellBasell MF 650W Isotactic Polypropylene, a commercial meltblowing grade homopolymer resin. The manufacturer states that polymerization was metallocene catalyzed, so the molecular weight distribution is expected to be low. Stated melt flow rate at 230 °C and a 2.16 kg mass was 500 g/10 min using ASTM D1238, and the density at 23 °C was 0.90 g/cm³ using ASTM D792.

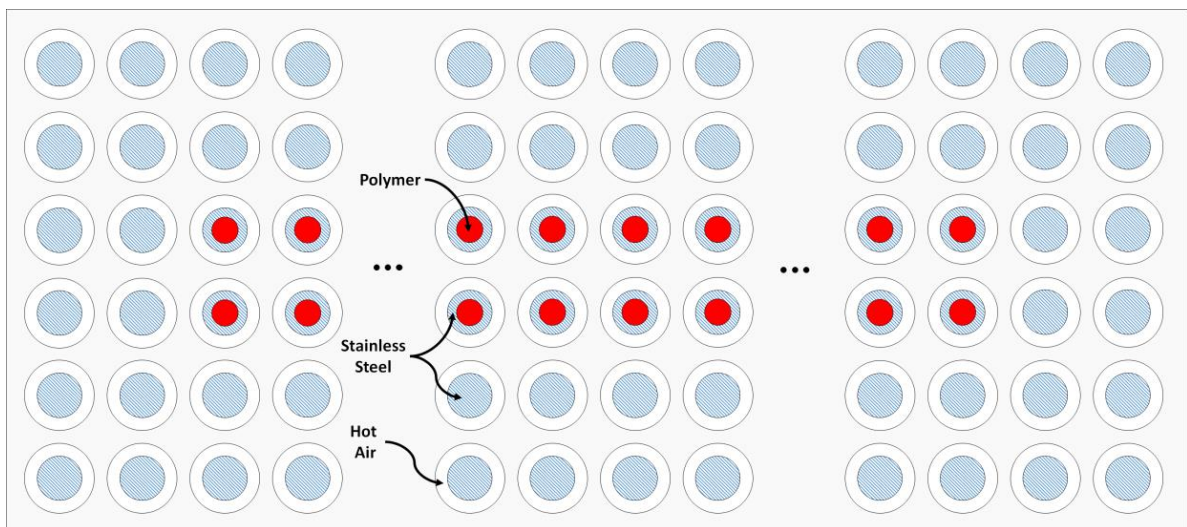
3.3.2 Dual-Row Meltblowing

A two-row meltblowing die was selected to study the unique annular spinneret design. The equipment and die used, termed the Spunblown® process, was manufactured by Biax-Fiberfilm Corporation [12], [13]. The die was 38 cm in width, contained two fiber spinning rows with a total of 368 spinnerets. The adjacent fiber forming spinneret rows were surrounded on all sides by two air-only (non-fiber-forming) rows, which serve to insulate the spinning fibers from cool air entrainment. The total number of air annuli, both those surrounding the fiber forming spinnerets and spinneret studs, was 1128. The inner diameter of the fiber forming spinnerets was 508 μm. Schematic representations of the specific die and system are displayed below.

Figure 3.2 (a) Schematic side view of the 2-row meltblowing process; (b) Schematic front view of the die face showing red polymer extrusion from the fiber forming spinnerets, blue hash steel spinneret wall and studs, and white hot air releasing annuli; (c) Relevant dimensions of the spinnerets (not shown: spinnerets extend 3.0 mm past the air annuli face and spinneret studs extend 1.5 mm past the same face).

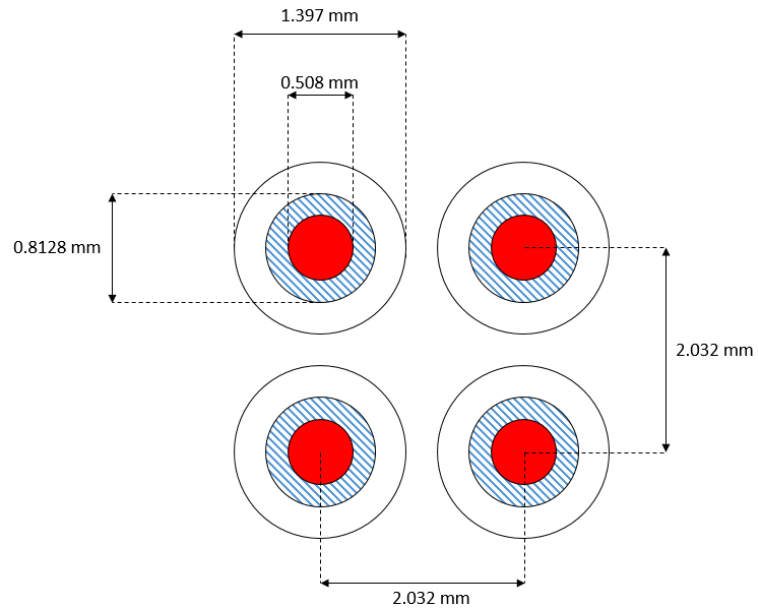


(a)



(b)

Figure continues to next page



(c)

In the multi-row meltblowing die design, molten polymer is pushed through a series of distribution plates and into 2.5 cm long cylindrical spinnerets. The spinnerets traverse an air cavity (see Figure 3.2a) and emit the polymer several millimeters in front of the die face. Other important process parameters were held nearly constant: die-collector-distance (DCD) was 40.0 cm, melt temperature was about 240 °C, die temperature was 220 °C, collector speed was 3.05 m/min, and collector suction was set to 40% of machine maximum. Samples were collected and analyzed from the full factorial variation of the parameters shown in s of substantial shot and fly.

Table 3.1, except for the condition of highest air temperature and speed, and lowest polymer throughput a condition which produced a mess of substantial shot and fly.

Table 3.1 Process variables and their specific conditions

Process Variable	Conditions
Air Cavity Temperature (°C)	166, 182, 240
Air Speed 1 cm in front of spinnerets (m/s)	46, 56, 68
Polymer Throughput (gram/hole/minute)	0.050, 0.100, 0.170

3.3.3 Ultra-High-Speed Videography

A Phantom v1612 Ultrahigh-Speed Camera was used visualize and track the rapid motions of the polymer jets and spinning fibers. The camera was equipped with a Canon 180 mm Macro lens whose face was positioned 18 cm from the fibers at the center of the die, giving a minimum spatial resolution of about 80 µm. Two plasma light sources (Hive Lighting, Killer Maxi Par Kit) capable of delivering 500,000 lux of continuous light was used to illuminate fibers directly, and as a backlight source. Video recordings were made for 1-2 second intervals for each of the 27 conditions varying air cavity temperature and pressure, and polymer throughput. Each condition was recorded at two video resolution and frame speed combinations: 128x800 at 58,252

frames/second, and 128x128 at 310,000 frames/second. Recording resolution does not affect spatial resolution.

3.3.4 High-Resolution Photography

A Canon EOS Rebel T6i, capable of recording images of 6000 x 4000 pixels, was used to capture high resolution photos of the spinning fibers very close to the spinneret (within 1 cm). The camera was equipped with a Canon 180 mm Macro lens and operated 30 cm from the spinnerets. The spatial resolution for this configuration was 3.5 μm , allowing accurate measurement of the polymer jet diameter in this region. The camera was also outfitted with a Canon Speedlite 430EX II flash to freeze the motion of the fibers. Flash pulses were provided to 1/4000th second.

3.3.5 Fiber Diameter Measurement

To measure fiber diameters in the collected webs, a sample from the center of the fabric was taken, sputtered using a Denton Desk V sputtering system, then examined using a Phenom Pro X scanning electron microscope (SEM). Ten detailed SEM images (1000 – 5000x magnification) were taken for each sample. Approximately 150-250 fiber diameters per sample were measured manually using National Institute of Health ImageJ software.

3.4 Results and Discussion

3.4.1 Fiber Diameter Distributions

Meltblown fiber diameters have previously been reported to be log-normally distributed, regardless of the mean fiber diameter. [8], [9], [17], [18] These distributions have the property that $\ln(D)$ is normally distributed, where D is the fiber diameter. Fiber diameters produced by the annular spinneret design follow this behavior for only a few cases. To describe these fiber diameter

distributions, we have implemented the Shapiro-Wilk test [19] for normality of both the ordinary and log transformed diameter distributions from the full factorial meltblowing experiment of the variables shown in s of substantial shot and fly.

Table 3.1. Test results, shown by the statistic W , were deemed sufficient to reject the null hypothesis that the distribution was normally distributed with a confidence of 95% or greater ($p \leq 0.05$). W can take the values (0,1] with higher values indicating that the distribution is closer to normal. Using this test for normality, we observe distributions that are normal, lognormal, somewhere in between, or neither, the character of which is diameter dependent. Inspection of the distributions not normally or log-normally distributed was required to tell if the distribution was a hybrid between normal and lognormal, or a distortion taking the distribution outside this “range”. This inspection showed that distributions not normal or log-normal but still with $W > 0.8$ for both ordinary and log-transformed distributions could be described as hybrid distributions, somewhere between normal and lognormal. When neither ordinary nor log-transformed distributions are normally distributed (i.e. $p_{\text{normal}}, p_{\text{lognormal}} > 0.05$) yet still for both $W > 0.8$ indicates that neither is far from normal. For distributions not normal or lognormal but with one $W < 0.8$, we categorize the distribution as skewed. There were no cases where both ordinary and log-transformed distributions had $W < 0.8$, and all skewed distributions had log-transformed $W > 0.8$. We term these distributions “skewed-lognormal” because they are close to lognormal ($W_{\text{lognormal}} > 0.95$), far from normal ($W_{\text{normal}} < 0.8$), but they are not lognormal because the log distributions have a positive skew (and $p_{\text{lognormal}} > 0.05$). While the W value of 0.8 is somewhat arbitrary, the inspection of these 26 distributions shows that it is an acceptable cutoff to accurately describe the distributions. To summarize, Table 3.2 shows the fiber diameter distributions organized into five

categories according to the results of the Shapiro-Wilk tests performed on the diameters and the logarithm of the diameters.

Table 3.2 Fiber diameter distributions as defined by Shapiro-Wilk test results. Subscripts of normal and lognormal indicate test result statistics from the fiber diameters and the logarithm of the diameters, respectively. All distributions observed satisfy one and only of the shown criteria.

Distribution observed	Defined by Shapiro-Wilk test criteria
Normal	$p_{\text{normal}} \leq 0.05$
Hybrid-normal	$p_{\text{normal}}, p_{\text{lognormal}} > 0.05$ and $W_{\text{normal}} > W_{\text{lognormal}} > 0.8$
Hybrid-lognormal	$p_{\text{normal}}, p_{\text{lognormal}} > 0.05$ and $W_{\text{lognormal}} > W_{\text{normal}} > 0.8$
Lognormal	$p_{\text{lognormal}} \leq 0.05$
Skewed-lognormal	$p_{\text{normal}}, p_{\text{lognormal}} > 0.05$ and $W_{\text{lognormal}} > 0.8 > W_{\text{normal}}$

Representative distributions for each are shown in Figure 3.3.

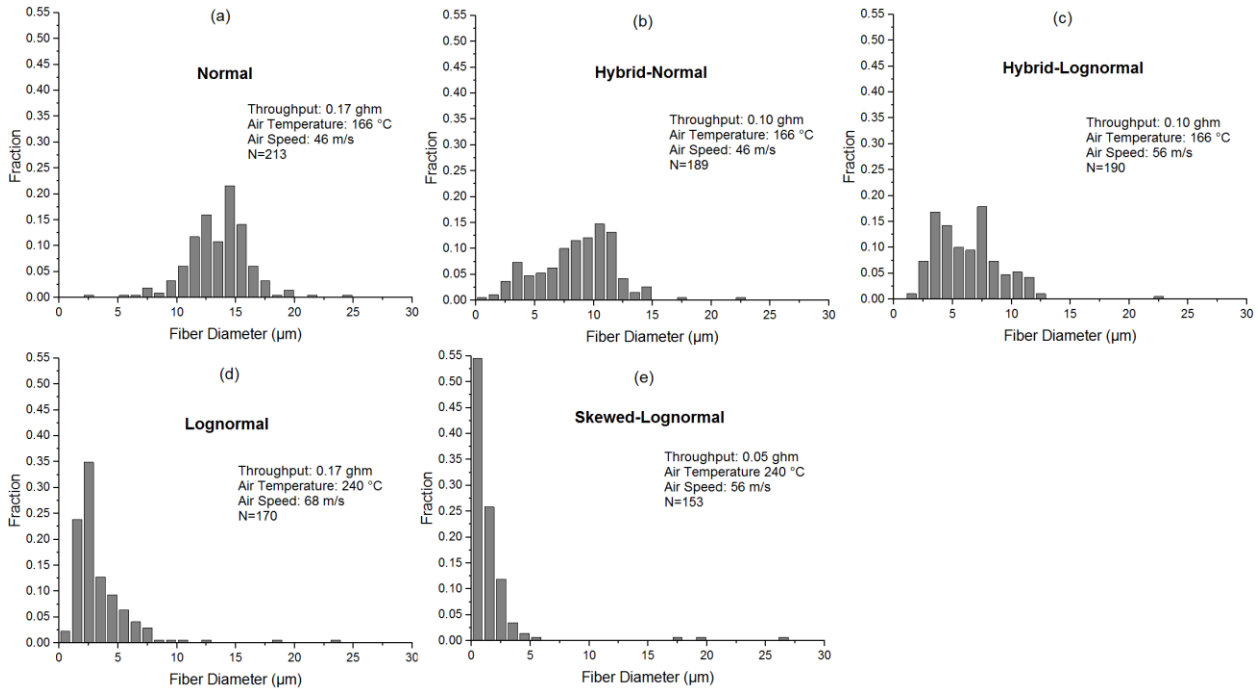


Figure 3.3 Representative fiber diameter distributions as histograms with 1 μm bin size.

Previous reports discussing meltblown fiber diameter distributions employ statistics appropriate for the lognormal distributions observed, namely, the geometric mean and a standard deviation or coefficient of variation. [9], [17], [18] The coefficient of variation, a measure of a

distribution dispersity, for a normally distributed variable is defined as the standard deviation divided by the mean. For the varied and often heavily skewed distributions observed for the annular spinneret design, we have chosen to focus on the median diameter and the standard deviation. We quantify the relative dispersity of the distribution as σ/D_{med} , the standard deviation divided by the median fiber diameter. The distribution type and this measure of dispersity are shown in Table 3.3 as they vary with the median fiber diameter for each fabric formed.

Table 3.3 Median fiber diameter, distribution type and distribution dispersity for each 26 samples collected. Distributions indicated by * are shown as histograms in Figure 3.3.

D_{Med} (μm)	Distribution Type	Dispersity (σ/D_{Med}) x100%
13.87	Normal*	19
11.84	Normal	25
10.98	Normal	26
9.59	Normal	28
9.35	Normal	34
8.97	Hybrid-Normal*	35
7.31	Hybrid-Lognormal	41
6.69	Hybrid-Normal	39
6.05	Hybrid-Lognormal*	43
4.94	Lognormal	51
4.24	Hybrid-Lognormal	74
3.49	Lognormal	69
3.39	Hybrid-Lognormal	77
2.71	Lognormal	94
2.68	Lognormal*	71
1.81	Lognormal	165
1.73	Lognormal	121
1.65	Skewed-Lognormal	163
1.39	Skewed-Lognormal	188
1.31	Skewed-Lognormal	143
1.24	Skewed-Lognormal	217
1.19	Skewed-Lognormal	158
0.94	Skewed-Lognormal	246
0.90	Skewed-Lognormal	192
0.90	Skewed-Lognormal*	346
0.76	Skewed-Lognormal	238

Table 3.3 shows that a relatively smooth transition from normal to skewed-lognormal occurs as the median fiber diameter decreases. This transition is accompanied by an increase in the fiber diameter dispersity. Underlying these shifts is the inability of the process to eliminate the presence of some large fibers for any condition. These few large fibers can greatly broaden the pore size distribution in the fabrics, and distort the mass portion of raw material that produces the more desirable fine fibers. This effect is best shown visually so Figures 3.3(a), 3(d), and 3(e) are reproduced to show the mass fraction histograms as well in Figure 3.4. Fiber masses are based on fiber cross sectional area and assuming constant polymer density for all fibers.

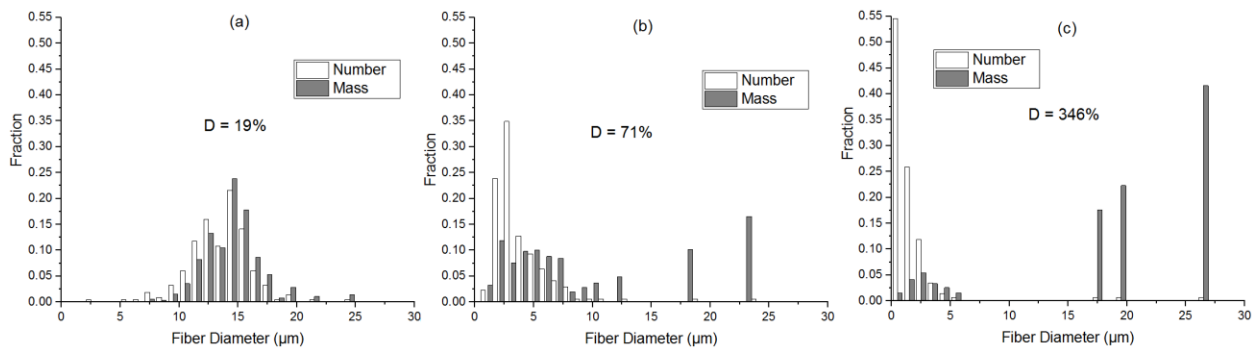


Figure 3.4 Fiber diameter distributions by number and by mass fraction, histograms with 1 μm bin size. Data sets were taken from Figures 3.3(a), (d), and (e), respectively for (a), (b), and (c). Dispersity: $D = \sigma/D_{\text{med}}$.

Figure 3.4 emphasizes the effect of a few large fibers on a fine fibrous sample: the large fibers can make up the majority of the fabric weight. A better understanding of the origins of these distributions was sought by using high speed videography and high resolution photography of the fiber spinning process.

3.4.2 Pulsation of the Polymer Jet

Meltblown fiber formation occurs three conceptual zones based on the distance from the spinneret. Very near the spinneret, the polymer jet rapidly accelerates to match the air velocity.

Farther downstream, turbulent bending instability motions cause the fibers to further attenuate.[20] Finally the fibers contact the suction belt, a process that can have a modest impact on the fiber diameter. (Samaneh citation?) Appropriate imaging techniques can be used to determine which zone(s) cause some large fibers to be formed in an otherwise narrow fiber sample. Ultra-high speed videography was used to observe the spinning fibers at intermediate distances from the spinnerets (~5-10 cm) where bending instability motions occur. For samples containing small median diameter fibers, an occasional much larger fiber was seen to pass through the field of view. One frame containing a large fiber in a fine fiber sample (1.19 μm median diameter in the fabric) is shown in Figure 3.5.



Figure 3.5 In the region of fiber bending instabilities, a large fiber is clearly visible along with many smaller fibers that are difficult to discern given the image resolution.

In accordance with the dispersity of fiber diameters for fine fiber samples, the disparity of large and small diameters was only clear for fine fiber samples, whose fabrics had median diameter of less than about 3 μm . Although the resolution of high speed video frames is insufficient to measure fiber diameters and produce histograms such as those in Figure 3.3, small fibers in the air stream greatly outnumbered the large fibers, just as they do in the fabrics. These observations make clear that the dispersity of a fiber diameter distribution has largely been determined by the time the fibers reach the region of bending instabilities and therefore give indication that dynamics near the spinneret shapes the fiber diameter distribution.

Ultra-high speed videography and high resolution photography were employed to study the behavior of the polymer jet near the spinneret (within 1 cm). At conditions producing large fibers, the polymer jet is stable with no noticeable change in the jet diameter, but wags slightly from side to side. For conditions producing small fibers, the jet still wags but its diameter oscillates or pulsates non-sinusoidally, and more dramatically for conditions producing smaller fibers.

Ultra-high speed videography was used to observe the dynamics of the pulsation at low resolution, while high resolution photography allowed for detailed observation and measurement of polymer jet diameters but frozen at random times during the period of pulsation. Images taken from an ultra-high speed cine of a sharply pulsating spinneret are shown in Figure 3.6.

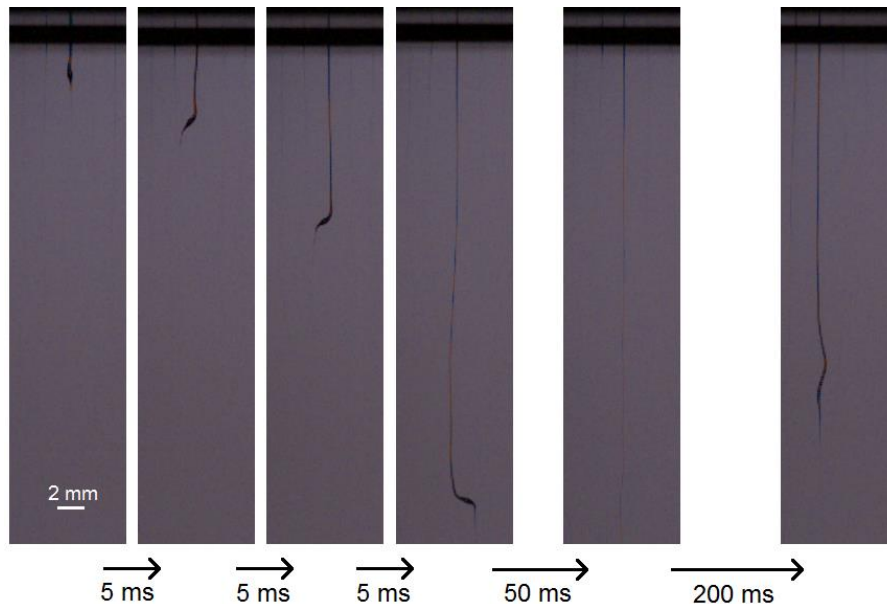


Figure 3.6 Top-down view of spinnerets from an ultra-high speed cine showing a sharp increase of polymer released from one spinneret into a larger fiber. Five spinneret columns are visible in this field of view, and the release of polymer from a second spinneret is visible in the rightmost image. The median fiber diameter collected from this condition was $0.76 \mu\text{m}$.

The pulsation of the polymer jet for all conditions occurs via a sharp increase of jet diameter followed by a gradual reduction to a stable minimum, then repeats. Because ten spinnerets are

visible in the video frame, the frequency and profile of the polymer jet fluctuation with time are accurately quantifiable in the ultra-high speed cines. Accurate measurement however, of the jet diameter was performed using the high resolution photos. High resolution photos taken from the same condition shown in Figure 3.6 have been arranged in Figure 3.7 to show the pulsation of the polymer jet that originates at every spinneret.

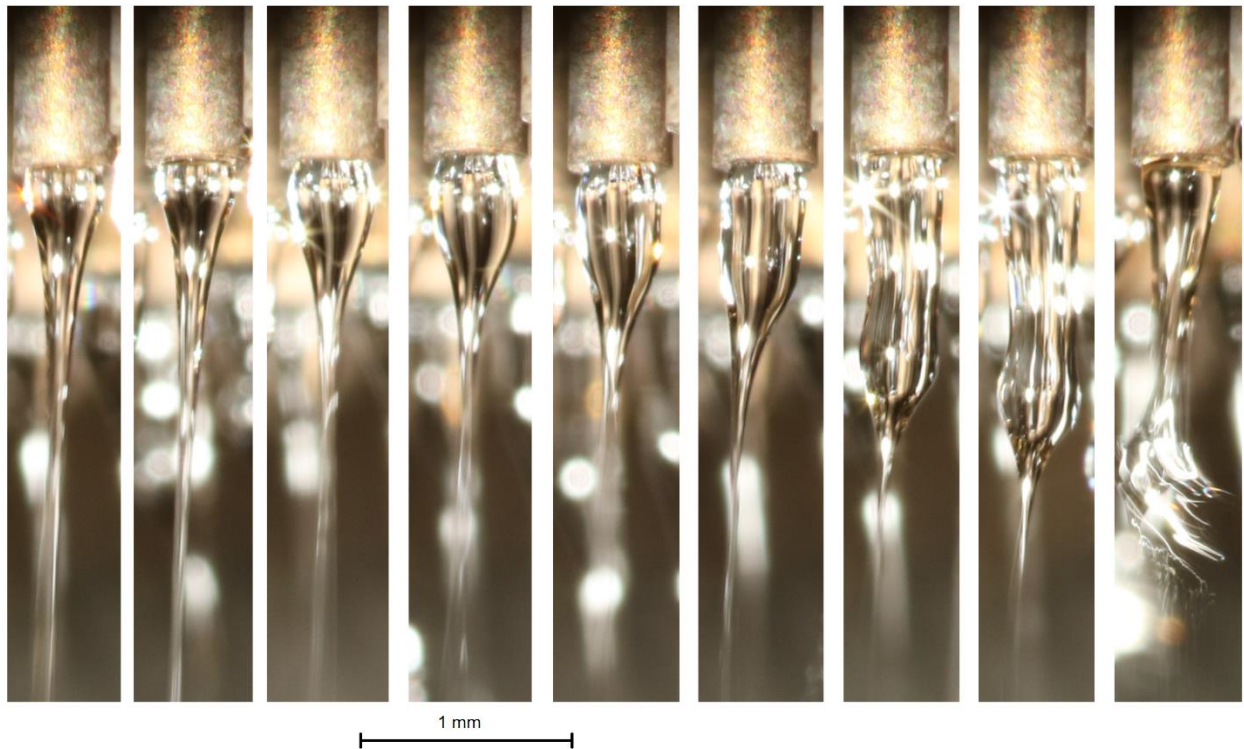


Figure 3.7 High resolution photos of the polymer jet issuing from a single spinneret at different moments during the jet pulsation.

Each image in Figure 3.7 shows the same spinneret at different moments during the pulsation of the polymer jet. Similar photos were taken for every condition both perpendicular to the polymer jet (as shown) and also facing inward slightly. Inward facing photos were taken to check for the possibility of filament pull-out, a situation that has been observed in melt-spinning. [21] Filament pull out was not observed to occur for any condition tested here. From the perpendicular photos, approximately 30 jets from every condition were measured to determine

their diameters at 3 mm from the spinneret outlet. Although photos were taken at random times with respect to the pulsation, it is assumed that 30 jet diameter measurements is a large enough sample to span the range of jet diameters for each condition, and give the amplitude of the polymer jet pulsation. Comparison of the pulsation amplitudes observed across conditions to the dispersity of the fiber diameters collected provides clear evidence that this pulsation causes large fibers to be formed in otherwise fine fiber samples. Jet pulsation amplitudes as well as processing conditions for each condition are appended to Table 3.3 and are reproduced below.

Table 3.4 Median fiber diameters, processing conditions, and jet pulsation amplitude.

D_{Med} (μm)	Air Temperature ($^{\circ}\text{C}$)	Air Speed (m/s)	Polymer Throughput (gram/ hole/ min)	Distribution Type	Dispersity (σ/D_{Med}) $\times 100\%$	Polymer Jet Pulsation Amplitude (in μm , at 3 mm from spinnerets)
13.87	166	46	0.17	Normal	19	21
11.84	182	46	0.17	Normal	25	36
10.98	166	56	0.17	Normal	26	14
9.59	182	56	0.17	Normal	28	39
9.35	166	68	0.17	Normal	34	39
8.97	166	46	0.1	Hybrid-Normal	35	25
7.31	182	46	0.1	Hybrid-Lognormal	41	72
6.69	182	68	0.17	Hybrid-Normal	39	47
6.05	166	56	0.1	Hybrid-Lognormal	43	36
4.94	182	56	0.1	Lognormal	51	107
4.24	240	46	0.17	Hybrid-Lognormal	74	61
3.49	240	56	0.17	Lognormal	69	54
3.39	166	68	0.1	Hybrid-Lognormal	77	57
2.71	182	68	0.1	Lognormal	94	132
2.68	240	68	0.17	Lognormal	71	72
1.81	166	46	0.05	Lognormal	165	97
1.73	166	68	0.05	Lognormal	121	125
1.65	166	56	0.05	Skewed-Lognormal	163	122
1.39	182	46	0.05	Skewed-Lognormal	188	236
1.31	240	46	0.1	Skewed-Lognormal	143	204
1.24	182	56	0.05	Skewed-Lognormal	217	247
1.19	240	56	0.1	Skewed-Lognormal	158	226
0.94	182	68	0.05	Skewed-Lognormal	246	358
0.90	240	68	0.1	Skewed-Lognormal	192	269
0.90	240	56	0.05	Skewed-Lognormal	346	498
0.76	240	46	0.05	Skewed-Lognormal	238	419

Conditions with jet pulsation amplitudes approaching the spinneret inner diameter (508 μm) show very sharp profiles and would be called “shot” by a naked-eye observer. Figure 3.6 shows shot in one of the sharpest pulsations observed, but Table 3.4 suggests that “shot” forms on a gradient of polymer jet pulsation. As the processing conditions are adjusted to produce smaller fibers, the polymer jet near the spinneret pulsates with increasing amplitude and sharpness.

Although the fiber was never seen to break at 3 mm from the spinneret, a sharp increase in jet diameter can deposit a large particle of polymer in the fibrous web. See Figure 3.8. Such particles observed in the web were not counted as fibers in the histograms above, but can further skew the mass distribution of polymer that forms fine fibers or large fibers and shot particles.



Figure 3.8 Shot particle; median diameter of fibers was 0.76 μm .

For moderate to high pulsation amplitudes, the frequency was easily measurable and highly reproducible for different spinnerets for the same processing conditions. For low pulsation amplitudes (less than about 50 μm) which occur at higher polymer throughputs, the jet diameter

appears to be constant with time in the ultra-high speed cines, so the frequencies for those conditions are not detectable. Although the ultra-high speed cines were not of high enough resolution to measure jet diameters, several key times of the pulsation were noted: the beginning of a jet diameter increase, maximum diameter, and time to return to minimum. Attributing the minimum and maximum jet diameters to those measured using the high resolution photos allows for the jet pulsation profile to be drawn. Such a sketch is shown in Figure 3.9.

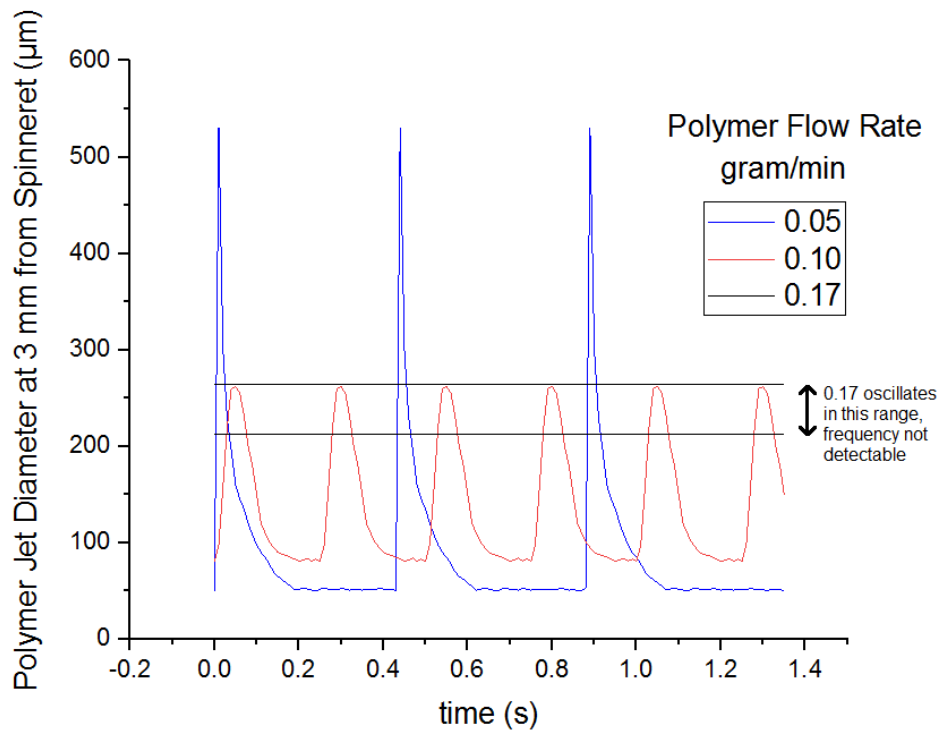


Figure 3.9 Polymer jet diameter profile with time, for three polymer flow rates. Air temperature was 240 °C, air speed was 56 m/s.

Due to the shape of the polymer jet profile, we term the behavior of the polymer jet a pulsation rather than an oscillation. The increase in jet diameter appears to come as a pulse arising from the release of polymer that accumulates at the tip of every spinneret. We propose this pulsation originates from the presence of a protected area immediately in front of the annular spinneret that is shielded from the high velocity air stream. At low polymer throughputs, polymer

accumulates in this region until it becomes large enough to be exposed to the high velocity air and is swept away into a larger fiber or shot particle. For higher polymer throughputs, the instability does not develop and the protected region remains nearly full at all times. The effect is to create a small reservoir between the spinneret and polymer drawing zone that prevents stable fiber formation at low polymer throughputs. The behavior is shown schematically in Figure 3.10.

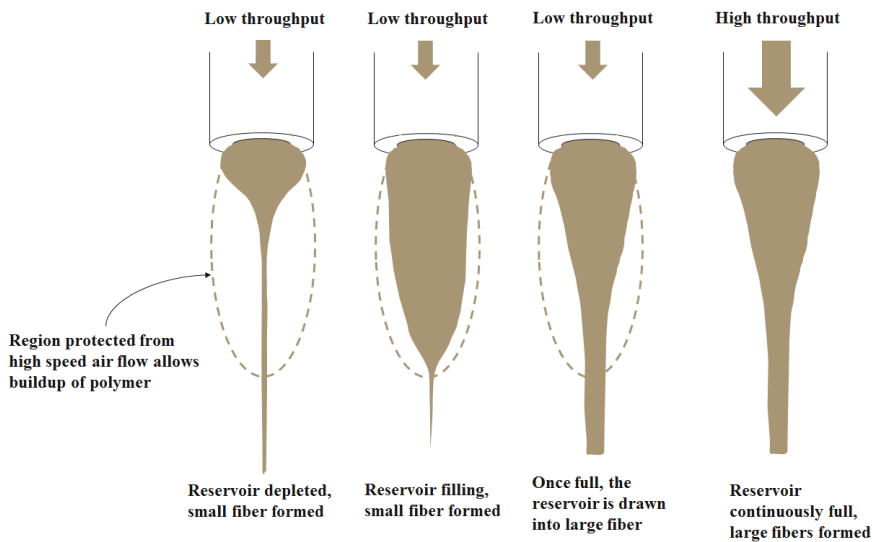


Figure 3.10 Polymer jet pulsation as caused by the annular spinneret aerodynamic configuration.

There is a natural high out flow from the filled reservoir, and a much lower out flow from a depleted reservoir. If the polymer throughput issuing from the capillary is high enough, the reservoir will remain full and fiber formation will be stable. When polymer throughput is less than this natural out flow, the reservoir can be depleted. When this happens, the fiber formed becomes much narrower, significantly reducing the flow out from the reservoir and allowing it to be refilled, repeating the process. The pulsation shown in Figure 3.6 directly shows that the pulsation causes large fibers to be formed, but Figure 3.10 shows that it also allows for very fine fiber formation. While the reservoir fills, polymer flow leaving the reservoir and forming a fiber is less than that

emitting from the capillary, indicating that the smallest fibers may not be formed either without this pulsation.

Examining the pulsation period for several processing conditions supports the protected-region explanation of the pulsation. Pulsation periods and their respective processing conditions are shown in Figure 3.11. Small error bars are indicative of the highly consistent pulsation frequency for different spinnerets of the same condition. This serves as validation that the polymer flow rate is very consistent at least across the spinnerets observed. It should be noted that the ultra-high speed video frame included ten adjacent spinnerets located near the center of the die, and that throughput consistency across the width of the die can and should be checked by comparing pulsation frequencies measured at various width positions.

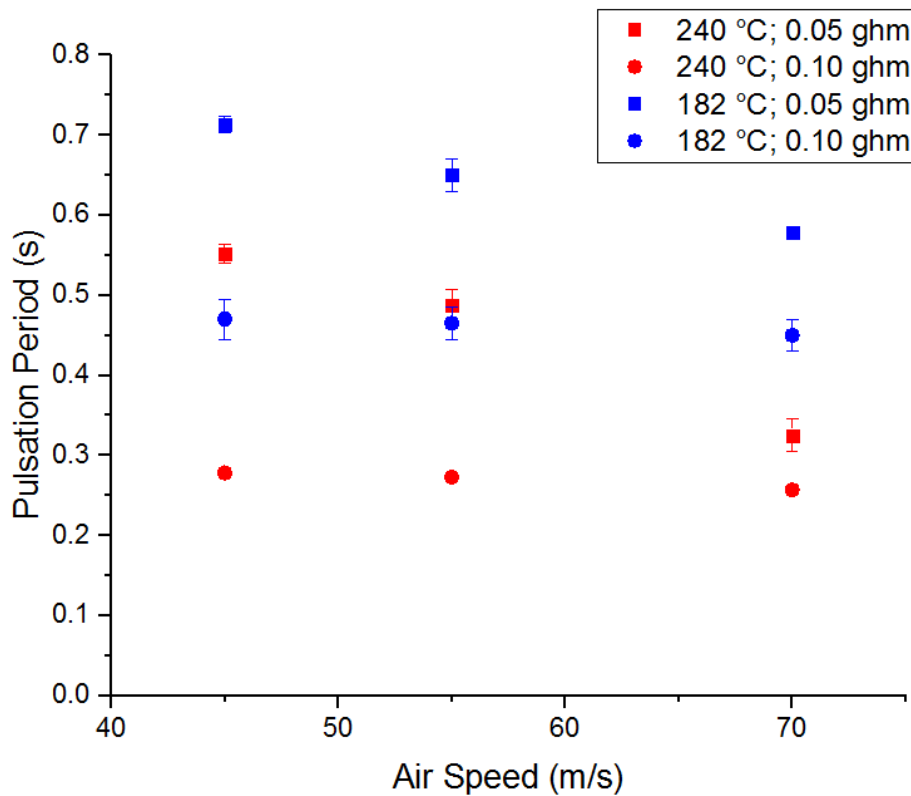


Figure 3.11 Jet pulsation period for high amplitude conditions.

Higher polymer throughputs yield more rapid pulsation (with lower amplitude), because the protected reservoir in front of the spinnerets can be filled more rapidly. Higher air speeds can increase the pulsation frequency if they reduce the size of the protected volume in front of the spinnerets, allowing the same throughputs to fill the reservoir more quickly. More turbulence around a spinneret annulus could subject the polymer jet to higher air speeds closer to the spinneret outlet, in effect reducing the volume of the protected region in front of the spinneret that is not exposed to high velocity air. Lower air temperatures translate to lower polymer temperatures for this process. The lower temperature polymer melt has greater viscosity and resistance to extension, requiring faster air to impart the necessary drag to sweep accumulated polymer into the air stream. Thus more polymer can accumulate at the tip of spinnerets when the melt is cooler, increasing the effective size of the reservoir and the pulsation period.

A similar fiber spinning instability, termed draw resonance, has been observed in melt-spinning technology [22], but the behavior of the pulsations are fundamentally different from those observed here. In melt spinning, a polymer (usually of higher molecular weight than meltblowing resins) is extruded from a capillary and taken up rapidly on a collecting roll. A pulsation of the thread diameter has been observed to occur there for moderate draw ratios, but the pulsation stabilizes at higher draw ratios. [23] Higher draw ratios correspond to faster fiber draw down and, in annular meltblowing, this increases the severity of the pulsations and results in fiber breakage. There is no reason to believe that reducing the polymer throughput or increasing the air speed further than what we have done here will result in anything other than a higher occurrence of shot. Also, melt spinning experiments have also shown that the spinline stability is enhanced (i.e. resonance amplitudes are reduced) by a higher polymer melt temperature. Holding polymer throughput and air speed constant, higher polymer jet temperatures, determined in large part by

the air temperature, yield higher pulsation amplitudes for every single condition in Table 3.4. These opposite trends in the pulsation behavior with processing conditions provide good evidence that the pulsation of the polymer jet in annular meltblowing cannot be explained by the same mechanisms that cause draw resonance in melt spinning.

3.5 Conclusions

We have reported on the character and causes of the fiber diameter distributions formed by the annular meltblowing spinneret design. Different from reports of the traditional slot-die design, the distributions are not lognormal for all conditions but range from normal to lognormal, and even to lognormal distributions with positive skew. The distributions give indication that large fibers cannot be eliminated entirely from the webs, even as processing conditions are adjusted to produce small fibers on average. Large fibers increasingly dominate the fabric weight as the median fiber diameter is reduced, a cause a significant broadening of the diameter distribution, relative to the median. We have attributed the origins of these fiber diameter distributions not to any mechanisms related to bending instabilities of the fibers at mid-distances from the spinnerets, but to a pulsation of the polymer jet very close to the spinneret outlet. The pulsation has been closely observed using ultra-high speed videography in conjunction with high resolution photography, and its nature described in relation to processing conditions. The pulsation appears to occur due to the existence of a protected region in front of each spinneret that is shielded from the high velocity air stream. The region allows for a buildup of polymer in that “reservoir” leading to the instabilities seen. All pulsation frequency and amplitude trends are explained using the protected-region hypothesis, but the fluid dynamics near the spinneret should be modeled to confirm this. Pulsation amplitude is directly related to the dispersity of the fiber diameter distribution, a fact which indicates the

pulsation causes the relative widening of the fiber diameter distributions as smaller fibers are formed.

3.6 References

- [1] S. Batra and B. Pourdeyhimi, *Introduction to Nonwovens Technology*. 2012.
- [2] INDA, “INDA | About Nonwovens <http://www.inda.org/about-nonwovens/>,” 2017. [Online]. Available: <http://www.inda.org/about-nonwovens/>.
- [3] D. H. Reneker and I. Chun, “Nanometre diameter fibres of polymer, produced by electrospinning,” *Nanotechnology*, vol. 7, pp. 216–223, 1996.
- [4] R. Butin, J. P. Keller, and J. Harding, “Non-Woven Mats by Melt Blowing,” 3849241, 1974.
- [5] M. E. S., G. M. Glenn, A. P. Klamczynski, W. J. Ortis, and L. H. C. Mattoso, “Solution Blow Spinning: A New Method to Produce Micro- and Nanofibers from Polymer Solutions,” *J. Appl. Polym. Sci.*, vol. 113, no. 4, pp. 2322–2330, 2009.
- [6] J. P. Keller and R. R. Buntin, “Melt-Blowing Die For Producing Nonwoven Mats,” 3825380, 1974.
- [7] R. Bresee and W. Ko, “Fiber Formation During Meltblowing,” *Int. Nonwovens J.*, vol. 12, pp. 21–28, 2003.
- [8] A. L. Yarin, S. Sinha-ray, and B. Pourdeyhimi, “Meltblowing : Multiple polymer jets and fiber-size distribution and lay-down patterns,” *Polymer (Guildf.)*, vol. 52, no. 13, pp. 2929–2938, 2011.
- [9] X. Wang and Q. Ke, “Experimental Investigation of Adhesive Meltblown Web Production Using Accessory Air,” *Polym. Eng. Sci.*, vol. 46, no. 1, pp. 1–7, 2006.
- [10] Y. C. Zeng, Y. F. Sun, and X. H. Wang, “Numerical Approach to Modeling Fiber Motion During Melt Blowing,” *J. Appl. Polym. Sci.*, vol. 119, pp. 2112–2123, 2010.
- [11] M. W. Milligan and B. D. Haynes, “Empirical models for melt blowing,” *J. Appl. Polym. Sci.*, vol. 58, no. 1, pp. 159–163, 1995.
- [12] E. C. A. Schwarz, “Apparatus and Process of Melt-Blowing A Fiberforming Thermoplastic Polymer and Product Produced Thereby,” 4380570, 1983.
- [13] E. Schwarz, “Apparatus and Process for Uniformly Melt-Blowing A Fiberforming Thermoplastic Polymer in a Spinnerette Assembly of Multiple Rows of Spinning Orifices,” 5476616, 1995.
- [14] C. Torobin, L., Finlow, “US Patent 6183670: Method and Apparatus for Producing High Efficiency Fibrous Media Incorporating Discontinuous Sub-Micron Diameter Fibers, and Web Media Formed Thereby,” 6183670, 2001.

- [15] L. B. Torobin, "Method and Apparatus for Producing Microfilaments," 4363646, 1982.
- [16] W. J. Li, C. T. Laurencin, E. J. Caterson, R. S. Tuan, and F. K. Ko, "Electrospun nanofibrous structure: A novel scaffold for tissue engineering," *J. Biomed. Mater. Res.*, vol. 60, no. 4, pp. 613–621, 2002.
- [17] D. H. Tan, C. Zhou, C. J. Ellison, S. Kumar, C. W. Macosko, and F. S. Bates, "Meltblown fibers: Influence of viscosity and elasticity on diameter distribution," *J. Nonnewton. Fluid Mech.*, vol. 165, no. 15–16, pp. 892–900, 2010.
- [18] C. J. Ellison, A. Phatak, D. W. Giles, C. W. Macosko, and F. S. Bates, "Melt blown nanofibers : Fiber diameter distributions and onset of fiber breakup," *Polymer (Guildf)*., vol. 48, pp. 3306–3316, 2007.
- [19] A. S. S. Shapiro and M. B. Wilk, "An Analysis of Variance Test for Normality (Complete Samples)," *Biometrika*, vol. 52, no. 3, pp. 591–611, 1965.
- [20] A. L. Yarin, S. Sinha-ray, and B. Pourdeyhimi, "Meltblowing : II-linear and nonlinear waves on viscoelastic polymer jets," *J. Appl. Phys.*, vol. 108, 2010.
- [21] C. Van Der Walt, M. A. Hulsen, A. C. B. Bogaerds, H. E. H. Meijer, and M. J. H. Bulters, "Stability of fiber spinning under filament pull-out conditions," *J. Nonnewton. Fluid Mech.*, vol. 175–176, pp. 25–37, 2012.
- [22] C. D. A. E. Han and R. R. Lamonte, "Studies on Melt Spinning. III. Flow Instabilities in Melt Spinning: Melt Fracture and Draw Resonance," *J. Appl. Polym. Sci.*, vol. 16, pp. 3307–3323, 1972.
- [23] R. J. Fisher and M. M. Denn, "A Theory of Isothermal Melt Spinning and Draw Resonance," *AICHE J.*, vol. 22, no. 2, pp. 236–246, 1976.

3.7 Supplementary Information

A secondary fiber spinning trial was conducted with a four fiber-spinning row die, with capillary inner diameters of 229 μm . Due to the smaller hole size, the fiber spinning window is limited to lower per hole throughputs. Fibrous samples were collected from the same air processing conditions as shown in Table 1 and with polymer throughputs ranging from 0.02 – 0.06 gram/hole/minute. In general, the processing window for producing shot-free fibers was quite narrow compared to the two fiber spinning row die with larger, 508 μm inner capillary diameter spinneret, so further experimentation was conducted with the larger capillary die. SEM microscopy was, however, performed for some of the samples collected from the smaller capillary die, allowing for fiber diameter measurement from that die geometry. For just two of these analyzed conditions, air speed (56 and 68 m/s), air temperature (166 °C), per-hole polymer throughput (0.05 ghm), and DCD (40 cm) were all identical from both the 508 μm (2-rows) and 229 μm (4-rows) inner capillary diameter dies, allowing for fiber diameter comparison from variations in capillary size and number of fiber spinning rows.

In a perhaps surprising result, *larger* capillary size appears to *decrease* median fiber diameter. The results dispel the intuitive notion that narrower capillaries will necessarily produce smaller fibers. The histograms of the manually measured individual fibers is shown in Figure 3.12.

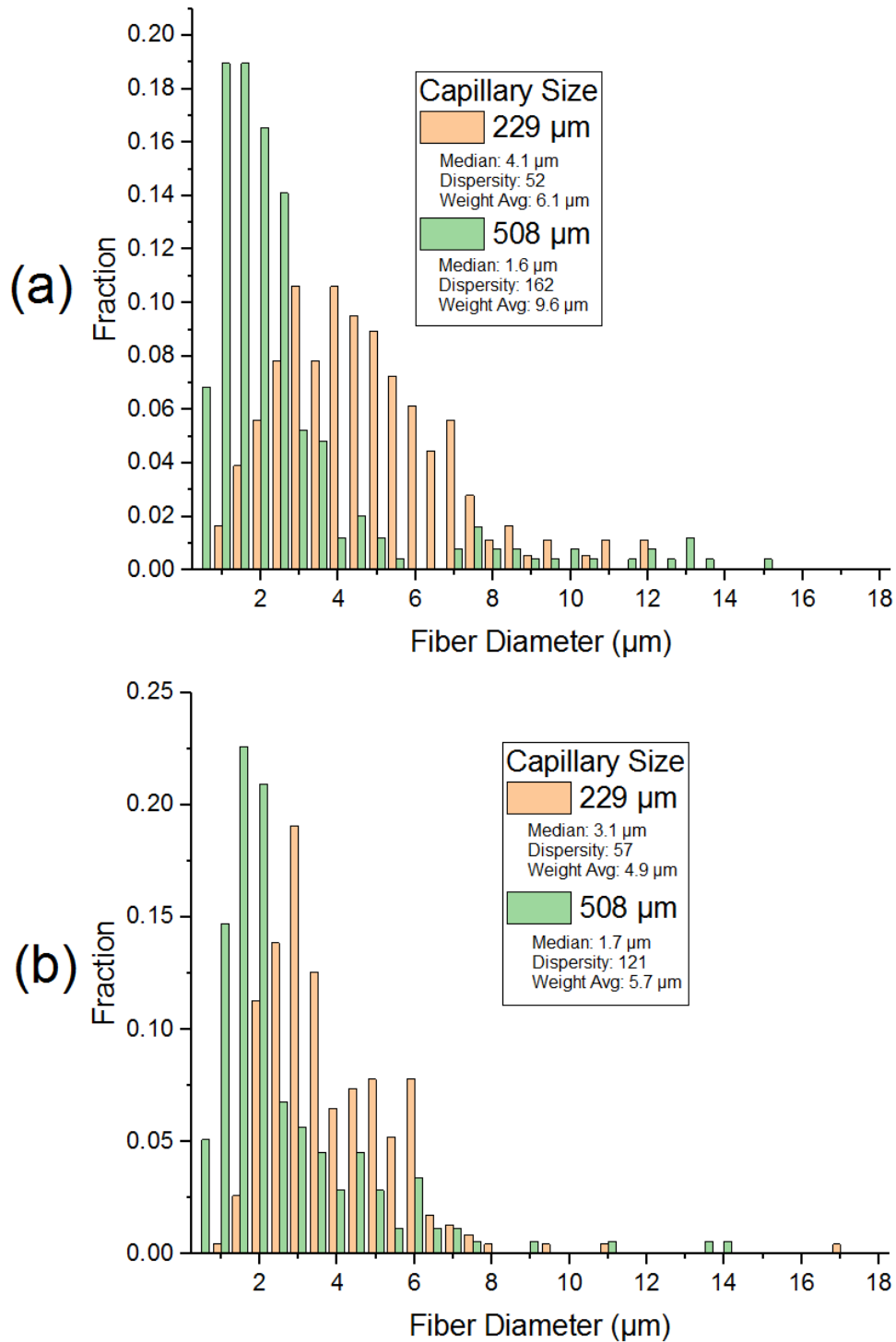


Figure 3.12: Fiber diameters from large (2-row) capillaries and from small (4-row) capillaries. For all diameters shown, air temperature was 166 °C, polymer throughput was 0.05 gram/hole/minute, and DCD was 40 cm (a) Air speed 56 m/s. (b) Air speed 68 m/s.

The polymer jet pulsation described above may describe these surprising trends, but more importantly, the result indicates that smaller capillary size may serve to stabilize the pulsation of the polymer jet. Note that the larger capillary produced more disperse (relatively wide) distributions than did the smaller capillary. Dispersity was shown above to correlate excellently to the severity, or amplitude, of the polymer jet pulsation. Due to the strong temperature gradients present in the air jet close to the spinnerets, a greater number of spinning rows for the smaller capillary die are expected to have wider fiber diameter distributions, not narrower. Moreover, the larger spinneret produced smaller median fiber diameters, but larger weight average fiber diameters which shows that the larger spinneret produced many small fibers, but a greater proportion of large fibers than did the smaller spinneret. Therefore, while it has not been observed directly, the trends seen show good evidence that the polymer jet from the large spinneret undergoes more severe jet pulsation than it does from the small spinneret.

If smaller capillary size serves to stabilize polymer jet pulsation, Figure 3.12 also highlights that jet pulsation can allow for the production of the finest meltblown fibers, even below 1 μm . Therefore, for some situations, the pulsation may be a desirable way to produce very fine fibers, but can also cause shot defects. More research into the causes and control mechanisms of the polymer jet pulsation is needed to find methods of producing submicron fibers at high throughput and, importantly, without the risk of causing shot.

4 Chapter 4 - High Throughput Multi-Row Meltblowing: Effects of Increasing Fiber-Forming Rows on Fiber Diameter Distributions and Web Defects

Stephen Barilovits, Eunkyong Shim, Saad A. Khan, Behnam Pourdeyhimi

Department of Chemical and Biomolecular Engineering and the Nonwovens Institute, North Carolina State University, Raleigh, NC (USA).

This chapter is under revision for publication.

4.1 Abstract

The annular meltblowing spinneret design allows for the production of fine fibers in two dimensions, which can create asymmetries not present in traditional single row meltblowing. Fiber diameters, distributions and incidence of spun fusion are reported for the meltblown production of fine fibers through a multi-row meltblowing design with two, four, and six spinning rows. Results show weak evidence that fiber diameters and distribution widths increase with increasing number of fiber spinning rows, and call into question the uniformity of polymer flow rate through spinnerets of different position on the array. Fiber fusion, fibers bonded to one another over significant distances in parallel, is observed at high rates (in some cases, >60% of all fibers are fused) and the rate increases with more spinning rows, higher polymer throughput, and higher die-collector-distance. Spun fusion in multi-row meltblowing may be reduced by increasing inter-spinneret distances, or by affecting the quench of molten fibers in the spinline prior to collection.

4.2 Introduction

A nonwoven refers to a sheet, mat, or web structure composed primarily of fibers and held together not by intricate weaving or knitting operations but by more rapid mechanical, chemical,

or thermal means. Nonwovens range from thin sheet-like products used in wipes, medical and industrial garments, to more lofty products used in insulation, cushioning, and filtration. They find use in a wide range of products and are often highly engineered and customized for specific applications. Applications such as filtration, medical barrier fabrics, acoustic and thermal insulation require many small pores in the fabrics for best performance – structures that are produced by the incorporation of very fine fibers. Technologies that specialize in producing the finest fibers include meltblowing, electrospinning, and solution blowing, and commonly produce fibers with diameters less than 2 μm [1]–[3]. Meltblowing, although it does not produce the smallest fiber diameters, is preferred industrially because it has significant cost, speed, and environmental advantages over the other methods.

Meltblowing produces fine fibers in a single continuous process from a thermoplastic resin. The process originated from work done by Van Wente at the US Naval Research Laboratory in the 1950's [4], and was patented and commercialized in large scale by Exxon in the 1970's [5], [6]. These works describe a fiber forming apparatus as a v-shaped nozzle through which thermoplastic polymer is extruded through a row fine capillaries to the openings at the tip. Two converging curtains of high velocity hot air are directed at an angle toward the capillary outlets causing rapid acceleration of the polymer jets into fine fibers. The fibers are carried by the air stream to a suction belt where they are collected. In many cases, fibers contact the collection belt while still partially molten, enabling the process to produce bonded fabrics in a single step. This “slot die” configuration has become the industry standard and the fiber formation process using this die geometry has been extensively examined both experimentally and by computational means [3], [7]–[10].

Meltblown fiber diameters typically range from 2-10 μm , sufficiently fine for most applications. Attempts to reduce meltblown fiber diameters come at a higher production costs and increased risk of producing “shot” defects, droplets of polymer that fail to produce continuous filaments. For specialized applications requiring finer fibers such as ultra-high efficiency air filtration, electrospun nanofibers may be incorporated at very low weight percentages into meltblown fabrics [11]. Meltblown fiber diameters are also distributed lognormally [10], [12], which gives rise to variable pore sizes in the fabrics. While such a characteristic may be desirable in some situations, such as air filtration, tight control of pore size is required in others, such as liquid filtration and tissue scaffolding [11], [13]. Efforts have been applied to improve the capabilities of the meltblowing process to produce fibers of controllable diameter and distribution, increase the assortment of compatible raw materials, while reducing costs and avoiding defects.

Over the years, advances in polymer chemistry and modifications to the slot-die geometries have improved the versatility of and reduced costs associated with meltblowing. The technology’s primary cost is the energy required to heat the large volumes of air needed to attenuate the fibers [8]. This cost can be reduced by appropriate resin selection for operation at lower air temperatures, but only to a point dictated by resin availability and the requirements of the fibers produced. Operation at higher polymer throughputs, likewise, can reduce the relative air handling costs but produce larger fibers and risk catastrophic “unzipping” of the slot die at higher pressures [14]. Such a ceiling to the overall throughput a machine is capable of delivering also sets a floor to the timeframe for producing a mass of fibers required to pay for the investment of the equipment.

To bypass some of these limitations and loosen the rheological requirements of resin necessary to produce fine fibers via meltblowing, a significant variations to the die geometry has been devised to allow for multiple fiber spinning rows. In this design, patented and commercialized

by Biax-Fiberfilm Corp, the polymer is extruded through cylindrical spinnerets each of which is surrounded by an annular air stream. See Figure 4.1.

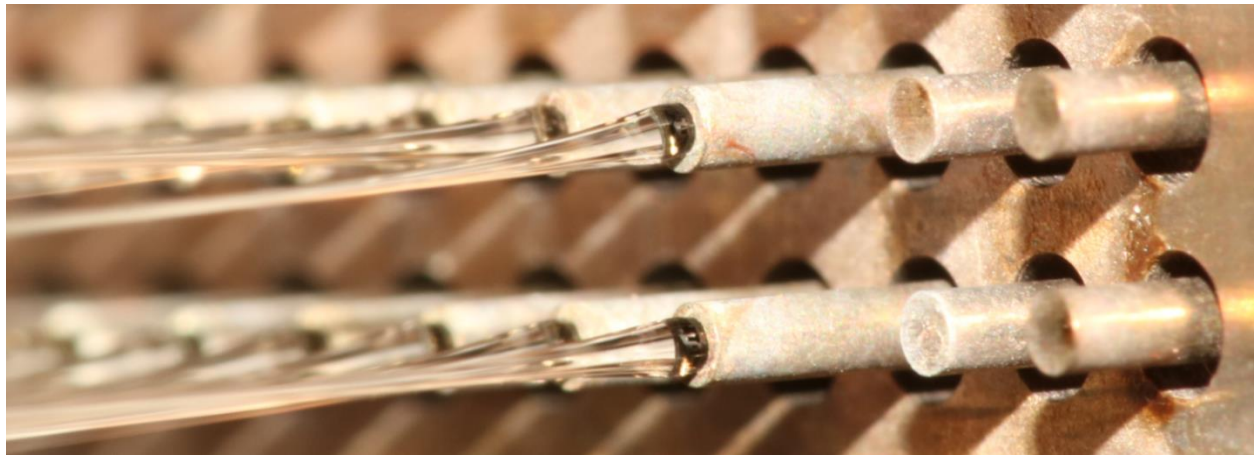


Figure 4.1 Annular meltblowing spinneret.

The fiber forming process and the fibers formed using the annular spinneret design have been investigated, giving understanding of the origins of the broad range of compatible resins and the fiber diameter distributions [15]. Such work was performed for a dual-row system, which is not commonly used industrially; instead, 4-12 rows are preferred to achieve higher throughputs than the single-row slot die. Multi-row effects, moreover, cannot be observed in a two-row system because, due to symmetry, both rows are exposed to the same air environment. Geometries with more than two rows contain both interior and perimeter spinnerets; the effect of this asymmetry on the fiber diameters, distributions, and other web properties is not yet known.

In this work, the effect of greater number of annular spinneret rows on fibers and webs formed is investigated. A 6-row die, modified to also spin fibers from 4 and 2 rows, was used to examine these effects. Air temperature, speed, polymer throughput, and die-collector-distance (DCD) parameters were varied for the same levels for each row-number configuration. The air temperature and velocity profile was mapped near the spinneret outlets and downstream. Fiber

diameters, measured by SEM image analysis, do not show a consistent variation based on number of fiber forming rows, showing that row number does not have a large effect on median fiber diameter. Likewise, diameter distributions are not measurably widened from increased number of fiber spinning rows. These results raise suspicion about the consistency of polymer throughput through capillaries of different location on the die face. In accordance with the observation that fiber diameter distributions are widened significantly by a pulsation of the polymer jet that occurs near the annular spinneret [16], these results further dispel the notion that the fiber diameter distribution width is mostly attributable to fibers being formed in an asymmetric air temperature environment characteristic of multi-row meltblowing.

Webs formed were also analyzed to assess the incidence of spun fusion defects, fibers that bond to one another in the air stream prior or collection. In all cases, increased number of fiber forming rows increased the portion of fibers involved in fusion. The results suggest that increased overall throughput achieved by greater number of fiber forming rows does not significantly broaden the distribution of single-fiber diameters, but increases the effective diameter by increasing the proportion of fibers fused to one another. Recommendations are made on techniques to reduce spun fusion in multi-row meltblowing.

4.3 Experimental

4.3.1 Material

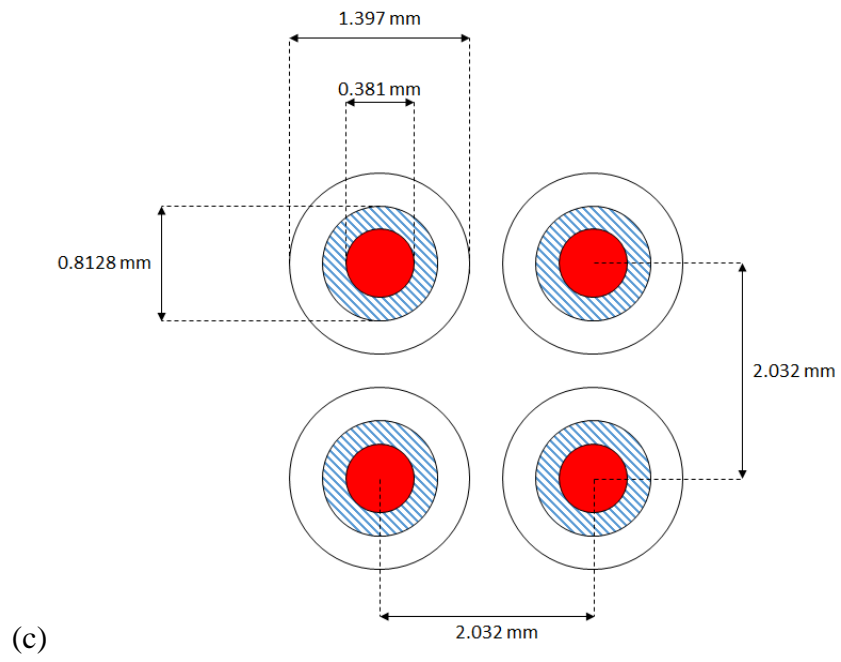
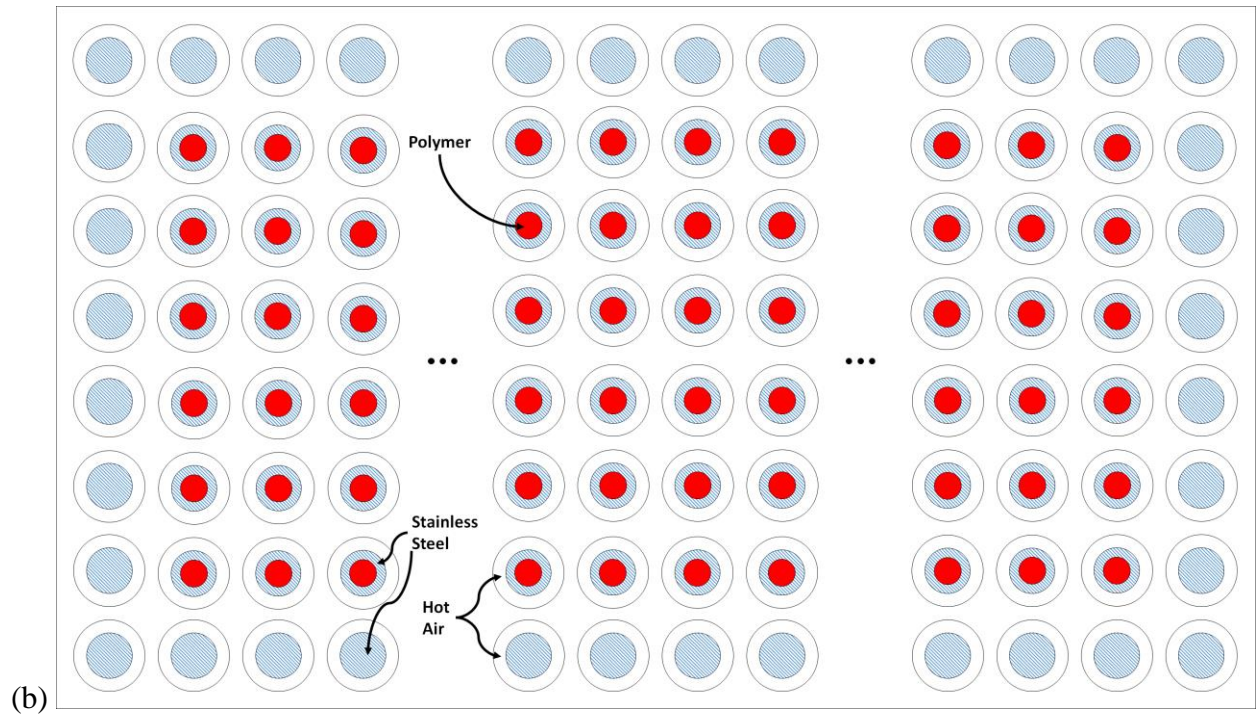
All experiments used LyondellBasell MF 650W Isotactic Polypropylene, a commercial meltblowing grade homopolymer resin. The manufacturer states that polymerization was metallocene catalyzed, so the molecular weight distribution is expected to be low. Stated melt flow

rate at 230 °C and a 2.16 kg mass was 500 g/10 min using ASTM D1238, and the density at 23 °C was 0.90 g/cm³ using ASTM D792.

4.3.2 *Multirow Meltblowing*

A lab-scale 6-row meltblowing die composed of cylindrical spinnerets coaxial with annular air outlets was selected for this study. The equipment and die used, termed the Spunblown® process, was manufactured by Biax-Fiberfilm Corporation [17], [18]. The die was 12.5 cm in width, contained six fiber spinning rows with a total of 366 spinnerets. The inner diameter of the fiber forming spinnerets was 381 μm. The fiber forming spinneret rows were surrounded by a perimeter air-only (non-fiber-forming) rows, which serve to insulate the spinning fibers from cool air entrainment. The total number of air annuli, both those surrounding the fiber forming spinnerets and spinneret studs, was 520. This die was then modified by the incorporation of a stainless steel plate placed in front of the polymer distribution plates and behind the entrance to the spinnerets which served to selectively block fiber forming rows. Matching gaskets, provided by the manufacturer, were placed on both sides of the blocking plate to prevent polymer leakage. Three plates were machined to the appropriate dimensions required to achieve the blocking of zero, two, and four of the spinneret capillaries, allowing the spinning of fibers from 6, 4 and 2 rows, respectively. Schematic representations of the die and system are displayed in Figure 4.2.

Figure 4.2 (a) Schematic side view of the multirow meltblowing process for six, four, and two fiber forming rows; (b) Schematic front view of the 6-row die face showing red polymer extrusion from the fiber forming spinnerets, blue hash steel spinneret wall and studs, and white hot air releasing annuli; (c) Relevant dimensions of the spinnerets (not shown: spinnerets extend 3.0 mm past the air annuli face and spinneret studs extend 1.5 mm past the same face).



In the multi-row meltblowing die design, molten polymer is pushed through a series of distribution plates and into 2.5 cm long cylindrical spinnerets. The spinnerets traverse an air cavity (see Figure 4.2a) and emit the polymer several millimeters in front of the die face. Hot air flows into the air cavity and escapes through the annuli surrounding the spinnerets and spinneret studs. In these experiments, four process variables were altered: air cavity temperature, air cavity pressure, polymer flow rate, and DCD. Their conditions spanned the range of typical safe use of the equipment and polymer and are shown in Table 4.1. DCD was not varied in the full factorial manner and was set to 40 cm for most conditions. DCD was set to 15 cm for conditions where air temperature was 182 °C, air cavity pressure was 68.9 kPa, and polymer throughputs were 0.07 and 0.17 ghm. DCD was set to 25 cm for conditions where air temperature was 240 °C, air cavity pressure was 68.9 kPa, and polymer throughputs were 0.07 and 0.17 ghm. Other important process parameters were held nearly constant: melt temperature was about 240 °C, die temperature was 220 °C, and collector suction was set to 40% of machine maximum. Collector belt speed was adjusted as appropriate to prevent fly formation, therefore, fabric basis weights were not held constant.

Table 4.1 Process variables and their specific conditions

Process Variable	Conditions
Air Cavity Temperature (°C)	182, 240
Air Cavity Pressure (kPa)	48.3, 68.9
Polymer Throughput (gram/hole/minute)	0.07, 0.170
Die-Collector-Distance (cm)	15.0, 25.0, 40.0

4.3.3 *Air Temperature and Velocity Profile*

The air temperature and velocity profiles in front of the spinnerets were measured using a K-type thermocouple and FlowKinetics FKT 2DP1A-C device with a 7.94 mm diameter Pitot tube attachment, respectively. Absolute velocity measurements require simultaneous air temperature

measurement, which was accomplished by mounting the thermocouple about two centimeters away from the Pitot tube in the positive x-direction (see Figure 4.3), so as not to disturb the air flow near the Pitot tube. Both devices were mounted on a robotically controlled stage (Benchtop PRO 2424 from CNC Router Parts) to take measurements at locations of a repeatable accuracy of ± 0.02 mm for an array of positions. The locations of the measured sites are shown in Figure 4.3, and were performed for each of the four air cavity temperature and pressure conditions shown in Table 4.1. The blocking plates block only polymer and do not affect the air flow, so the air profile is consistent for all numbers of fiber spinning rows.

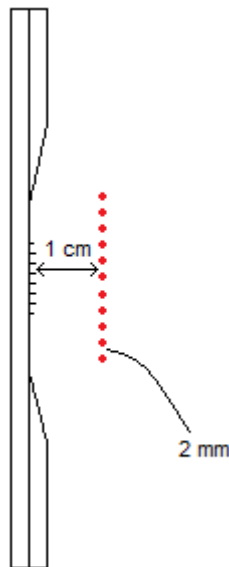


Figure 4.3 Side schematic view of the locations where temperature and velocity measurements were measured.

FlowKinetics FKT Series pressure and temperature monitoring system was used to continually record data averaged over each half second. The probes were held at each position for 15 seconds and values reported here were averaged over the last 5 seconds of that hold time. This procedure allowed the thermocouple to equilibrate to the new temperature of each position.

4.3.4 *Fiber Diameter Measurement*

To measure fiber diameters in the collected webs, a sample from the center of the fabric was taken, sputtered using a Denton Desk V sputtering system, then images recorded using a Phenom Pro X scanning electron microscope (SEM). At least ten detailed SEM images (1500 – 5000x magnification) were taken for each sample. Fiber diameter measurements were performed using proprietary software package, AutoFiber, developed by Mann+Hummel Group. After manual removal of errant diameters such as fused fibers, this method was previously verified to give the same diameters as complete manual measurement as performed using National Institute of Health ImageJ software (see supplementary info). Between 100 and 700 individual fibers were measured for each condition. Statistical analysis was performed using the capability and npar1 way procedures from the Statistical Analysis Software, SAS 9.1.

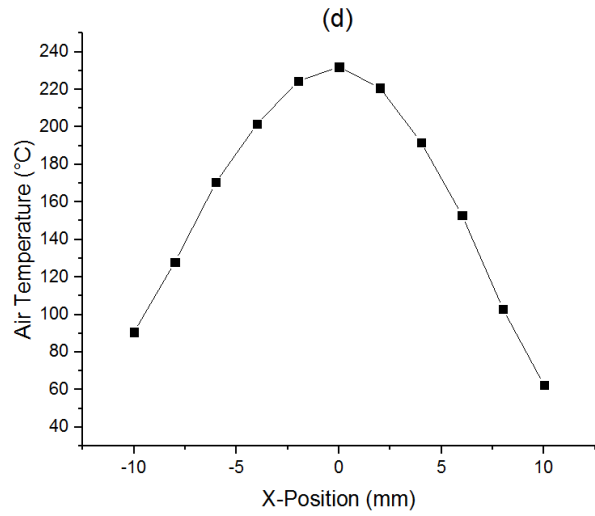
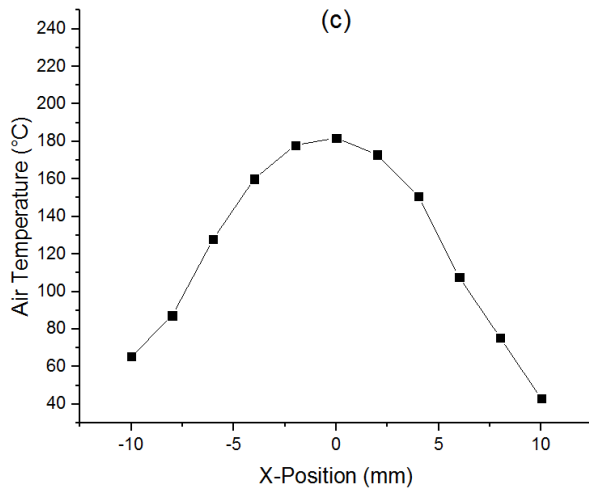
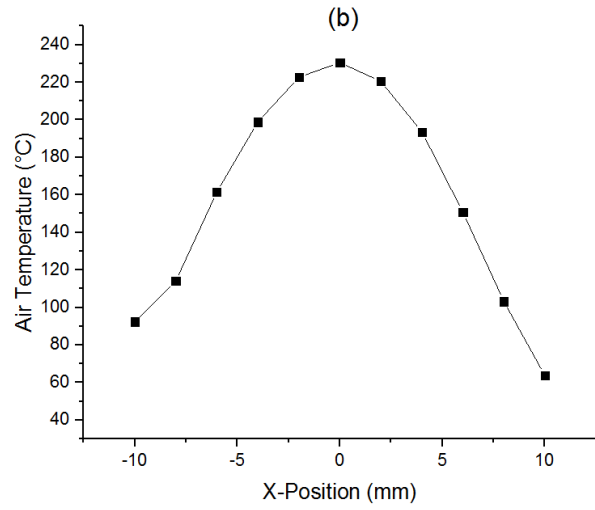
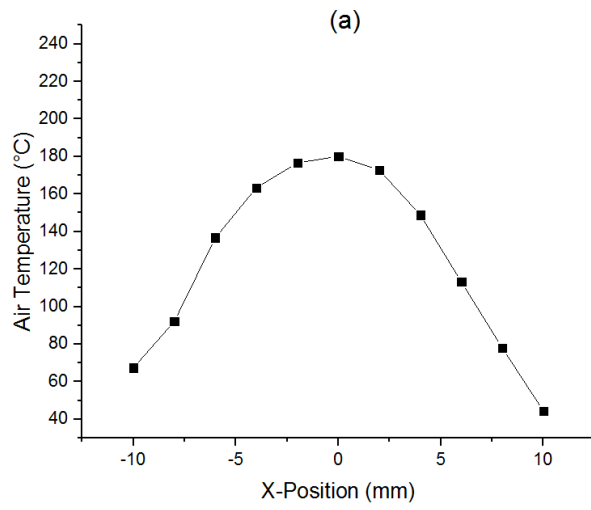
4.4 **Results and Discussion**

4.4.1 *Air Temperature and Velocity Profile*

In investigating the effects of increasing number of spinning rows on the fibers and webs formed, understanding of the attenuating air environment is especially important. It is assumed that the polymer flow rate through each spinneret is constant. Therefore the temperature at which the polymer melt emerges from the capillaries into the air stream should also be independent of the spinneret location. The principal difference between fibers spun from interior and perimeter rows, therefore, lies in the air environment fibers are exposed to after emerging from the spinnerets. Previous empirical modeling of the fiber diameters produced by the annular spinneret design show that final fiber diameter can be accurately predicted by knowledge of air and polymer conditions very close to the die; in other words, this region is the most critical to fiber formation.

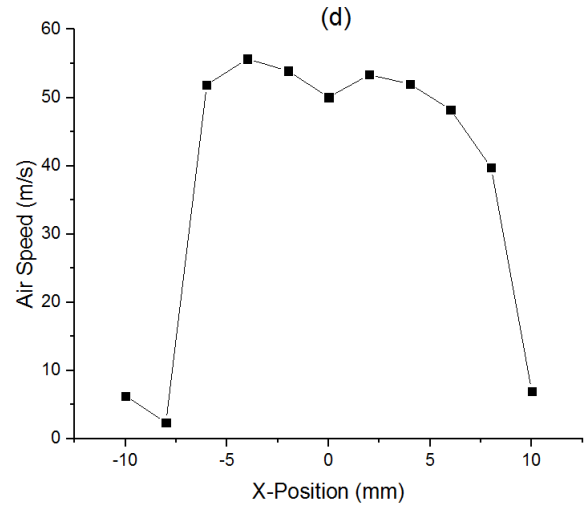
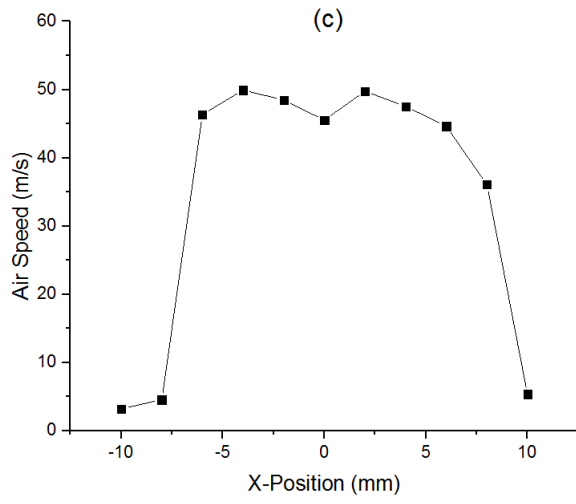
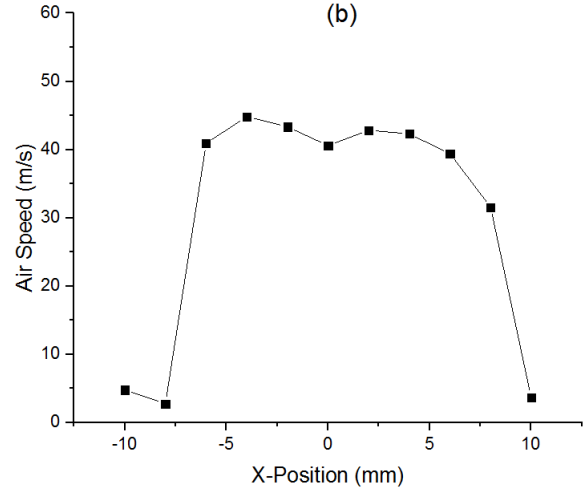
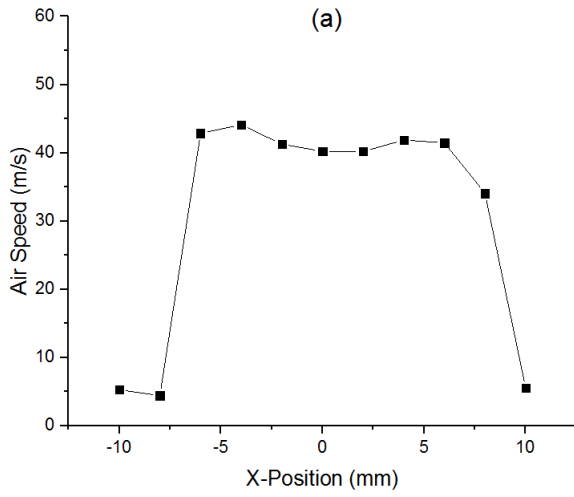
The air temperature and velocity was measured for the array of points shown in Figure 4.3, with measurements concentrated in the region of most interest one centimeter in front of the capillary outlets. The measurements at these near-spinneret positions are shown in Figure 4.4 for each combination of air cavity temperature and pressure.

Figure 4.4 Air temperature and velocity measured across the air stream 1 cm in front of spinnerets. Spinnerets were “dry”, i.e. no fibers were formed during the measurement. Measurement type by numeral: I. Air Temperatures; II. Air Speeds. Air cavity conditions by letter: (a) 48.3 kPa, 182 °C; (b) 48.3 kPa, 240 °C; (c) 68.9 kPa, 182 °C; (d) 68.9 kPa, 240 °C.



I.

Figure continues to next page.



II.

Capillary outlets are located at odd millimeter values on both sides of the origin: ± 1 , ± 3 , and ± 5 mm. Figure 4.4 can therefore be used to estimate the air environment of fibers emitting from each spinneret row. Figures 4.3I and 4.3II show that the air speed varies less significantly than does the air temperature for different spinneret rows. This is due to the fact that air heat dissipates more rapidly than does air momentum. Air speed did increase slightly at higher temperatures for same cavity pressure conditions.

Figure 4.4 also shows two experimental artifacts that should be noted. First, the air speed profile was measured with a pitot tube with diameter more than half that of the air stream width. Such a configuration can cause the narrow air stream to accelerate around the tube head, altering static pressure readings and giving artificially high air speed readings, especially near the edge of the high velocity stream. The air profile within the high velocity stream is therefore likely flatter than Figure 4.4II suggests, with air speeds closer to the values measured at the center ($X = 0$). A smaller diameter Pitot tube or hot wire anemometer should be used for more accurate readings. Second, the true zero position in the x-dimension, the origin from which all measurement points were determined, appears to be closer to +1 mm, giving the slightly asymmetric profiles seen. Nevertheless, air temperature differences dwarf air speed difference when comparing fibers originating from different spinneret rows. Air temperature within the air stream shows a parabolic profile, with the region where fibers originated from the two center spinnerets (± 1 mm) has a higher air temperature and flatter profile than fibers originating from other rows (± 3 and ± 5 mm).

4.4.2 *Fiber Diameters and Distributions*

Given the air heat gradient present in the fiber forming region, it is intuitive that the fiber diameters and distributions vary based on row number. To examine the effect of row number on

fiber diameters, irrespective of absolute diameter, diameters from each processing condition and row number are shown in Figure 4.5 as relative to the average diameter produced for all row numbers of the same condition. Diameters are expressed as mean diameters with error bars according to the standard error of the distribution.

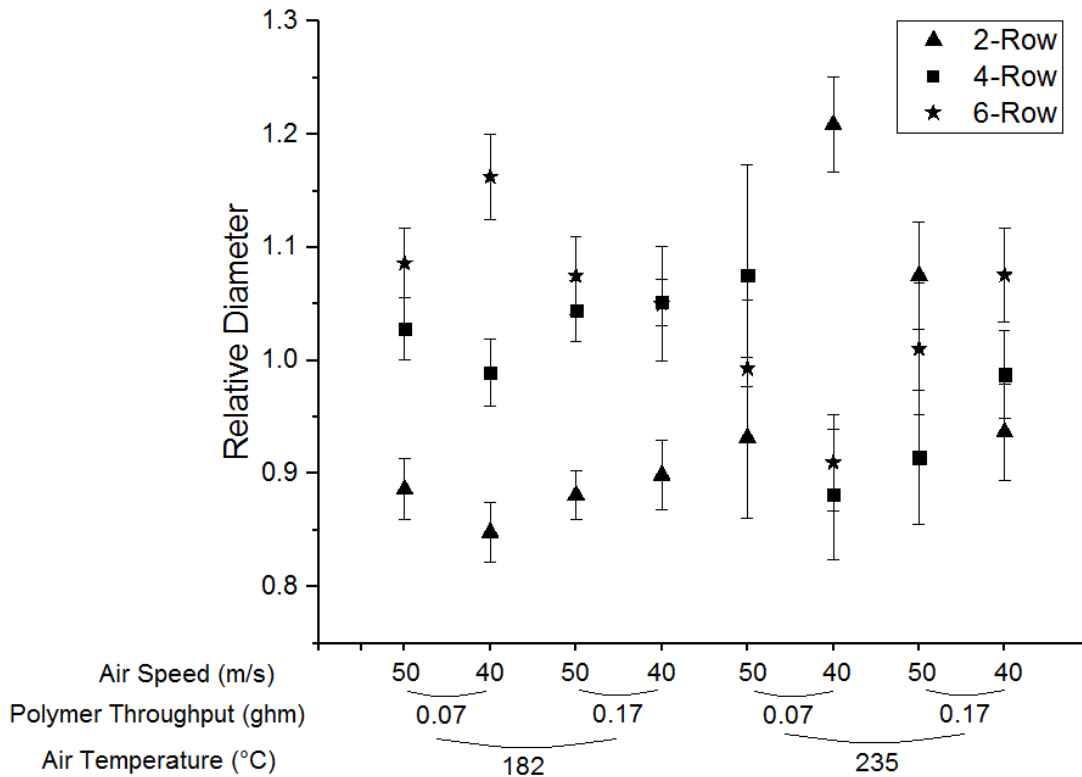


Figure 4.5 Fiber diameter for different number of spinning rows relative to the average for all rows, for various processing conditions.

Figure 4.5 shows weak evidence of a dependence of fiber diameter on number of rows. Generally, two rows produce finer fibers than four or six, except for two of the conditions where two rows produced larger fiber diameters. Given the air profiles shown in Figure 4.4, 2-row fibers are expected to be more insulated from cooler room air than fibers produced from 4 or 6 rows, hence the 2-row case is expected to produce finer fibers. For the conditions where the expected trend is clear, the increase of average fiber diameter from 2-row to 6-row is about 20%. This

relatively small effect with respect to the diameter distributions increases the difficulty of finding a clear trend but emphasizes the role of conditions affecting the polymer jet very close to the spinneret, the importance of which has been previously discussed [15]. Perimeter fibers spun in the 6-row case are expected to enter cooler air more quickly than fibers spun from the 2-row case, but may still nearly reach the fiber size of the 2-row fibers before the cool air causes the fibers to solidify, preventing further attenuation. It would be beneficial to investigate the effect of elimination of the air curtain row, the air annuli that do not spin fibers. In this study, even the 6-row case contained one insulating air curtain row, which could mitigate the effects of row number on fiber diameter. In any case, these results show that only modest reduction of fiber diameter can be gained by the incorporation of more than one air curtain row. As alteration of processing parameters such as air temperature and polymer throughput cause clear and significant change to fiber diameter [15], these results cast doubt on the economic viability of fiber diameter reduction by incorporating more air curtain rows. Additional air curtain rows will certainly increase the energy consumption of the process, and with an uncertain and at most modest effect on fiber diameter.

In addition to fiber diameters, diameter distributions are expected to be affected by the number of spinning rows. If perimeter rows produce larger fibers than interior rows, increasing row number can widen the fiber diameter distributions. To test whether the distributions were affected by number of spinning rows, the fiber diameters were analyzed using the Kolmogorov-Smirnov two sample test. This sensitive statistical test is appropriate for continuous variables and determines the probability that two random sampled data sets come from the same empirical distribution function. [19] The tests were performed for row pairs for all 40 cm DCD conditions combined, as well as for row pairs from each condition separately (shown in supplementary

information). The cumulative diameter distributions of fibers formed with two, four, and six rows are shown in Figure 4.6. Interestingly, the cumulative distribution shows that 2-row fibers have the smallest diameter for larger fibers, and the largest diameter for smaller fibers. This is revisited below.

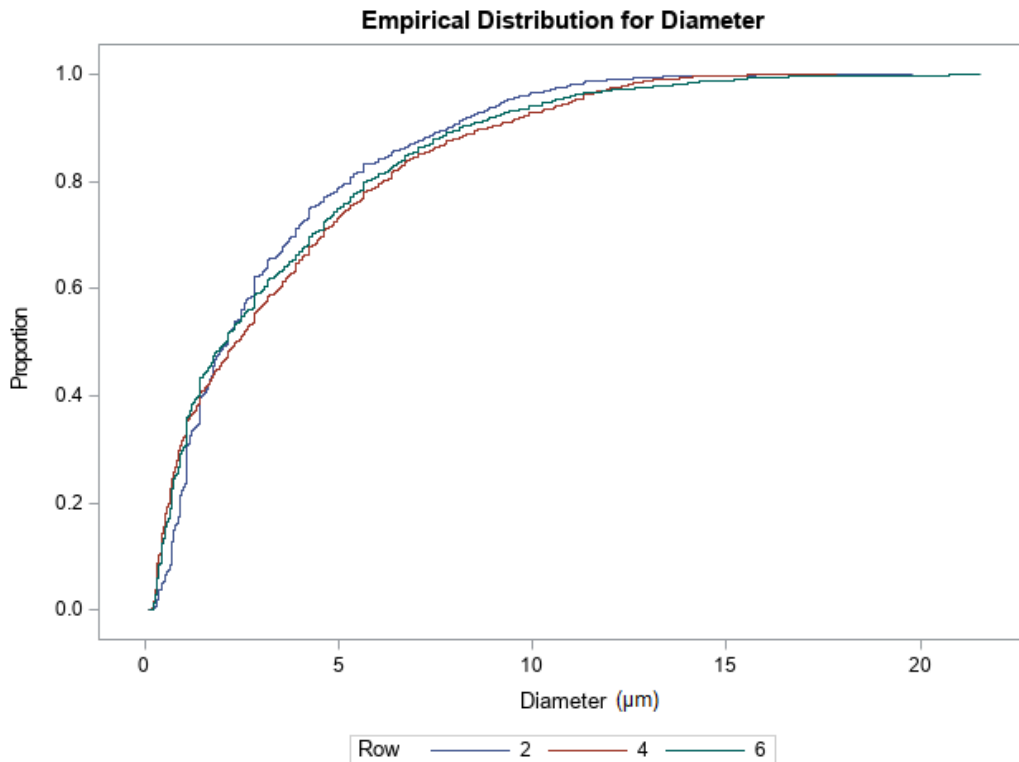


Figure 4.6 Cumulative fiber diameter distributions from all conditions where DCD = 40 cm, for two, four, and six fiber spinning rows. Each distribution results from approximately 3000 fiber diameters measured.

With a 95% confidence level, fibers from two spinneret rows form a different diameter distribution from four and six rows ($p < 0.001$). Four and six row distributions were not significantly different ($p = 0.07$). These indicate that most of diameter distribution change occurs between two and greater row numbers. Surprisingly, Kolmogorov-Smirnov test statistic values show that, while the diameter distribution from two rows is statically distinct from both four and six rows, the 2-row distribution more closely resembles that formed from 6-row than from 4-row.

Another unintuitive result that principally highlights the small impact that the increasing number of fiber spinning rows has on the fiber diameters and distributions.

Diameter distributions from a two-row annular spinneret design have been investigated and shown to have various shapes based on the processing conditions [16]. In that work, fiber diameter distribution width, or dispersity, was described by the standard deviation relative to the median fiber diameter, similar to a coefficient of variance for a normal distribution but applicable to the skewed distributions characteristic of meltblown fiber diameters. This fiber diameter distribution dispersity was calculated for each sample collected, and results compared between samples formed from different number of spinning rows. Dispersities for each row number, averaged across all 40 cm DCD conditions are shown in Figure 4.7 (all dispersities are shown in supplementary material).

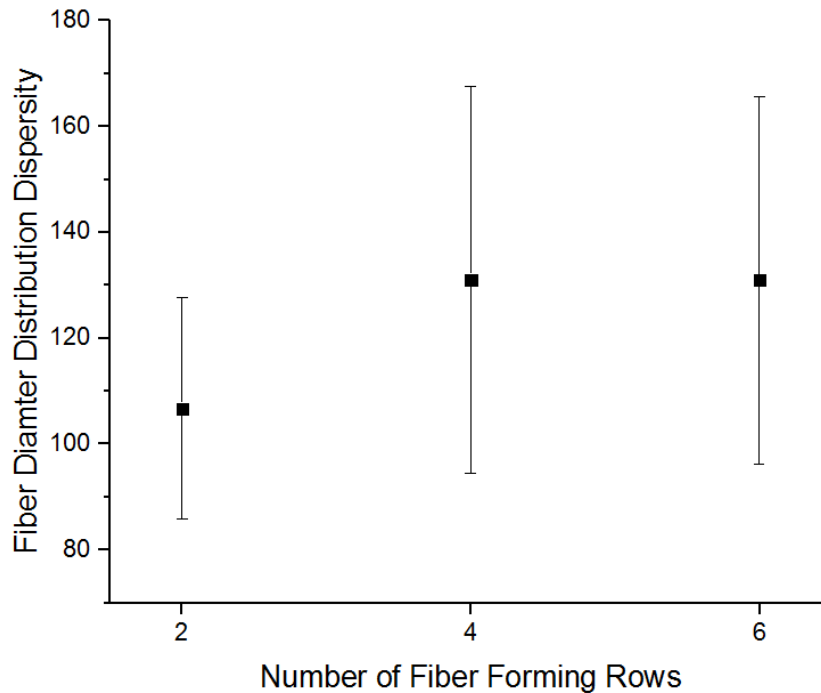


Figure 4.7 Fiber diameter distribution dispersivity for all conditions (where DCD = 40 cm), spun from 2, 4, and 6 spinneret rows.

Fiber diameter distributions, given their variability between conditions, are not significantly wider for greater number of spinning rows. Four and six row conditions showed higher diameter dispersivity for conditions of lower polymer throughput, lengthening the error bars associated with those row numbers. Distributions widths are known to be highly dependent on polymer jet pulsation near the spinnerets, the severity of which is throughput dependent. [16] Greater variability in the distribution widths between conditions at higher row number therefore could plausibly arise from uneven polymer flow rates through capillaries of different rows. Higher flow rates through center spinnerets and lower flow rates through perimeter spinnerets would mitigate any increase of average fiber diameter from increasing number of spinning rows. Furthermore, more severe polymer jet pulsation has been shown to reduce small fiber diameters, but also increase the diameter of large fibers. Variable polymer jet pulsation for higher number of spinning rows could explain the interesting trend seen in Figure 4.6, that 2-rows produced larger

small-diameter fibers, but smaller large-diameter fibers. Flow rates were not monitored for each spinneret, but results here give some suspicion about the assumption of uniform polymer throughputs for dies of greater row number. The assumption can be tested by high speed observation of polymer jet pulsation frequency of perimeter and interior spinnerets [16]. Such an experiment would become increasingly challenging for greater number of spinning rows, but would be easier to implement and less likely to interfere with the flow rates than methods that involve contact with the polymer melt.

4.4.3 Web Defect: Spun Fusion

In the measurement of fiber diameters discussed above, all diameters refer to individual fibers, not ropes, fused fibers, shot particles, or any other web defects. While most web defects are seldom observed in the SEM images fiber fusion is commonly observed, for all samples of all conditions. Spun fusion refers to the situation where molten fibers contact one another in the air stream prior to solidification and lay down. The result is fibers fusion, fibers bonded in parallel over a long distance which reach the collection belt essentially as one larger fiber. Fused fibers may contain two or several fibers in a bonded bundle, with some containing as many as 20 fibers or more. Spun fusion bonding is distinct from interfiber bonding on the collection belt, which causes the bonding of fibers at high angles, but leaves fibers isolated from one another over most of their length. The latter case is often desirable because it can create bonded meltblown fabrics for appropriate DCDs [15], while the former is considered an undesirable web defect.

SEM images, the same used to determine individual fiber diameters above, were analyzed manually to determine the severity of fiber fusion, expressed as a fraction of all fibers that are

fused. Fibers and fused fibers from each SEM image were counted to determine this fraction using the method shown in Figure 4.8.

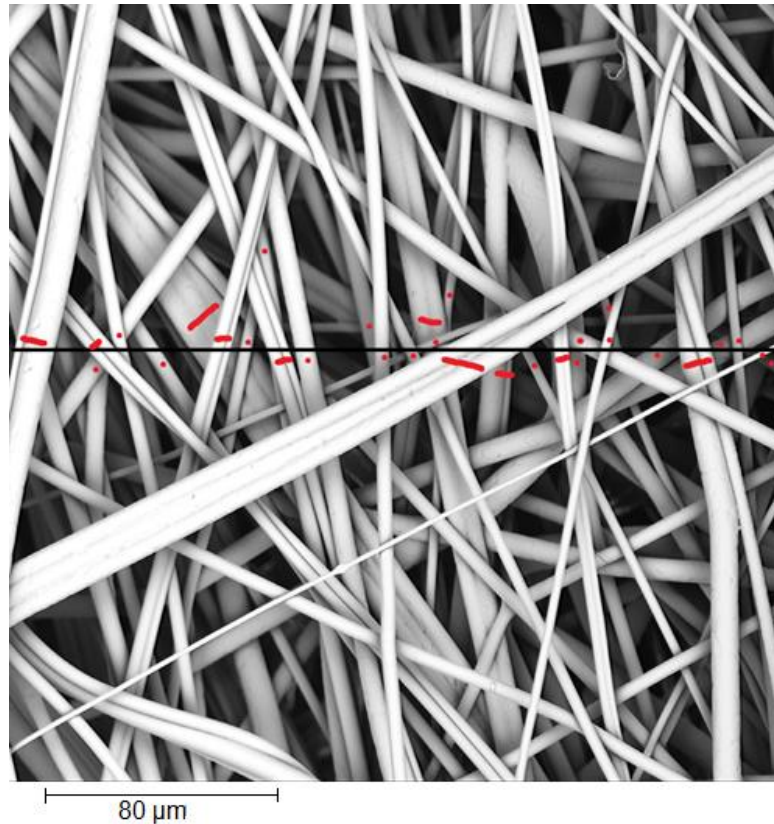


Figure 4.8 Fiber fusion counting procedure: a line is drawn approximately perpendicular to the machine direction of the fiber orientation. Individual and fused fibers are counted that cross this line. This procedure applied to this image gives 43 fibers total (fused or individual), 22 fibers involved in 10 fusions. 22/43 or 51% of fibers are fused.

All SEM images were analyzed in this manner to investigate the effects of processing conditions and number of spinning rows on the fraction of fiber fusion. Effects of the each processing condition, averaged across the other processing conditions, are shown in Figure 4.9. Except for Figure 4.9(d), all DCDs were 40 cm.

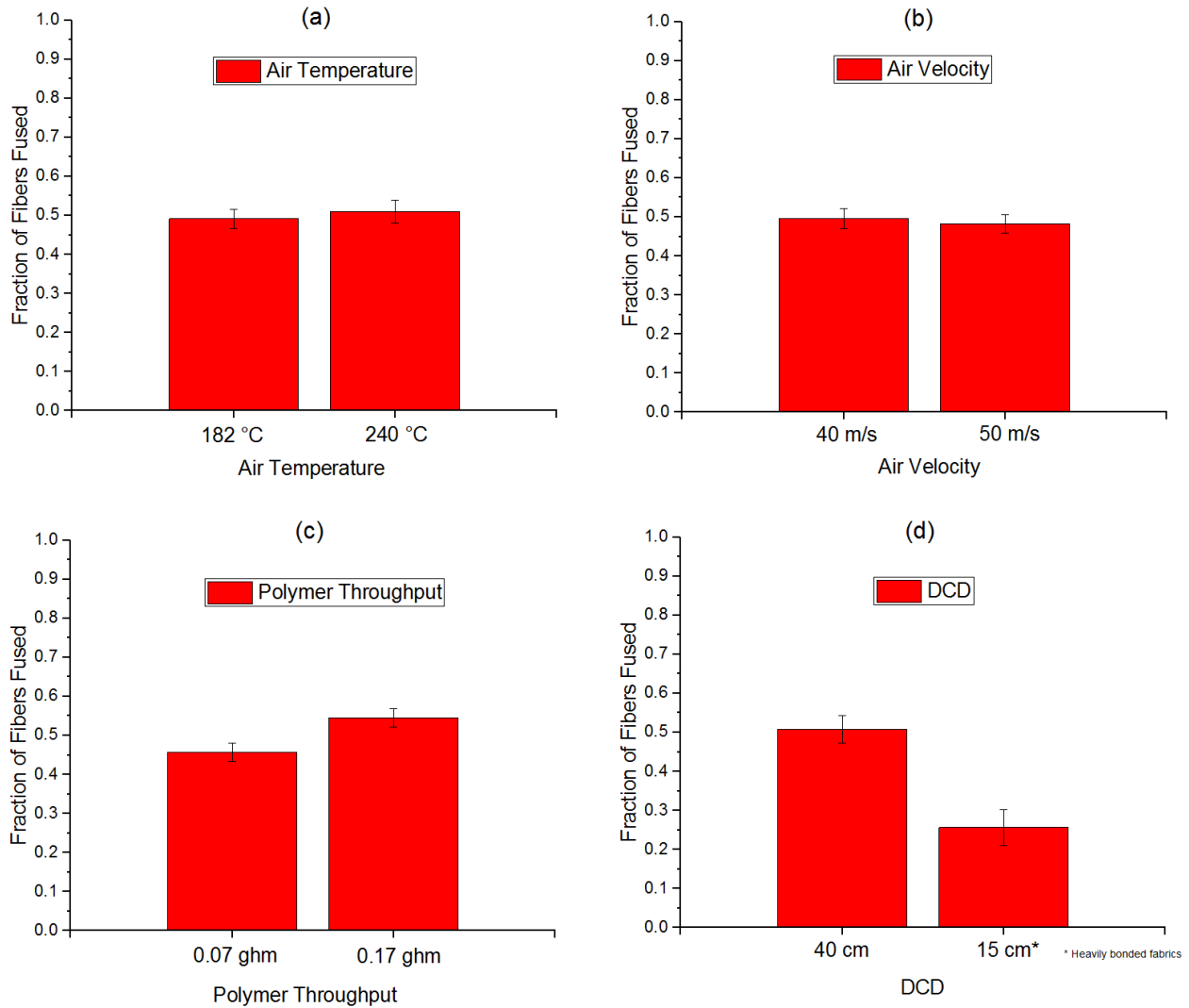


Figure 4.9 Effect of processing conditions on the incidence of fiber fusion. (a) Air temperature effects (for DCD = 40 cm, averaged across row number, air velocity, and polymer throughput); (b) Air velocity effects (for DCD = 40 cm, averaged across row number, air temperature, and polymer throughput); (c) Polymer throughput effects (for DCD = 40 cm, averaged across row number, air temperature and air velocity); (d) DCD effects (averaged across all conditions and row number).

Lower DCD and polymer throughputs produced lower fiber fusion rates, while air temperature and velocity had no significant effect. Significant reduction in fiber fusion was achieved by reducing the DCD to a level that also produced heavily bonded samples. Thus shortening DCDs below the bonding distance, the maximum DCD at which fibers contact the collection belt while still molten, can reduce the distance over which fibers may contact one

another while still molten. Thus DCD variations below the bonding distance can have a significant impact on fiber fusion because, beyond the bonding distance, fibers have solidified and further spun fusion cannot occur. Higher polymer throughputs increase fiber fusion rates because they produce larger fibers which cool more slowly than fine fibers [15], which increases their bonding distance and the chance that fibers will fuse. Higher air temperature may increase fiber fusion for a wider air temperature range than is varied here by keeping the fibers molten longer in a high temperature air stream, but the effect could be mitigated by faster polymer jet attenuation caused by higher air temperatures. In the same way that lower polymer throughputs reduce fiber fusion by creating small fibers that cool more rapidly, air processing conditions that produce smaller fibers are expected to reduce fiber fusion. Therefore higher air velocities, similarly over a wider range than is studied here, could reduce fusion since those conditions also cause faster polymer jet attenuation.

Figure 4.10 shows the effect of the number of fiber forming rows on fiber fusion rates.

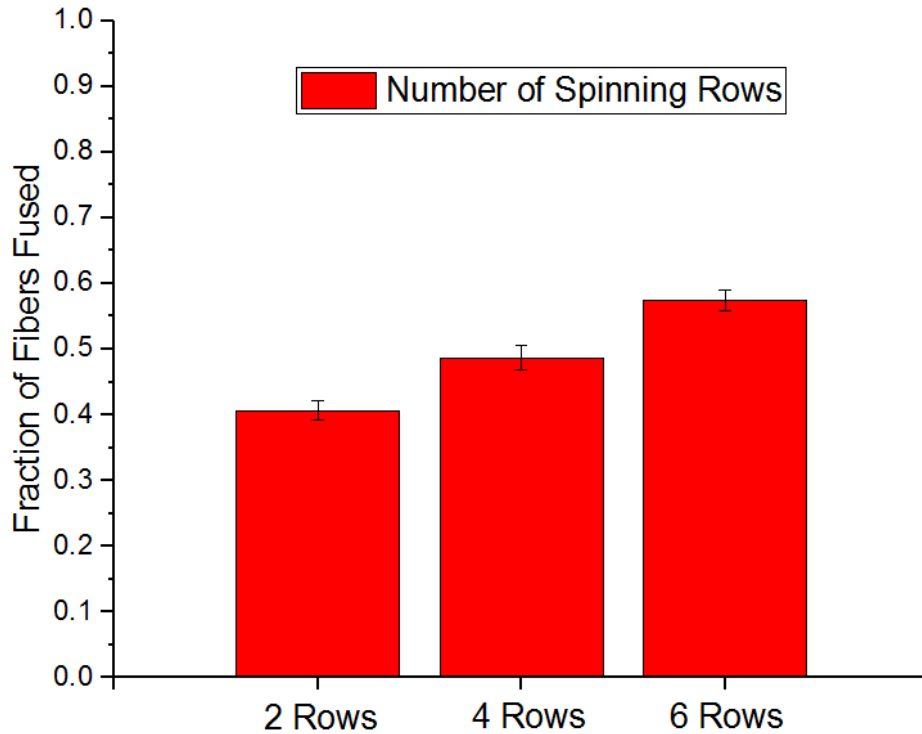


Figure 4.10 Fiber fusion rates for all processing conditions (where DCD = 40 cm) for fibers spun from 2, 4 and 6 fiber forming spinneret rows.

Figure 4.10 confirms the anticipated effect of fiber density within the air stream on spun fusion. Given the spinneret spacing and motion paths of the fibers, the trend is expected to continue for higher row numbers. Meltblown fibers undergo bending instabilities and whipping motions at intermediate distances from the spinneret outlets, while they are still molten. Side-to-side motions of the spinning fibers for a similar spinneret design have been shown to extend past 2 mm, the distance between spinnerets, within 2 cm from the spinneret outlets [15]. This means that fibers may begin contacting one another just 2 cm downstream from the spinnerets. The bending instabilities only grow from there; side-to-side motions of 18 mm were observed to take place 12 cm from the spinnerets. For spinnerets separated by just 2 mm, these bending instabilities can allow fibers separated by up to 9 rows to contact and fuse 12 cm from the spinnerets. With bonding

distances of 20 to 35 cm, fibers from opposite perimeter rows of a 12 or 16 row die, the most that are commercially available, will be able to fuse.

Spun fusion increases the effective diameter of fibers formed via meltblowing. The significant rates observed of fibers involved in fusion, sometimes over 60%, could therefore undermine the intended benefits of a multi-row meltblowing design of lower cost and increased production rates of fine fibers. The results here show that spun fusion could be reduced by increasing the spinneret-spinneret distance. A reduced spinneret density on the die will reduce the chance fibers contact one another in the air stream. Such a modification will not necessarily increase air handling costs, because for a given processing condition, the air volumes used are related to the number of air annuli, not to their density. A much reduced spinneret density would require larger dies and likely cause greater volumes of cool room air to be entrained into the attenuating air stream because nearby air annuli will not as effectively insulate one another. Alternatively, spun fusion could be reduced by targeted control of the fiber quench conditions, rather than allowing fibers to crystallize according to the upstream processing conditions. If low DCDs reduce fiber fusion rates then fibers that are intentionally quenched closer to the die than the bonding distance (by cooling water or air jets, for example) will not be able to fuse after crystallizing. Each of these modifications may reduce effective fiber diameter by reducing the incidence of fiber fusion, but are expected to increase individual fiber size. Modifications to the die geometries and/or spinning quench conditions provide ample opportunity for further investigation to utilize the tradeoffs involved to create unique and controllable fiber structures.

4.5 Conclusions

We have extended the understanding of the fiber formation process of an annular meltblown spinneret design to include the effects of increasing the number of fiber forming spinneret rows. A 6-row die was modified to also spin from only 4-rows and 2-rows, allowing a comparison of the fibers and webs formed for the same processing conditions, but for varied number spinning rows. Despite the sharp air temperature gradient across the air stream, which presumably exposes fibers spun from perimeter rows to cool air earlier in the spinning process than fibers spun from interior rows, individual fiber diameters and distributions were not significantly altered by increasing row number. This surprising result raises doubt about whether the polymer throughput is consistent between interior and perimeter spinnerets because inconsistent throughput can explain the trends seen.

Fabrics were also analyzed for the occurrence of spun fusion, a web defect involving fibers bonded over long distances in parallel. A greater fraction of fibers were fused to one another for higher per-capillary polymer throughput, higher DCD, and more spinning rows. Increasing overall throughput with additional spinneret rows therefore increases effective fiber diameter by spun fusion. For some conditions, more than 60% of all fibers observed are fused to one another. For a high number of spinning rows, spun fusion may be reduced by increasing the spinneret spacing or by quenching the spinning fibers before collection. Either method will likely reduce spun fusion rates at the cost of increasing individual fiber diameters.

4.6 References

- [1] D. H. Reneker and I. Chun, "Nanometre diameter fibres of polymer, produced by electrospinning," *Nanotechnology*, vol. 7, pp. 216–223, 1996.
- [2] M. E. S., G. M. Glenn, A. P. Klamczynski, W. J. Ortis, and L. H. C. Mattoso, "Solution Blow Spinning: A New Method to Produce Micro- and Nanofibers from Polymer Solutions," *J. Appl. Polym. Sci.*, vol. 113, no. 4, pp. 2322–2330, 2009.
- [3] R. L. Shambaugh, "A Macroscopic View of the Melt-Blowing Process for Producing Microfibers," *Ind. Eng. Chem. Res.*, vol. 27, pp. 2363–2372, 1988.
- [4] V. Wente, "Superfine Thermoplastic Fibers," *Ind. Eng. Chem. Res.*, pp. 342–346, 1955.
- [5] J. P. Keller and R. R. Buntin, "Melt-Blowing Die For Producing Nonwoven Mats," 3825380, 1974.
- [6] R. Butin, J. P. Keller, and J. Harding, "Non-Woven Mats by Melt Blowing," 3849241, 1974.
- [7] V. Bansal and R. L. Shambaugh, "On-line Determination of Diameter and Temperature during Melt Blowing of Polypropylene," *Ind. Eng. Chem. Res.*, vol. 5885, no. 97, pp. 1799–1806, 1999.
- [8] B. Haynes, "An experimental and analytical investigation on the production of microfibers using a single hole melt blowing process," University of Tennessee Knoxville, 1991.
- [9] A. L. Yarin, S. Sinha-ray, and B. Pourdeyhimi, "Meltblowing : Multiple polymer jets and fiber-size distribution and lay-down patterns," *Polymer (Guildf.)*, vol. 52, no. 13, pp. 2929–2938, 2011.
- [10] D. H. Tan, C. Zhou, C. J. Ellison, S. Kumar, C. W. Macosko, and F. S. Bates, "Meltblown fibers: Influence of viscosity and elasticity on diameter distribution," *J. Nonnewton. Fluid Mech.*, vol. 165, no. 15–16, pp. 892–900, 2010.
- [11] S. Batra and B. Pourdeyhimi, *Introduction to Nonwovens Technology*. 2012.
- [12] X. Wang and Q. Ke, "Experimental Investigation of Adhesive Meltblown Web Production Using Accessory Air," *Polym. Eng. Sci.*, vol. 46, no. 1, pp. 1–7, 2006.
- [13] W. J. Li, C. T. Laurencin, E. J. Caterson, R. S. Tuan, and F. K. Ko, "Electrospun nanofibrous structure: A novel scaffold for tissue engineering," *J. Biomed. Mater. Res.*, vol. 60, no. 4, pp. 613–621, 2002.
- [14] G. F. Ward, "Meltblown nanofibres for nonwoven filtration applications," *Filtr. Sep.*, vol. 38, no. 9, pp. 42–43, 2001.

- [15] S. Barilovits, E. Shim, S. a Khan, and B. Pourdeyhimi, "Experimental Investigation of a Multi-Row Meltblowing Fiber Formation Process and Web Structures," *Pending Publ.*, 2018.
- [16] S. Barilovits, E. Shim, S. A. Khan, and B. Pourdeyhimi, "Meltblown Polymer Jet Pulsation: Observations and Effects on Fiber Diameter Distribution in an Annular Meltblowing Spinneret Design," *Pending Publ.*, 2018.
- [17] E. C. A. Schwarz, "Apparatus and Process of Melt-Blowing A Fiberforming Thermoplastic Polymer and Product Produced Thereby," 4380570, 1983.
- [18] E. Schwarz, "Apparatus and Process for Uniformly Melt-Blowing A Fiberforming Thermoplastic Polymer in a Spinnerette Assembly of Multiple Rows of Spinning Orifices," 5476616, 1995.
- [19] B. P. Flannery, S. Teukolsky, W. H. Press, and W. T. Vetterling, *Numerical Recipes in C: The Art of Scientific Computing*. 1988.

4.7 Supplementary Information

4.7.1 *Fiber Diameter Measurement Using a Semi-Automated Method*

Auto-Fiber is a proprietary software developed by Mann+Hummel Group and is designed to analyze SEM images to rapidly determine fiber diameters. Software results may include fused fibers, ropes, shot particles, or other non-fiber measurements and manual removal of such incorrect measurements is required. Even with the manual assistance, the process is much faster than direct measurement of the fiber diameters using software such as National Institute of Health ImageJ. To determine if the diameters produced by measuring individual fibers manually (using ImageJ software) are equivalent to the diameters measured from the same SEM images using a semi-manual method with AutoFiber, the fiber diameter distributions are compared using the Kolmogorov-Smirnov two sample test. Fibers were produced using a two-row annular meltblowing die of different dimensions to that studied here; conditions and details are described in a previous study [15]. The distributions are shown in Figure 4.11 as cumulative distributions, with test P-values shown. The P-value indicates the probability that the two samples tested originate from the same distribution.

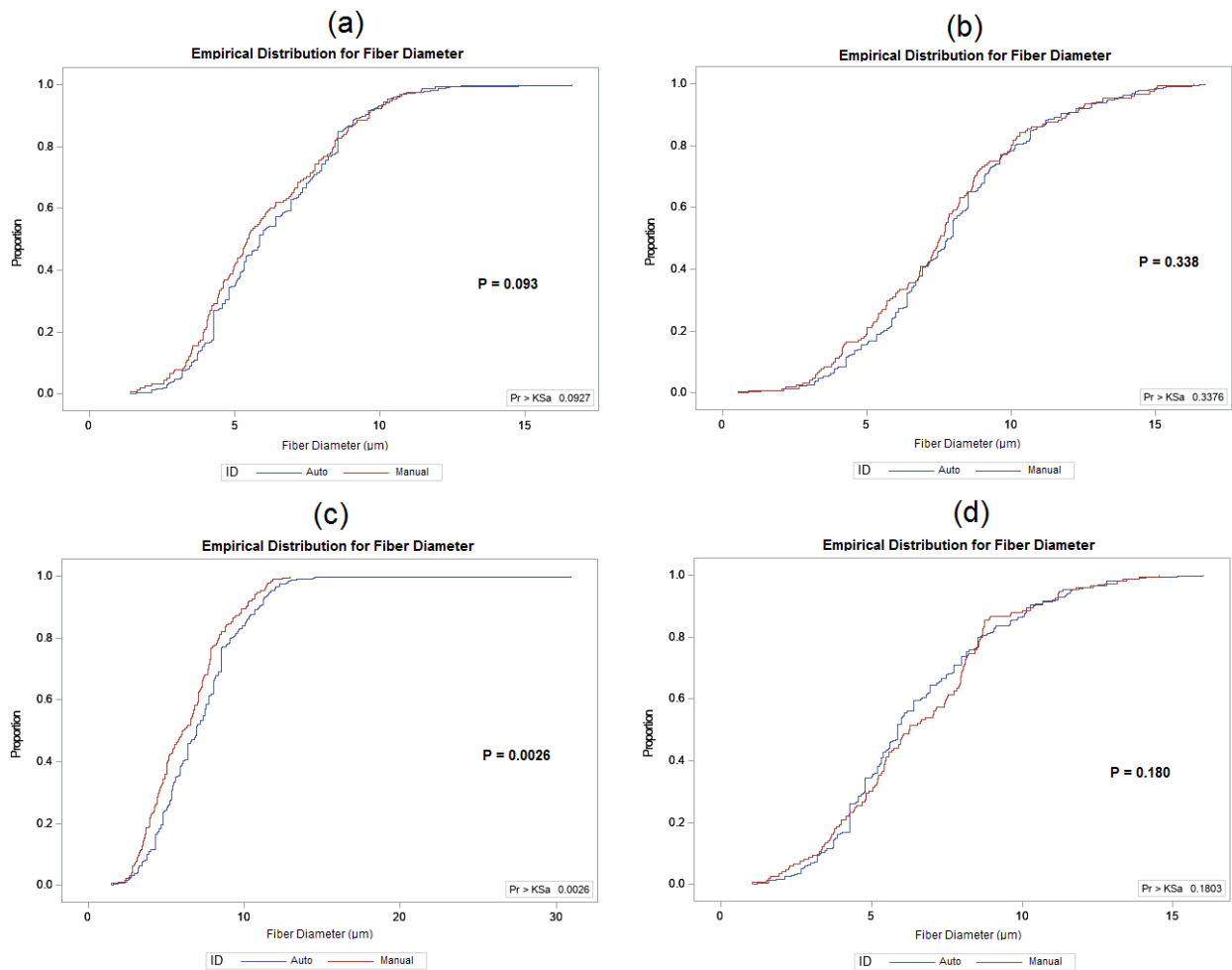


Figure 4.11 Fiber diameter distributions as determined manually (using ImageJ software) shown in red, and using a semi-automated program (AutoFiber from Mann+Hummel Group) shown in blue. Kolmogorov-Smirnov two sample test p-values shown. Processing conditions: (a) air temperature of 166 °C, air speed of 55 m/s, polymer throughput of 0.10 ghm, DCD of 15 cm; (b) air temperature of 166 °C, air speed of 55 m/s, polymer throughput of 0.10 ghm, DCD of 20 cm; (c) air temperature of 166 °C, air speed of 55 m/s, polymer throughput of 0.10 ghm, DCD of 30 cm; (d) air temperature of 166 °C, air speed of 55 m/s, polymer throughput of 0.10 ghm, DCD of 40 cm.

With a 95% confidence level, only for one of the conditions shown, Figure 4.11(c), do the manual and semi-automated diameters differ. Recognizing the variability that may occur for manual measurement, especially in selection fibers for measurement up to an arbitrary depth into the fabric, we deem that the semi-automated method gives satisfactory fiber diameter

measurements. AutoFiber software with manual removal of incorrect measurements is therefore used in this study to determine the individual fiber diameters produced for all samples collected.

4.7.2 Processing Conditions and Fiber Diameter Distributions

Processing conditions varied for the levels shown in Table 4.1 are arranged for identifying purposes in Table 4.2.

Table 4.2 Processing condition by condition identifying number. Fabrics formed from all condition for 2, 4, and 6 fiber spinning rows.

Condition Number	Air Temperature (°C)	Air Cavity Pressure (kPa)	Polymer Throughput (ghm)	DCD (cm)
1	182	68.9	0.07	40
2	182	48.3	0.07	40
3	182	68.9	0.17	40
4	182	48.3	0.17	40
5	182	68.9	0.17	15
6	182	68.9	0.07	15
7	240	68.9	0.07	40
8	240	48.3	0.07	40
9	240	68.9	0.17	40
10	240	48.3	0.17	40
11	240	68.9	0.17	25
12	240	68.9	0.07	25

Distribution dispersities, the standard deviation divided by the median fiber diameter, for each condition and row number are shown in Table 4.3.

Table 4.3 Fiber diameter distribution dispersities for each condition and number of fiber spinning rows.

Condition Number	2-Row	4-Row	6-Row
1	94	64	72
2	87	56	58
3	41	40	44
4	38	23	52
5	44	27	33
6	50	33	45
7	136	315	165
8	130	245	162
9	106	114	181
10	80	68	75
11	37	58	66
12	153	181	155

Fiber diameter distributions for each condition, specified by number of spinning rows, are shown in Figure 4.12. Kolmogorov-Smirnov test values are also shown for each pair.

Figure 4.12 Fiber diameter distributions as cumulative distributions for all samples collected. Distributions in blue are for the sample collected from the 2-row case, red from the 4-row case, and green from the 6-row case. Table 4.2 displays processing conditions for each condition number. Kolmogorov-Smirnov two sample test p-values shown: P_{2/6} shows the p-value results when 2 and 6-row distributions are compared, analogously for the other two pairs.

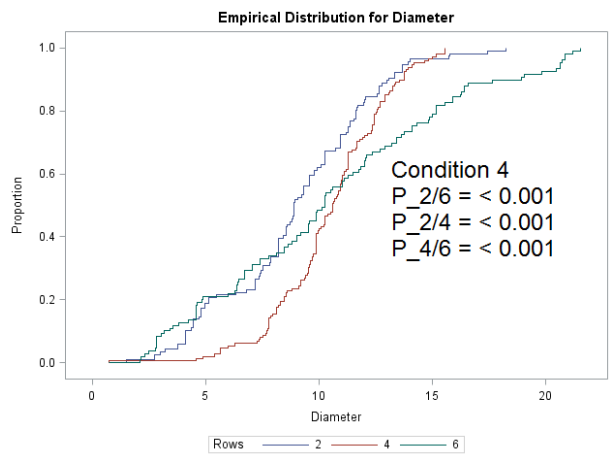
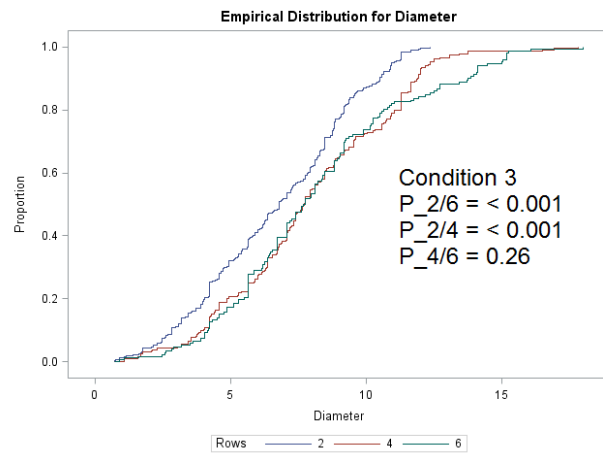
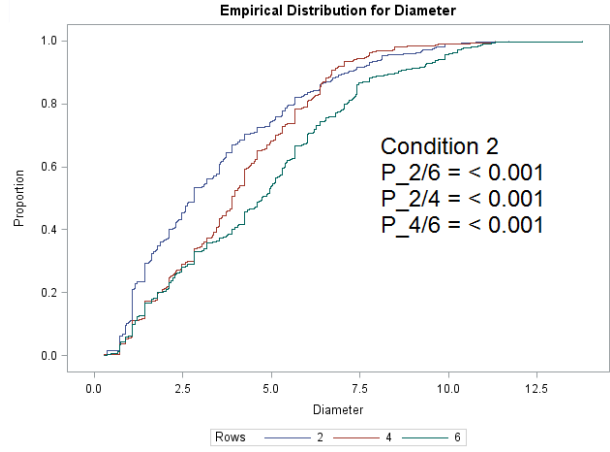
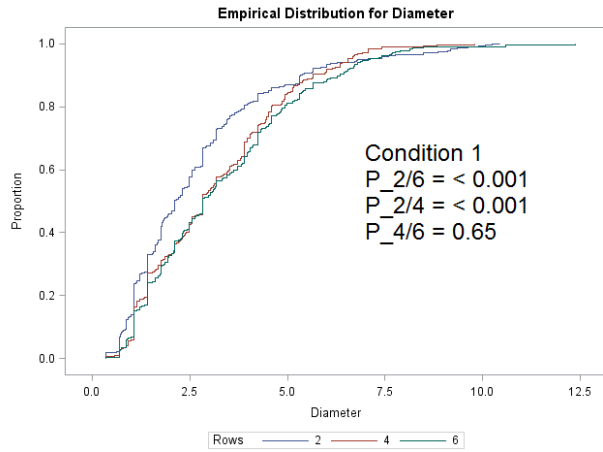


Figure continued on next page.

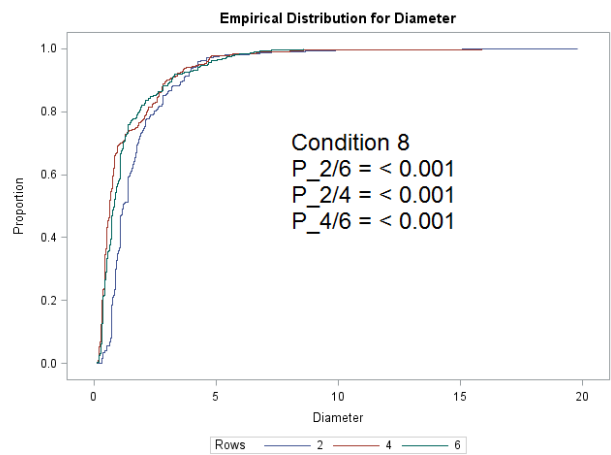
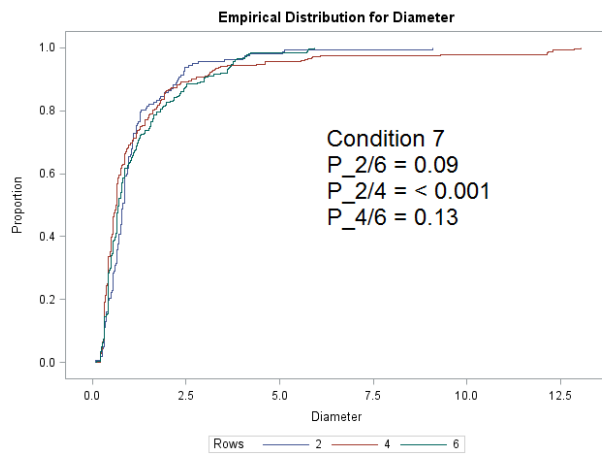
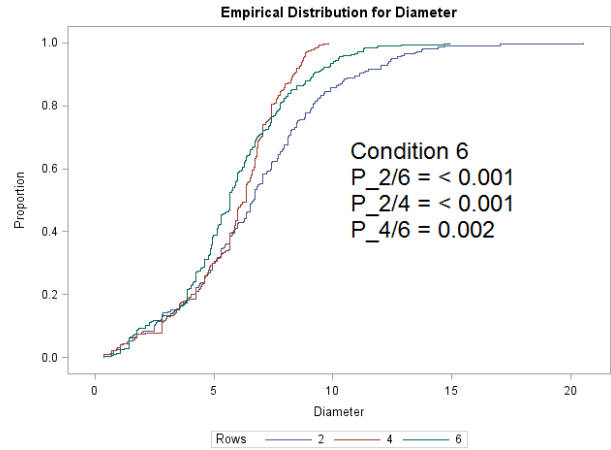
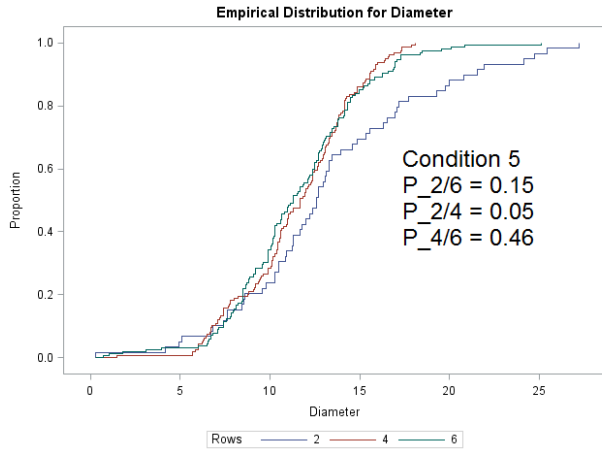
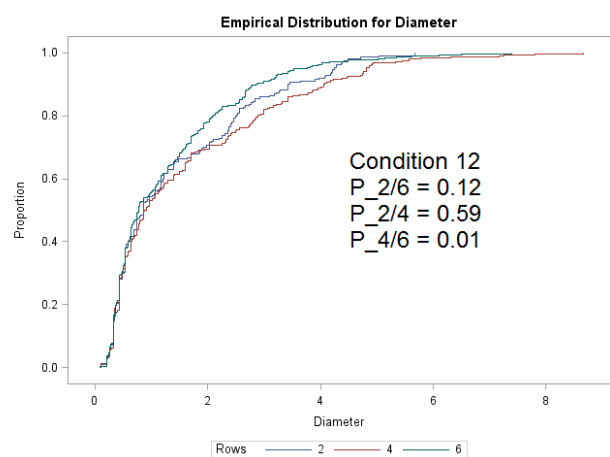
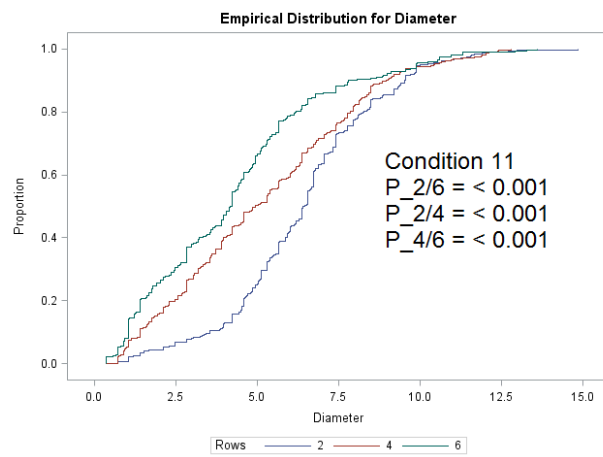
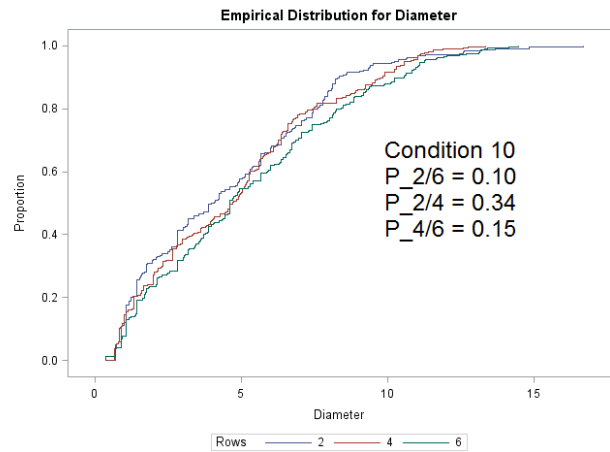
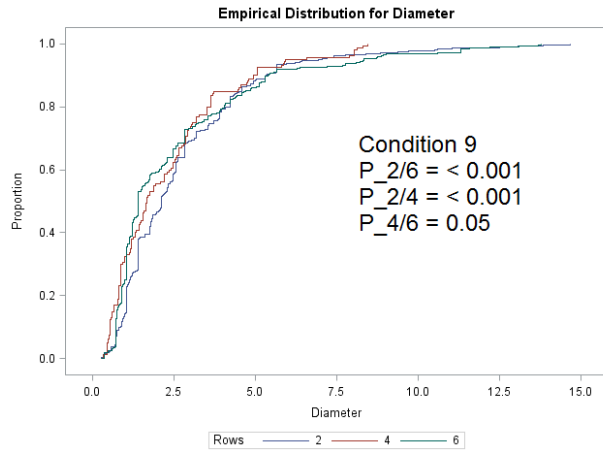


Figure continued on next page.



5 Chapter 5 - Summary and Conclusions

The objective of this study was to improve, through experimentation, the understanding of the multi-row meltblowing fiber and web formation process. Although the process was originally developed and commercialized decades ago, no publicized systematic investigation of the process has yet been performed. Extensive collective knowledge of the process exists among its users and developers in the industry, but this knowledge is diffuse by nature. Newcomers may need to rely on rumors circulated from few sources, spend precious time and material learning by trial and error what others already know, or anticipate this result, opting instead to adopt the more well-studied technology. Purported capabilities of the process to form fine yet strong fibers at high throughput (i.e. low cost) and do this with a wide array of polymer resins would make the technology highly attractive and likely to be used by many for years to come. The experiments in this study were therefore motivated to obtain an understanding of the process limitations and to explain the fiber diameters, their distributions, and web structures formed.

The work can be divided into two main parts: first, a detailed study of the annular spinneret design and second, an investigation of high-throughput spinning using multiple rows. Given the numerous variables involved, experiments were designed to examine the effects of only the most critical process parameters. Process variables included polymer throughput, air speed, air temperature, Die-Collector Distance (DCD), number of spinning rows, and capillary size. Critical observations were often made with various imaging techniques, such as infrared thermography, ultra-high speed videography, high resolution photography, and electron microscopy.

A single polypropylene resin, LyondellBassell MF650W, was used for all experiments and was chosen because it is popularly used and known to be easily processed by the equipment. The

polymer flow and thermal properties were used as guides for selecting appropriate processing conditions and to put fiber diameter attenuation into a physical context. Without risking any thermal degradation, tests show that this polymer can be spun into fibers between about 120 - 250 °C, which translates to a zero-shear viscosity range of 10 – 290 Pa*s.

The annular spinneret design was studied using a two-row meltblowing configuration, the symmetry of which eliminates most multi-row effects. Using a spinneret size of 508 μm inner diameter, fibers were formed with median diameters ranging from 0.76 to 13.8 μm for variations in polymer throughput, air temperature, and air speed. Air temperature and speed profiles measured without spinning fibers allow for estimation of the air environment surrounding the fibers during spinning. On-line observation of the polymer jets very close to the spinnerets was performed using high-resolution infrared thermography. The results confirmed calculations that significant heat transfer occurs between the air and polymer inside the capillaries prior to spinning, allowing rapid alteration of the polymer temperature. Infrared thermography also showed that thicker polymer jets cool more slowly than do narrower jets. An empirical model using inputs of polymer flow behavior at the calculated temperature at which polymer emerges from the spinnerets and the air temperature and speed very close to the spinnerets proved to accurately estimate the median fiber diameter produced across a wide array of processing conditions. This result most importantly shows that total fiber diameter attenuation, while complex and caused by several mechanisms, is largely determined by polymer properties and the attenuating air environment very close to the spinnerets.

The webs formed were analyzed to determine autogenous bonding distances and the incidence of spun fusion defects. Bonding distances were determined by inspecting SEM images of fibers collected at various DCDs for only the two-row meltblowing case. In correspondence

with IR thermography of polymer jets showing that large jets cool more slowly than narrow jets, conditions spinning larger and warmer fibers were associated with greater bonding distances. Higher polymer throughput, higher air temperature, and lower air velocity increased the maximum DCD required to produce fabrics where some portion of the fibers were bonded.

Fiber diameter distributions formed by the annular spinneret show a greater diversity of distributions than has been reported for those made from the traditional slot die. Distribution shapes varied from normal, to lognormal, to skewed-lognormal as the median fiber diameters declined. This shape transition occurs because even when most fibers become very narrow, some large fibers are spun for all processing conditions. In effect, the diameter distribution widths do not follow the median fiber diameter, so smaller median diameter samples have a wider relative diameter distribution width. Fibers were collected from the symmetric two-row meltblowing system, showing that these diameter distributions originate from the spinneret configuration rather than from any multi-row effects.

Several important dynamics of the spinning process were observed using visible light imaging. Ultra-high speed videography capable of monitoring the fiber path undergoing rapid bending motions showed that these motions begin much closer to the spinneret for smaller fibers. In the analysis of these fiber motions, it was noted that some fibers were much larger than others at the same distance from the die. To examine this further, the high-speed imaging was performed close to the spinnerets. This revealed that a clearly visible pulsation of the polymer jet, an oscillation of its diameter, occurred for conditions that spin small fibers. The pulsation occurred simultaneously at essentially identical frequencies for different spinnerets. The pulsations of all observed spinnerets were randomly phase-shifted from one another, indicating that the pulsations are aerodynamic or polymer property in origin, rather than due to pressure fluctuations of the

extruder. High-resolution stop-motion photography was used to clearly visualize the polymer jet in this region and allow measurement of the polymer jet diameter at different times. Polymer jet pulsation amplitudes are shown to correspond well to the relative width of the fiber diameter distributions, indicating that the pulsation can, in large part, explain the fiber diameter distributions characteristic of the process.

One of the principal advantages of multi-row meltblowing is the possibility of forming fine meltblown fibers at higher single-pass throughput than is possible using the traditional die. Sheets were collected using a meltblowing die with inner capillary diameters of 381 μm and containing two, four, and six fiber-forming spinneret rows. Fiber diameters and distributions were only modestly affected by the number of spinning rows, but in general, more capillary rows spun fibers with slightly larger diameters and wider diameter distributions. The effects were admittedly weaker than expected and call into question the uniformity of polymer throughput across the two-dimensional array of spinnerets. In any case, the results further highlight the relative importance of polymer jet pulsation and its dominating role in determining fiber diameters and distributions.

Fabrics formed from spinneret row number variations were analyzed for the incidence of spun fusion web defects. Spun fusion is similar to roping but occurs when partially molten fibers contact, wrap around, and bond to one another in the air stream prior to collection. The result is that two or more fibers are collected essentially as one larger and not cylindrical fiber. A greater number of spinning rows showed a clear and consistent trend in increasing the proportion of fibers fused. The increased throughput achieved by adding fiber-spinning rows also increases the density of fibers in the air stream and the chance that fibers will contact one another. Thus, while more spinning rows only modestly increases *individual* fiber diameters, the *effective* fiber diameters are

more significantly increased. Suggestions to reduce spun fusion include increasing spinneret or row spacing and affecting the rapid quenching of molten fibers closer to the spinnerets.